

Diss. ETH No. 15504

**DESIGN AND OPERATION OF SIMULATED MOVING
BED PROCESSES FOR FINE CHEMICAL AND
PHARMACEUTICAL SEPARATIONS**

A dissertation submitted to the
SWISS FEDERAL INSTITUTE OF TECHNOLOGY ZURICH

for the degree of
DOCTOR OF TECHNICAL SCIENCES

presented by
STEFANIE ABEL
Dipl. Chem.-Ing.
born on May 10th, 1973
Citizen of Germany

Accepted on the recommendation of
Prof. Dr. M. Mazzotti (ETH Zurich), examiner
Prof. Dr. M. Morbidelli (ETH Zurich), co-examiner
Prof. Dr. M. Morari (ETH Zurich), co-examiner

Zurich 2004

Acknowledgements

Arriving at the end of my time as a Ph.D. student at ETH, I would like to thank everybody who worked with me and supported me during this wonderful time.

First of all I want to thank Prof. Marco Mazzotti, who accepted me as a Ph.D. student in his group and gave me the chance to work on this extraordinary project. I am very grateful to him for many interesting discussions and his continuous support.

I am also very grateful to Prof. Massimo Morbidelli and Prof. Manfred Morari for accepting to be my co-examiners and supporting me as my 'second and third boss' in this common project.

My special thanks goes to Gültekin Erdem, who worked together with me on the control part of this project. Without him, the SMB controller would still be fantasy. Thanks, Gültekin, we were a great team.

Many many thanks also to Norbert for his patience and his encouragement.

Finally I want to thank all the nice people I met here at IVUK/IPE and at Hönggerberg, who made the time here very special for me.

Zusammenfassung

Aufgrund von immer strengeren Auflagen und ökologischen Bedenken geht der Trend in der Lebensmittelindustrie, der agrochemischen und pharmazeutischen Industrie sowie im Bereich der Biotechnologie immer stärker in Richtung hochreiner Produkte und rückstandsfreier Prozessführung. Diese Entwicklung fordert neue Technologien, insbesondere für Trennprozesse, die, sobald sie eingeführt sind, auch besser gesteuert werden können. Die präparative Chromatographie, insbesondere die Simulated Moving Bed (SMB) Technologie, wurde als Trenn- und Aufreinigungsprozess in den oben genannten Industriezweigen immer bedeutender. Dies ist auf die hohe Flexibilität und Effizienz sowie den hohen Reinheitsgrad der Produkte, der mit dieser Technologie erreicht werden kann, zurückzuführen. Heutzutage wird die SMB Technologie in diesen Industriezweigen bevorzugt für schwierige Trennaufgaben angewandt wie zum Beispiel die Trennung von Enantiomeren. Sie ist auch interessant für komplexe Trennaufgaben wie der Trennung von Bio-Molekülen oder von Naturstoffen, die aus mehreren schwer charakterisierbaren Komponenten bestehen. Daher gibt es zur Zeit eine grosse Zahl von möglichen Anwendungen der SMB Technologie im kleinen Massstab, die ein neues SMB Schema fordern, das die Flexibilität und Vielseitigkeit dieser Technologie ausnutzt. Für die sachgerechte Eingliederung von SMBs in die Produktion ist es wichtig, dass robusten Regelungsprozesse angewendet werden können. Dieser Aspekt der Prozesssteuerung muss angegangen werden. SMBs bestehen aus mehreren chromatographischen Kolonnen mit Zu- und Abläufen, deren Position im Kolonnen-Karusell periodisch weitergeschaltet wird. Daher erreichen SMBs nur einen zyklischen Stationärzustand, bei dem die Gemischzusammensetzungen sich periodisch ändern und haben eine nicht-lineare Dynamik mit Totzeiten und benötigen eine langwierige Analysetechnik für die Qualitätskontrolle der Produkte. Diese Eigenschaften stellen eine Herausforderung sowohl für die SMB Prozesstechnik als auch für die Regelung dar.

Das Ziel dieser Arbeit ist die Bandbreite der Anwendungsgebiete für SMB Technologie zu erweitern. Dabei sollen nicht nur chirale Trennungen, sondern auch Mehrkomponententrennungen in mehrere Fraktionen berücksichtigt werden, wie z.B. die Trennung von Bio-Produkten. In diesem Zusammenhang wurden zwei neue SMB Schemata realisiert: das SMB mit Lösungsmittelgradient (SG-SMB) und die SMB Trennung in drei Fraktionen (3F-SMB). Darüber hinaus wurde die Möglichkeit der Kombinierung von SMB und Kristallisation betrachtet. Um ein Werkzeug für die sachgerechte Implementierung von

SMBs in Produktionsabläufe zur Verfügung stellen zu können, wurde ein optimierendes Regelungsschema für SMBs entwickelt und getestet. Diese technischen Neuerungen die in dieser Arbeit untersucht wurden, werden im Folgenden kurz beschrieben:

- Bei einem SMB mit Lösungsmittelgradient (SG-SMB) besteht die mobile Phase aus einer Mischung von zwei oder mehr Lösungsmitteln. Das SG-SMB strebt eine Verbesserung der Trennleistung an, indem ein Gradient in der Lösungsmittelzusammensetzung, im Gegensatz zu dem ursprünglichen isokratischen SMB Konzept, angewendet wird. Verschiedenen Zusammensetzungen der mobilen Phase entsprechen unterschiedliche Rückhaltezeiten für die adsorbierten Stoffe, was durch unterschiedliche Adsorptionsisothermen charakterisiert werden kann. In dieser Arbeit wird eine SMB Anlage untersucht, bei der Lösungsmittelmischungen mit zwei verschiedenen Zusammensetzungen jeweils am Feed- und am Lösungsmittelzulauf zugegeben werden. Dadurch stellen sich zwei verschiedene Zusammensetzungen der mobilen Phase jeweils in den ersten und den letzten beiden Abschnitten der Anlage ein. Um diesen Prozess zu optimieren wurden die Kriterien für die Auslegung von SMBs mit linearen und nicht-linearen Isothermen gemäss der Gleichgewichtstheorie für diesen Prozess-Modus erweitert. Es wird gezeigt wie der Bereich vollständiger Trennung hergeleitet werden kann und wie die optimalen Betriebsparameter gefunden werden können. Schlussendlich wird der SG-SMB Modus mit dem isokratischen Modus bezüglich Produktivität und Lösungsmittelverbrauch verglichen und Versuchsergebnisse werden gezeigt.

- Eine SMB Anlage in kleinem Massstab wurde als eine Modifizierung einer kommerziellen ÄKTATMexplorer Anlage entwickelt und für die Trennung von verschiedenen Mischungen von Nukleosiden verwendet. Sowohl eine Trennung in zwei Fraktionen wie auch in drei Fraktionen wurde durchgeführt. Letztere wurde durch die Anwendung einer neuen SMB Konfiguration bzw. Betriebs-Modus (3F-SMB) ermöglicht. Experimente demonstrieren die Durchführbarkeit der 3F-SMB Trennung und bestätigen die prognostizierten Tendenzen die aus dem Adsorptionsverhalten der aufzutrennenden Komponenten hergeleitet wurden.

- Die Kombination von SMB und Kristallisation wird anhand einer Fallstudie für die Trennung der Enantiomere der Trögerschen Base untersucht. Es ist bekannt, dass die Produktivität einer SMB-Trennung mit steigender Reinheitsanforderung absinkt. Das Ziel des kombinierten Prozesses ist es die Gesamtproduktivität zu erhöhen, und zwar durch die Anreicherung der beiden Fraktionen durch SMB bis zu einer bestimmten Reinheit,

welche niedriger ist als gefordert, und anschliessender Aufreinigung durch den billigeren Kristallisationsprozess. [1]. In dieser Fallstudie konnte festgestellt werden, dass für das gewählte System tatsächlich eine Verbesserung erzielt werden kann, welche stark von der gewählten Reinheitsgrad im SMB Schritt abhängt [2, 3].

- Es wird eine neue optimierende adaptive Regelungsstrategie für SMBs vorgeschlagen: ein linearisiertes Prozess-Modell mit reduzierter Ordnung, das die periodische Natur des Prozesses widerspiegelt, wird für die Optimierung und Regelung verwendet. Die Stellgrössen sind dabei die vier internen Durchflussraten, welche über die externen Flussraten kontrolliert werden können. Der Prozess-Output besteht aus den Raffinat- und Extrakt-Konzentrationen, woraus die Ausbeute und die Reinheit der Produkte direkt bestimmt werden kann. Die Konzentrationsmessungen von Extrakt und Raffinat werden zusammen mit einem Kalman Filter als Feedback Information verwendet um Ungenauigkeiten des Prozess-Modells auszugleichen und um Prozess-Störungen zu bewältigen. Die Einschätzung des Anlagenstandes, die der Kalman Filter berechnet, wird für eine mehrstufige Vorhersage der Produktkonzentrationen verwendet. Diese dienen als Basis für die Berechnung der optimalen Anpassungen der Input-Parameter bzw. der internen Durchflussraten, die die Produktivität maximieren und den Lösungsmittelverbrauch minimieren, abhängig von einer festgelegten Mindestreinheit der Produkte. Die Realisierung dieses Konzepts wird diskutiert und die Implementierung mit einem simulierten 8-Säulen-SMB wird bewertet. Es wird gezeigt, wie die optimierende Regelungsstrategie es ermöglicht die SMB Anlage bei optimalen ökonomischen Bedingungen zu betreiben und wie sie mögliche Prozess-Störungen und Ungenauigkeiten des Prozess-Modells bewältigt.

Dieser Teil der Arbeit ist das Ergebnis einer Zusammenarbeit mit einem weiteren Doktorand, Gültekin Erdem (Prof. M. Morari), in einem Gemeinschaftsprojekt dreier ETH Institute: Prof. M. Mazzotti (Institut für Verfahrenstechnik), Prof. M. Morbidelli (Institut für Chemie- und Bio-Ingenieurwissenschaften) und Prof. M. Morari (Institut für Automatik).

Abstract

The evolution of food, agrochemical, pharmaceutical and biotechnology industries is clearly moving towards purer products and cleaner processes, due to stricter regulations and growing environmental concerns. This trend calls for better technologies, particularly separation process technologies, which are better controlled once implemented. Preparative chromatography, particularly using SMBs, has been increasing its importance as a separation and purification process in the above mentioned industries, since it is flexible, energy efficient and achieves high purity performance. Nowadays, the SMB technology is adopted in these industries for difficult applications, such as the resolution of enantiomers, and it is considered attractive for complex separation tasks, such as bio-separations or separation of natural compounds involving a number of difficult-to-characterize compounds. Therefore, there are now a large number of potential small-scale applications of the SMB technology that call for a new SMB paradigm, which exploits the flexibility and versatility of the technology. Proper implementation of SMBs in production will require the application of robust control techniques. The issue of process control under uncertainties has to be addressed. SMBs are constituted of several chromatographic columns with inlets and outlets, whose position within the column carousel switches periodically. Therefore SMBs reach only a cyclic steady state, where compositions change periodically and exhibit nonlinear dynamics with dead-times and lengthy analytic techniques for product quality assessment. These features pose fundamental questions and challenges on both SMB technology and control theory.

The aim of this work is to broaden the range of SMB applications and include not only chiral separations but also multi-component multi-fraction separations, e.g. bio-separations. In this context two new SMB paradigms have been realized, i.e. the solvent gradient SMB (SG-SMB) and the three fraction SMB (3F-SMB). Furthermore, the possibility of combining SMB and crystallization is considered and in order to provide a tool to implement the SMB process properly in production, an optimizing control scheme for SMBs has been developed and tested. These technical innovations investigated in this work are described briefly below:

- In the solvent gradient mode (SG-SMB) the mobile phase consists of a mixture of two or more solvents. The SG-SMB aims at further improving separation performance by applying a gradient in solvent composition in contrast to the original isocratic SMB concept. To different mobile phase compositions corresponds a different retention behavior of the solutes, i.e. different adsorption isotherms. In this work a SMB unit is studied with solvent mixtures of two different compositions entering the unit at the feed and desorbent inlet ports, respectively. Thereby two different mobile phase compositions are established in sections 1 and 2, and sections 3 and 4, respectively. To optimize this process the equilibrium theory design criteria for SMB separations with linear and nonlinear isotherms are extended to describe this operation mode. It is shown how the region of separation is derived and how the optimal operating conditions can be found. Finally the solvent gradient mode is compared with the isocratic mode in terms of productivity and solvent consumption and experimental results are shown.
- A desktop SMB unit developed as a modification of the commercial ÄKTA™-explorer working platform has been utilized for the separation of different mixtures

of nucleosides. Both two fraction and three fraction SMB separations have been carried out, the latter made possible by the adoption of a new SMB configuration and operating mode (three fraction SMB, 3F-SMB, operation). Experiments demonstrate the feasibility of the 3F-SMB operation, and confirm the trends predicted based on considerations about retention of the components to be separated along the unit.

- The combination of SMB and crystallization is investigated in a case study for the separation of the enantiomers of Troger's base. It is well known that the productivity of an SMB separation decreases with increasing purity constraint. The goal of the combined process is to increase the overall productivity by enriching the two fractions by SMB up to a certain purity, which is lower than the target purity, and complete the purification by a crystallization step, which is usually cheaper than SMB [1]. It was found that an improvement for the chosen system is indeed possible, and it strongly depends on the chosen purity limit for the SMB process [2, 3].

- A new optimization based adaptive control strategy for the SMB is proposed: A linearized reduced order model, which accounts for the periodic nature of the SMB process is used for the optimization and control purposes. The manipulated variables are the four internal flow rates, which can be controlled via external flows. The outputs of the process include the raffinate and extract concentrations, from which the product yield and purities can be determined directly. Concentration measurements at the raffinate and extract outlets are used as the feedback information together with a Kalman filter to remove model errors and to handle disturbances. The state estimate from the Kalman filter is then used for the multi-step prediction of the outlet concentrations. These serve as the basis for the calculation of the optimal input adjustments, which maximize the productivity and minimize the desorbent consumption subject to constraints on product purities. The realization of this concept is discussed and the implementation on a virtual eight column SMB platform is assessed. It is shown how the optimizing control strategy enables to run the SMB plant at its economical optimal conditions and how it handles possible disturbances and model uncertainties.

This part of the work is the outcome of a collaboration with another Ph.D. student, Gültekin Erdem (Prof. M. Morari), in a joined project involving three institutes at ETH, i.e. Prof. M. Mazzotti (Institute of Process Engineering), Prof. M. Morbidelli (Institute for Chemical and Bio-Engineering) and Prof. M. Morari (Automatic Control Laboratory).

Table of Contents

1	Introduction	1
1.1	Simulated Moving Bed technology	2
1.2	Separation design	4
1.3	Modeling of SMB processes	7
2	Solvent Gradient SMB (SG-SMB) for linear isotherms	9
2.1	Introduction	9
2.2	Retention Behavior in Mixed Solvents	10
2.3	Solvent Gradient Simulated Moving Bed (SG-SMB)	12
2.4	Operating Conditions for Complete Separation	14
2.5	The Region of Complete Separation	15
2.5.1	Complete separation region for a fixed pair (x_2, x_3)	15
2.5.2	Complete separation region for a fixed value of x_2	16
2.5.3	Complete separation region	20
2.5.4	Effect of retention model parameters	21
2.5.5	Effect of mobile phase composition	22
2.6	SG-SMB Design and Operation	24
2.6.1	Choosing an operating point	25
2.6.2	Tuning the separation performance	27
2.7	Discussion and Conclusions	28
3	Solvent Gradient SMB (SG-SMB) for Langmuir isotherms	34
3.1	Introduction	34
3.2	Solubilities and adsorption isotherms	34
3.2.1	Solubility	35
3.2.2	Nonlinear competitive adsorption isotherms	36

3.3	Operating conditions for complete separation in nonlinear SG-SMBs	37
3.3.1	The 'open loop'-configuration	37
3.3.2	The 'closed loop'-configuration	40
3.4	Discussion and conclusion	41
4	Experimental implementation of the SG-SMB concept	47
4.1	Experimental setup	47
4.2	SG-SMB separation of α -ionone enantiomers	47
5	Three fraction SMB	52
5.1	Design criteria for linear adsorption isotherms	54
5.2	Performance analysis	57
6	SMB separation of nucleosides into two fractions and three fractions	64
6.1	Introduction	64
6.2	Chromatography of nucleosides	64
6.3	Two fraction SMB separation	66
6.3.1	Experimental setup	66
6.3.2	2-1-2-1 configuration	69
6.3.3	2-2-2-0 configuration	71
6.4	Three fraction SMB separation	72
6.4.1	Experimental setup	72
6.4.2	Results	74
6.5	Concluding remarks	77
7	Optimizing Control of SMBs	79
7.1	Introduction	79
7.2	SMB model	81
7.3	SMB Control	82

7.3.1	Simplified SMB model	84
7.3.2	State estimation	89
7.3.3	Optimization	89
7.4	Simulation results for a linear adsorption isotherm	92
7.4.1	Base Case	92
7.4.2	Model/plant mismatch: adsorption isotherms	94
7.4.3	Model/plant mismatch: column packing	97
7.4.4	Step disturbance	98
7.4.5	Ramp disturbance	98
7.5	Conclusions	101
8	Experimental implementation of SMB control	103
8.1	System characterisation: SMB separation of nucleosides	103
8.2	Online monitoring	109
8.2.1	Sensor setup	109
8.2.2	Measurement results	112
8.2.3	Comparison of online monitoring results and simulation	115
8.3	SMB control	117
9	Conclusions and Outlook	120

1 Introduction

The Simulated Moving Bed (SMB) is a continuous chromatographic multi-column separation process, which is well established for the adsorption based separation of hydrocarbons as well as fine chemicals. This technology is widely used particularly for the separation of enantiomers, which have identical physical properties, making it impossible to separate them by any of the classical separation processes [4, 5, 6, 7]. The SMB technology covers a broad range of production scales from the laboratory units, which use chromatographic columns with a 0.46 cm internal diameter, to the multi-ton production units licensed by Novasep for chiral separations with column diameters between 20 and 100 cm, to the largest SMB unit licensed recently in South Korea by the Institute Française du Pétrole with a column diameter of 8 m for the production of 700'000 tons per year of p-xylene. New applications are envisaged in the near future, particularly in the emerging area of bio-separations, e.g. for the purification of enzymes, peptides, antibiotics, monoclonal antibodies and natural extracts [8]. These days advances in the field of biotechnology are fast. An increasing number of active agents can be synthesized, which makes it necessary for the pharmaceutical industry to reduce the time to market more and more and to significantly speed up the synthesis of samples and trial phases of drugs. In the era of the human genome project more and more often the word 'pharmacogenomics' is heard, which comes from the words pharmacology and genomics. It holds the promise that by understanding an individual's genetic makeup it might one day be possible to even produce personalized drugs with greater efficiency and safety. This enormous scientific progress is also a challenge for engineers to provide appropriate, efficient and flexible processes that are also applicable on larger scales.

SMB technology is often adopted for difficult applications, such as the resolution of racemates, and it is considered attractive for complex separation tasks, such as bio-separations or separations of natural compounds involving a number of difficult-to-characterize components. Therefore it can be stated that a large number of potential small-scale applications of the SMB technology exists. The main advantages of SMB technology are on the one hand the highly efficient continuous operating mode with a higher productivity and lower solvent consumption than in batch column chromatography [6], and on the other hand the adaptiveness of the process, which can substantially save time, e.g. by making the development of an enantioselective chemical synthesis unnecessary. Chromatography in general is a very flexible and mild separation technique, well suited especially for sensitive

products. Moreover, SMB can be easily scaled up [6, 9].

The scope of this work is to develop new SMB paradigms, which exploit the flexibility and versatility of the technology and thus provide the above mentioned industries with improved state of the art processes. Furthermore, proper implementation of SMBs in production will require the application of robust control techniques. On the one hand the issue of process control under uncertainties is addressed. On the other hand the control scheme is designed to optimize the separation online in terms of productivity and solvent consumption. This will allow economic operation and achieving product specifications while coping with process disturbances and long-term modifications of system characteristics, e.g. aging of the stationary phase and of the column packing.

1.1 Simulated Moving Bed technology

The Moving Bed technology is based on a continuous chromatographic countercurrent separation process. The principle of operation can be best described with reference to the true countercurrent process, the True Moving Bed (TMB), which is schematically drawn in Figure 1.1.

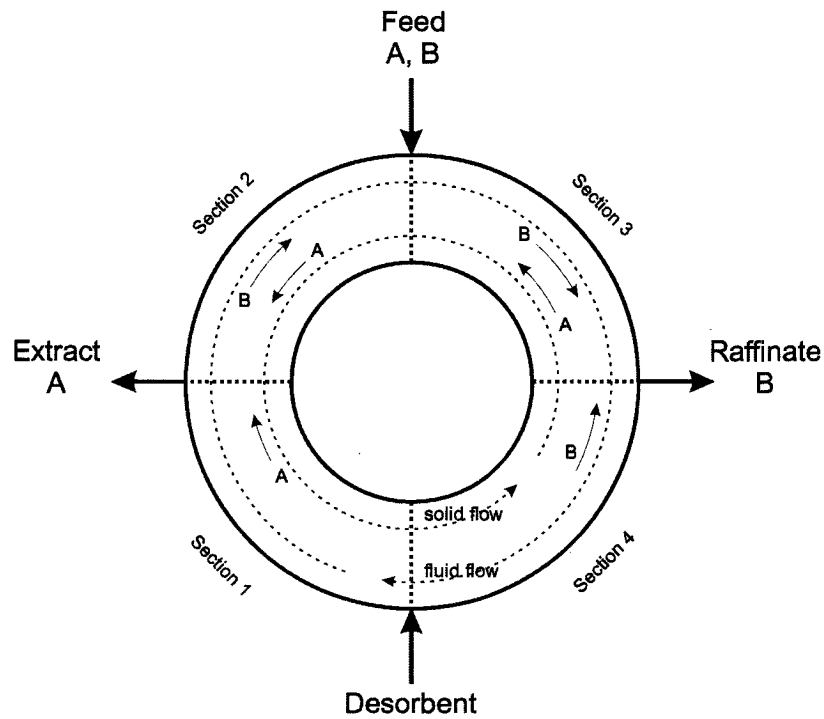


Figure 1.1: Scheme of the conceptual True Moving Bed (TMB) process.

The conventional Moving Bed process realizes the separation of a feed mixture into two fractions by exploiting a countercurrent contact of the solid and the fluid phase [4, 10]. The separation principle is the different adsorption affinity of the components on the solid phase. The unit is divided into 4 sections by the inlet and outlet streams, where the feed enters between sections 2 and 3. The products are withdrawn in the extract stream between sections 1 and 2 and in the raffinate stream between sections 3 and 4, whereas the direction of the fluid flow is defined going from section 1 to 4. Sections 1 and 4 regenerate the solid phase and the solvent, respectively, which is necessary for their continuous recycle. With reference to the TMB in Figure 1.1 and a binary system under complete separation conditions, the ratio between fluid and solid flow rates in the four sections has to be chosen so that the more retained adsorbate A is carried by the solid phase to the extract outlet, while the less retained adsorbate B is conveyed by the fluid phase to the raffinate port.

The True Moving Bed (TMB) process described above is a conceptual process, since the significant technical problems due to the solid phase movement cannot be solved in practice. The SMB technology overcomes these problems: instead of physically moving the solid phase, fixed-bed columns are used, whereas one or more columns form a section ($V_j = S_j V$, where V_j and V are the volume of the j th section and of a fixed-bed column of the SMB unit, respectively; S_j is the number of subsections, i.e. columns, in the j th section of the SMB unit).

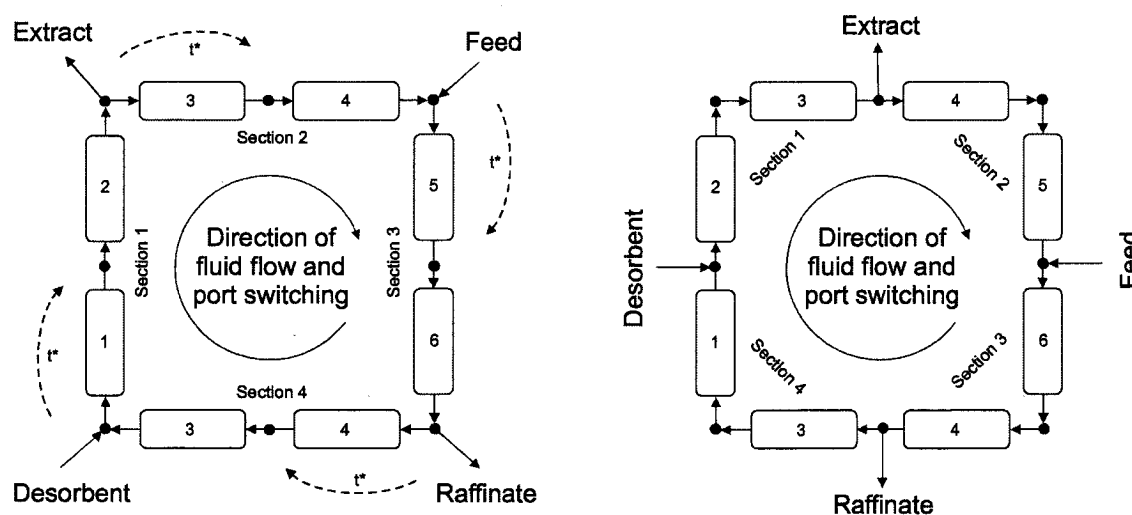


Figure 1.2: Scheme of an 8-column closed loop Simulated Moving Bed unit. Column configuration 2-2-2-2.

The solid flow is practically simulated by switching all the inlet and outlet ports periodically by one column position in the direction of the fluid flow, as illustrated in Fig. 1.2. This simulates a solid flow equivalent to $Q_s = V(1 - \varepsilon^*)/t^*$, where t^* is the time period between two successive switches of the inlet and outlet ports and $\varepsilon^* = \varepsilon + (1 - \varepsilon)\varepsilon_P$ is the overall void fraction of a column with ε being the bed void fraction and ε_P the porosity of the solid phase particles. To calculate the net fluid flow rate in an SMB, $Q_j^{net} = Q_j - V\varepsilon^*/t^*$, the fluid amount that is trapped in a column and is moved at each port switch backwards in the direction of the solid flow, has to be averaged over the time t^* and subtracted from the fluid flow rate Q_j . In case extra column dead volume is considered, the amount of fluid trapped in it has to be subtracted as well. Using these quantities one can define the flow rate ratio m_j for each section of the unit. The equation of m_j , Equ. (1.1), and the importance as key parameters for process design can also be derived directly from the constraints obtained from Equilibrium Theory, as shown in [11].

$$m_j = \frac{\text{net fluid flow rate}}{\text{solid flow rate}} = \frac{Q_j t^* - V\varepsilon^* - V_j^D}{V(1 - \varepsilon^*)}, \quad j = 1, \dots, 4. \quad (1.1)$$

SMB and TMB units are considered to be equivalent and to achieve in principle the same separation performance provided the geometric and kinematic equivalence relationships are fulfilled [4, 10, 12]:

$$\frac{V}{t^*} = \frac{Q_s^{TMB}}{1 - \varepsilon^*} \quad (1.2)$$

$$Q_j^{SMB} = \left[Q_j^{TMB} + \frac{Q_s \varepsilon^*}{1 - \varepsilon^*} \right], \quad (1.3)$$

The SMB can be operated in a closed loop configuration, as shown in Fig. 1.2, where the regenerated solvent coming from section 4 is directly recycled to section 1, or in an open loop configuration, where the fluid coming from section 4 is withdrawn and recycled indirectly.

1.2 Separation design

In order to design the operating conditions of an SMB, it is necessary to know the adsorption behavior of the system under consideration. For sufficiently low feed concentrations a linear adsorption isotherm can be assumed:

$$q_i = H_i c_i, \quad (1.4)$$

where q_i is the amount adsorbed on the solid phase, H_i the Henry's constant, c_i the concentration in the liquid phase, and i is the component index. For this simple case of a linear isotherm the necessary and sufficient conditions for complete separation of two components B and C with $H_B > H_C$ consist of the following inequalities (see [10] for details):

$$H_B < m_1 \quad (1.5)$$

$$H_C < m_2 < m_3 < H_B \quad (1.6)$$

$$\frac{-\varepsilon_P}{1 - \varepsilon_P} < m_4 < H_C \quad (1.7)$$

These conditions define a region in the four-dimensional operating parameter space yielding complete separation of B and C in the frame of the ideal equilibrium model based on a TMB, whereas the equivalence between SMB and TMB is exploited. Usually only the triangular projection of this region onto the (m_2, m_3) plane is used for graphical representation (see Fig. 1.3a), but it has to be kept in mind that this applies only provided also the constraints on m_1 and m_4 are fulfilled and the operating point in terms of m_1 and m_4 is chosen in the region of complete regeneration shown in Fig. 1.3b.

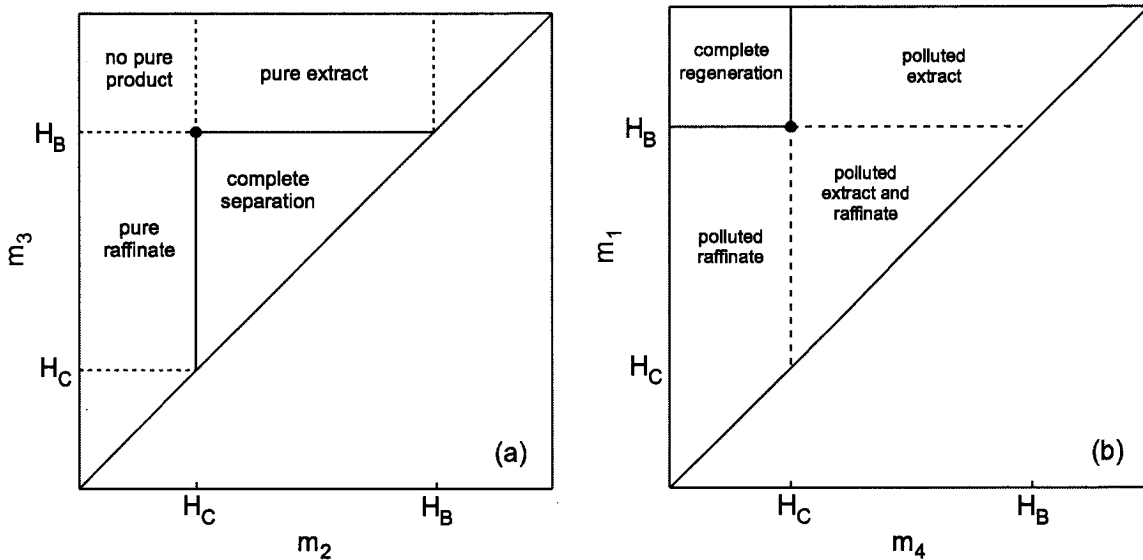


Figure 1.3: Linear adsorption isotherm: (a) region of complete separation in the (m_2, m_3) operating parameter space; (b) region of complete regeneration in the (m_4, m_1) operating parameter space.

In contrast to the linear adsorption behavior, in case of non-linear adsorption isotherms the region of complete separation depends on the concentration of the components in the

feed. Among others, a very common and well investigated isotherm type is the Langmuir isotherm, which has been adopted frequently in this work. This adsorption theory is based on the assumption of a maximum number of sites for monolayer adsorption on the solid phase for which the components in the fluid phase compete. For a binary mixture the competitive Langmuir isotherm for component i writes as follows:

$$q_i^* = \frac{\Gamma_i k_i c_i}{1 + k_B c_B + k_C c_C} \quad (i = B, C) \quad (1.8)$$

where k_i and Γ_i are the equilibrium constant and the saturation loading capacity of the i -th component, respectively.

The boundaries for the region of complete separation in the (m_2, m_3) plane can be derived from equilibrium theory, which is described in detail in [10]. The triangular region of complete separation shrinks with increasing feed concentration c_F and the vertex shifts towards lower m_2 and m_3 values, as shown by an example in Fig. 1.4. Eventually, the region becomes too narrow for robust operation.

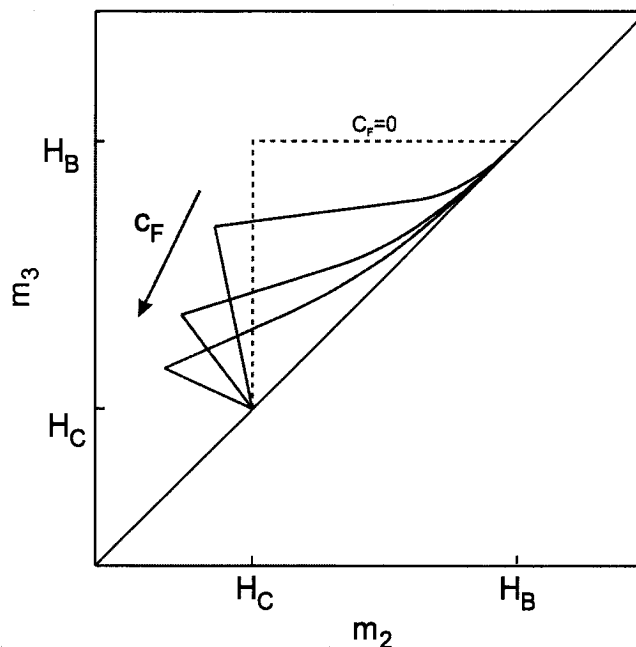


Figure 1.4: Region of complete separation in the (m_2, m_3) operating parameter space for a Langmuir isotherm with $k_B = 0.0321$ l/g, $k_C = 0.0175$ l/g, $\Gamma_B = 165$ g/l, $\Gamma_C = 220$ g/l, for different feed concentrations $c_{F,B} = c_{F,C} = 0, 2, 5, 8$ g/l.

In general, economic process operation is sought. The SMB performance can be assessed

using the following parameters [10]. The productivity PR , which can be defined as the amount of pure product recovered per unit time and amount of solid phase, should be maximised:

$$PR = \frac{\text{amount separated per time}}{\text{volume solid phase}} = \frac{Q_F c_F}{n_{col} V} = \frac{(m_3 - m_2)(1 - \varepsilon^*) c_F}{n_{col} t^*} \quad (1.9)$$

and the desorbent requirement DR , defined as the mass of desorbent required to recover a unit mass of product, should be minimized:

$$DR = \frac{\text{desorbent consumption}}{\text{amount separated}} = \frac{Q_D + Q_F c_D}{Q_F c_F} = \frac{1}{c_F} \left[\frac{m_1 - m_4}{m_3 - m_2} + c_D \right] \quad (1.10)$$

Equ. (1.9) shows that for constant t^* and c_F the productivity increases with the distance to the diagonal in the (m_2, m_3) plane. In case the difference $(m_1 - m_4)$ as well as c_F and c_D are constant, the desorbent requirement decreases with increasing distance from the diagonal, as seen from Equ. (1.10). Therefore the optimal operating point in terms of productivity and desorbent requirement would be the vertex of the triangular region of complete separation. In practice usually a safety margin for a more robust operation is applied and an operating point further inside the region of complete separation is chosen.

1.3 Modeling of SMB processes

Process simulation is a very important aspect in the field of SMB. The process design criteria are based on the TMB and derived from equilibrium theory assuming infinite column efficiency while mass transfer resistance and axial dispersion are neglected. This means that the design criteria can be used to assess the process and to find a reasonably good operating point, but they can never completely reflect the behavior of the real process.

SMB models of various complexity have been reported in the literature and a good summary can be found in [13]. SMB models are constituted of a column model, i.e. the material balance equations for a single chromatographic column, and node balance equations that connect the single column models one to the other to make the whole SMB. The simulations in this work have been carried out using a detailed one-dimensional column model, the lumped solid diffusion model. This model accounts for all the phenomena taking place in the column: accumulation in the fluid and solid phases, convection and axial dispersion in the fluid phase, and mass transfer assuming that solid diffusion is the rate limiting step [14]. The detailed column model consists of the following material balance

equations (symbols are defined in the Notation section):

$$\varepsilon^* \frac{\partial c_i}{\partial t} + (1 - \varepsilon^*) \frac{\partial q_i}{\partial t} + u \frac{\partial c_i}{\partial z} = \varepsilon D_{L,i} \frac{\partial^2 c_i}{\partial z^2} \quad (1.11)$$

$$\frac{\partial q_i}{\partial t} = a_p k_i (q_i^* - q_i) \quad (1.12)$$

$$q_i^* = f(c) \quad (1.13)$$

The system of PDEs is converted to a system of ODEs by a space discretization based on the method of finite differences. The system of ODEs is then integrated using the black box solver package 'lsoda' from Lawrence Livermore national laboratory, which solves the initial value problem for systems of first order ODEs with automatic method switching for stiff or non-stiff problems.

2 Solvent Gradient SMB (SG-SMB) for linear isotherms

2.1 Introduction

Recent developments in the field of SMB have highlighted the possibility of further improving the separation performance by applying non-standard operation modes. On the one hand, schemes where additional operational degrees of freedom are available have been proposed, such as the VARICOL[®] process where ports and columns are switched in an asynchronous manner [15, 16], or the POWERFEED process where the internal and external flowrates are varied during the time period between two successive port switches [17, 18, 19]. On the other hand, it has been proposed to optimize each SMB section separately, by tuning operating conditions such as temperature [20], pressure in supercritical applications [21, 22, 23], or the mobile phase composition, as it will be discussed in the following two chapters.

SMBs are usually operated in the liquid phase under isocratic conditions, i.e. at constant temperature, pressure, and mobile phase composition, thus letting the components to be separated adsorb according to the same adsorption isotherm in the four sections of the unit. However, the separation of enantiomers as well as bio-separations are often based on rather small selectivities, e.g. between 1.1 and 1.2. In these cases productivity can be boosted by operating the SMB unit in the gradient mode where the conditions in each section are chosen independently in order to reduce adsorptivity and retention times in sections 1 and 2, and to increase them in sections 3 and 4.

The benefits of such an approach have been demonstrated for an SMB where supercritical carbon dioxide is used as a solvent. In this case in fact, the operating pressure and density have a significant effect on retention, and by applying a pressure gradient (with the pressure decreasing from section 1 to section 4) productivity can be significantly improved with respect to the constant pressure operation. This has been demonstrated both experimentally [21, 23], and theoretically [24, 22], and represents a very promising concept with potential for concrete applications. Another possibility is that of operating sections 1 and 2 at a higher temperature than sections 3 and 4; the advantages and limitations of this approach have been recently investigated theoretically [20], but no temperature gradient SMB has been experimentally tested so far.

Gradient elution chromatography is widely used for analytical purposes, and exploits the effect of mobile phase composition on the retention behavior of solutes. How this

concept can be applied to the SMB technology and how SMBs can be operated in the solvent gradient mode is described in this chapter, whereas also other approaches can be found in recent contributions to the literature [25, 26, 27]. The typical solvent gradient implementation involves the use of two solvents with different properties, e.g. a more and a less polar one, and the tuning of their relative composition along the SMB unit.

The objective of this approach is to derive design criteria for binary SMB separations operated in the solvent gradient mode, where for the sake of simplicity the concentration of the solutes is low enough that their adsorption isotherms are linear (see Equ. 1.4). Allowing for solvent composition changes along the SMB unit increases the number of degrees of freedom, thus making the overall optimization of the separation a more complex problem. In addition to the adsorption equilibria, several other physical properties such as viscosity, density, and solubility depend on the mobile phase composition. These have an important impact on SMB operation and optimization, through their effect on pressure drop, column efficiency, and maximum allowable feed concentration of the species to be separated. As a consequence, optimizing solvent gradient SMBs requires a fairly large amount of physico-chemical data. However, knowing the complete separation region in terms of fluid flow rates and switch time as a function of the solvent composition profile in the SMB is a prerequisite to tackle and master the overall optimization problem. Therefore, it is the objective of this work to determine the complete separation region in the operating parameter space, and to clarify the features of solvent gradient operation, without actually attempting to identify optimal operating conditions, e.g. optimal solvent gradient profile and optimal operating point.

2.2 Retention Behavior in Mixed Solvents

It is well known in analytical chromatography that changing the mobile phase composition, e.g. either changing the ratio between a polar and an apolar solvent, or changing the pH of the solution, modifies significantly the retention behavior of the solutes. For example, the effect of increasing the water content in a water/methanol mixture on the Henry's constants of the enantiomers of α -ionone on a Nucleodex- β -PM, Macherey-Nagel, Düren, Germany, 30 \times 4 mm, stationary phase: heptakis-(2,3,6-per-O-methyl)- β -cyclodextrin bonded to silica gel; particle diameter: 5 μ m) is illustrated in Figure 2.1.

It is rather clear that changing the mobile phase composition modifies at the same time the affinity of the solutes for the fluid phase, i.e. their solubility, as well as their ad-

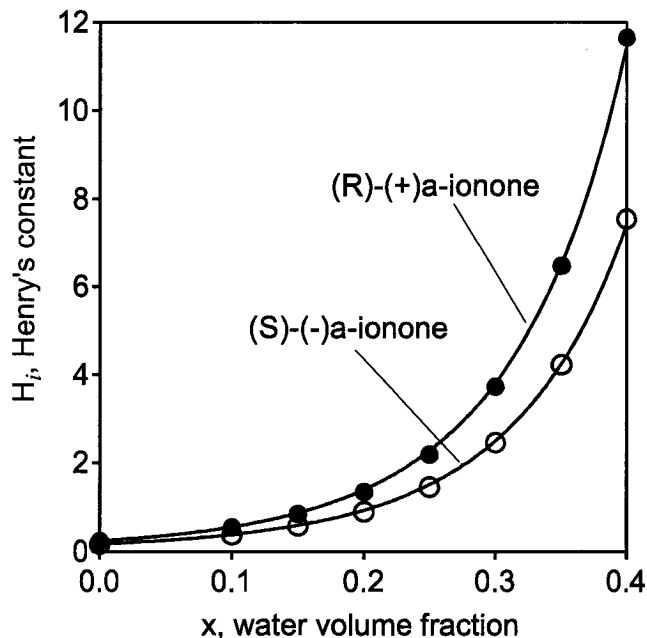


Figure 2.1: Enantiomers of α -ionone in methanol/water mobile phases. Henry's constants as a function of the water volume fraction, x . Symbols are the measured values at 20°C, whereas solid lines are calculated using Eq. (2.1) and the following dimensionless parameter values: $H_A^0 = 0.24$, $H_B^0 = 0.17$, $k_A = 0.75$, $k_B = 0.80$, $n_A = 10.85$, and $n_B = 9.80$.

sorptivity on the stationary phase. The latter effect may be due either to modifications of the distribution of the surface charges in the different fluid environments, or to true competitive adsorption of one or both solvents on the stationary phase itself. Most likely, both phenomena are present to a certain extent. However, in the following we will be content to describe data such as those in Figure 2.1, in an empiric way, namely using the following nonlinear interpolating function:

$$H_i = H_i(x) = \frac{H_i^0}{(1 - k_i x)^{n_i}} \quad (i = A, B), \quad (2.1)$$

where x represents the fraction (normally, a volume fraction) of the solvent (indicated in the following as solvent W), with elution strength smaller than the other (indicated in the following as solvent S); H_i^0 is the Henry's constant at $x = 0$, i.e. where only solvent S is used; k_i and n_i are positive parameters describing the effect of x on retention. Since selectivity is given by the ratio H_A/H_B , it is also a function of mobile phase composition unless $k_A = k_B$ and $n_A = n_B$. The data in Figure 2.1, where x represents the water volume fraction are well described using the parameter values (all dimensionless): $H_A^0 = 0.24$, $H_B^0 = 0.17$, $k_A = 0.75$, $k_B = 0.80$, $n_A = 10.85$, and $n_B = 9.80$. In this case selectivity is 1.41 in pure methanol, and increases to 1.54 in a solution with 40% volume of water.

2.3 Solvent Gradient Simulated Moving Bed (SG-SMB)

Let us refer to the closed-loop configuration shown in Figure 2.2, where the outlet stream from section 4 is recycled to section 1 after mixing with the desorbent stream. A composition profile for the mobile phase can be established in a simple way by feeding two different mobile phase compositions through the desorbent and feed ports. Let us indicate the volume fraction of the weak solvent W in the desorbent and in the feed with the symbols, x_D and x_F , respectively. Within the unit the mobile phase composition will be intermediate between the two inlet compositions. In particular, if $x_D < x_F$, i.e. the desorbent is richer than the feed in the solvent with the greater elution strength, then retention times will be smaller in sections 1 and 2 than in sections 3 and 4.

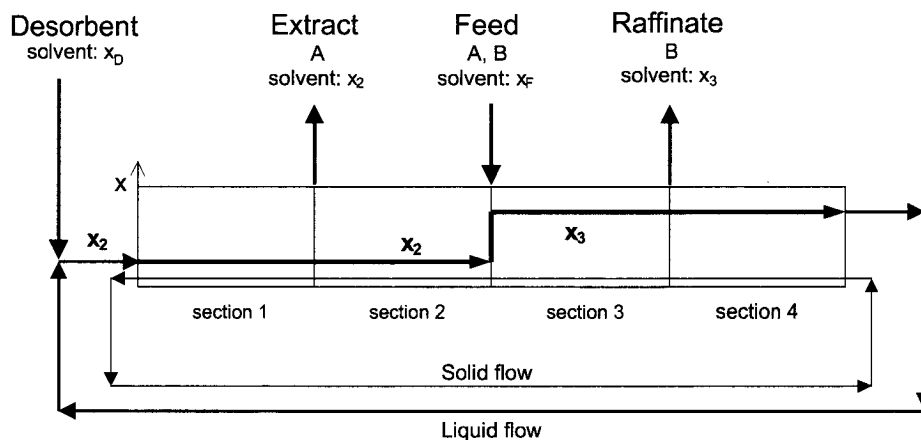


Figure 2.2: Mobile phase composition profile in a closed loop SG-TMB unit where the external mobile phase compositions are x_D and x_F , with $x_D \leq x_2 \leq x_3 \leq x_F$.

This situation is illustrated in Figure 2.2 for a TMB; the mobile phase composition profiles in each section are flat at steady state, in a TMB unit where axial dispersion is neglected. In the following we identify the solvent W fraction in sections 1 and 2 as x_2 , and that in sections 3 and 4 as x_3 . These values for given inlet compositions $x_D < x_F$ depend on the external and internal flow rates, and are calculated through the balances for solvent W at the desorbent and the feed nodes:

$$x_F Q_F + x_2 Q_2^{TMB} = x_3 Q_3^{TMB} \quad (2.2)$$

$$x_3 Q_4^{TMB} + x_D Q_D = x_2 Q_1^{TMB}, \quad (2.3)$$

where Q represents volume flow rates, and for the sake of simplicity volume changes upon mixing have been neglected. The inequalities $x_D \leq x_2 \leq x_3 \leq x_F$ follow from these

equations.

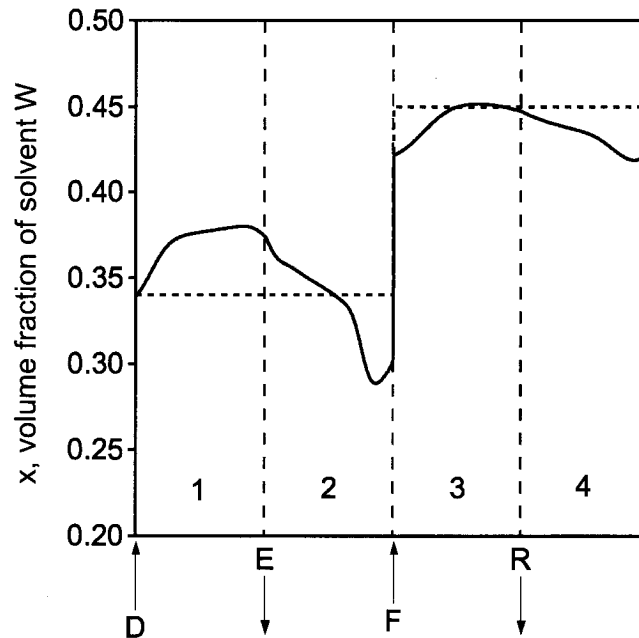


Figure 2.3: Comparison between the mobile phase composition profile in a SG-TMB (broken line) and in the equivalent SG-SMB with a 2-2-2-2 configuration (solid line). In the latter case, the profile is calculated for cyclic steady state conditions, and plotted at the end of the period between two port switches, just before the next port switch.

In a SG-SMB the composition profile is less regular, due to the non-steady state nature of its behavior, and the profile drawn in Figure 2.2 represents only an idealization of the real profile. The latter depends on the operating conditions; it can be pretty close to the TMB one, but also rather different. An example of such a profile is illustrated in Figure 2.3; this has been calculated using a standard lumped solid diffusion model of the SG-SMB [14]. The operating conditions reported in the caption of the figure were designed to attain $x_2 = 0.34$ and $x_3 = 0.45$; the profile corresponds to a point in time at the end of a time period between two port switches, immediately before the switch. It is worth noting that the desired x_2 and x_3 values are shown by the horizontal broken lines in the figure, and that these correspond to the space and time average of the actual concentration profiles attained in sections 1 and 2, and 3 and 4, respectively. The difference between the profiles in Figures 2.2 and 2.3 stems from the intrinsic difference between the countercurrent TMB process and the simulated countercurrent SMB process.

It is worth noting that the analysis that follows applies also to the case of an SMB operated in an open-loop configuration, i.e. without direct recycle of the stream coming

out of section 4. Since the stream entering section 1 is just the desorbent stream, then in this case $x_2 = x_D$, and Eq. (2.3) does not apply.

The above discussion clarifies similarities and differences between TMB and SMB behavior in the solvent gradient operation mode. Despite these differences, it is convenient to use the TMB model to identify feasible operating regions in the operating parameter space at least as a first approximation, and then to translate these into flow rates and switch time of the equivalent SMB unit. A direct analysis of the SMB unit with the usual detailed models can be performed afterwards as a refinement step. This approach will be followed in our analysis. SMB and TMB units are considered to be equivalent and to achieve in principle the same separation performance provided geometric and kinematic conversion rules are fulfilled [4, 12].

2.4 Operating Conditions for Complete Separation

With reference to the SG-TMB unit in Figure 2.2, the following conditions on the flow rate ratios are necessary and sufficient to achieve complete separation in the case where adsorption isotherms are linear, i.e. $q_i = H_i(x)c_i$ [4, 12]:

$$H_A(x_2) < m_1 \quad (2.4)$$

$$H_B(x_2) < m_2 < H_A(x_2) \quad (2.5)$$

$$H_B(x_3) < m_3 < H_A(x_3) \quad (2.6)$$

$$m_4 < H_B(x_3) . \quad (2.7)$$

Since Henry's constants depend upon the mobile phase composition through the parameter x , the lower and upper bounds of the m_j values to be adopted depend on the mobile phase composition as well. The parameters x_2 and x_3 can be calculated through the solvent balances (2.2) and (2.3), which can be recast in terms of flow rate ratios and accounting for overall material balances at the feed and the desorbent nodes as follows:

$$m_3(x_F - x_3) = m_2(x_F - x_2) \quad (2.8)$$

$$m_1(x_2 - x_D) = m_4(x_3 - x_D) . \quad (2.9)$$

Note that these two equations apply also in the case of porous particles, i.e. $\varepsilon_p > 0$, since the solvents are considered non-adsorbable.

Solving Eqs (2.8) and (2.9) for x_2 and x_3 in terms of x_D , x_F , and the flow rate ratios, and substituting the resulting expressions in Eqs (2.4) to (2.7) yields a set of inequalities in the four unknowns m_j ($j = 1, \dots, 4$). This is a nonlinear system due to the nonlinear dependence of H_i on x through Eq. (2.1), which defines a region in the four dimensional space spanned by the four flow rate ratios. In the frame of equilibrium theory the points belonging to this region allow achieving complete separation of species A and B, i.e. pure A in the extract and pure B in the raffinate. The boundaries of this region depends only on the external mobile phase compositions x_D and x_F , and on the retention behavior of the solutes, which is described by Eq. (2.1).

In order to apply this result to the design of the separation in the gradient mode, it is worth developing a geometrical representation of the complete separation region [10]. This can be done rather effectively following a step by step approach, which can be easily extended also to the case of nonlinear isotherms, and is presented in the next section.

2.5 The Region of Complete Separation

In this section we consider the separation problem for fixed mobile phase composition in the desorbent, x_D , and in the feed, x_F . The objective is to define operating conditions in terms of flow rate ratios m_j , i.e. in terms of fluid and solid flow rates in the TMB unit (and in terms of fluid flow rates and switch time for the corresponding SMB unit) that lead to complete separation. The procedure to determine the complete separation region is outlined in various steps in the following. With illustrative purposes, as a model system a mixture of two components A and B is considered; the relative composition of the two species need not be specified since adsorption follows the linear isotherm (1.4). The corresponding parameters in Eq. (2.1) are $H_A^0 = 2.12$, $H_B^0 = 1.41$, $k_A = k_B = 0.95$, and $n_A = n_B = 1$. The complete separation region will be calculated for $x_D = 0$ and $x_F = 0.9$.

2.5.1 Complete separation region for a fixed pair (x_2, x_3)

When the values of x_2 and x_3 are fixed, the upper and lower bounds in Eqs (2.4) to (2.7) are known and independent from the flow rate ratios. The projection of the corresponding complete separation region onto the (m_2, m_3) plane is a rectangle, of which only the portion above the diagonal, i.e. where $m_3 > m_2$, allows having a positive feed flow rate. The case where $x_2 = 0.2$ and $x_3 = 0.6$ is illustrated in Figure 2.4; we will call this *the*

complete separation region for the given (x_2, x_3) pair. It is worth considering all the regions drawn in the figure beside the complete separation rectangle 1. In region 2 the raffinate is polluted with component A, in region 3 the extract is polluted with component B, and in region 4 both extract and raffinate contain both A and B. In regions 5 and 6 both A and B exit the unit entirely in the raffinate or entirely in the extract, respectively. Regions 7, 8, and 9 are not feasible since in the frame of a linear adsorption analysis either component A (in region 7), or component B (in region 8), or both (in region 9), cannot leave the unit and therefore accumulate indefinitely. In reality, their hold-up is upper bounded by the achievement of saturation conditions either in the fluid or in the adsorbed phase. In this case the linear description is no more valid, and must be replaced by a nonlinear analysis.

However, in the SG-TMB the four m_j values must fulfill also the solvent balances Eqs (2.8) and (2.9); this reduces the number of degrees of freedom from four to two only. In particular, the operating point in the (m_2, m_3) plane must belong to the operating line defined by Eq. (2.8). With reference to Figure 2.4, only the points belonging to the segment along the operating line (2.8) that intersects the rectangle are compatible with the mobile phase compositions x_2 and x_3 , and allow achieving complete separation.

At the same time the flow rate ratios m_1 and m_4 must be one proportional to the other according to Eq. (2.9) and fulfill inequalities (2.4) and (2.7). The following inequality, which is derived by combining the three equations just mentioned, guarantees that there exists a finite range of feasible values of m_4 (and hence of m_1):

$$(x_3 - x_D)H_B(x_3) \geq (x_2 - x_D)H_A(x_2) . \quad (2.10)$$

This is actually a constraint on the pair (x_2, x_3) ; only combinations of mobile phase composition levels that fulfill the last inequality allow for the achievement of regeneration of the solid phase in section 1 and of the mobile phase in section 4. Eq. (2.10) implies that x_3 must be strictly larger than x_2 ; how much larger depends on the specific functional form of $H_A(x)$ and $H_B(x)$. It is worth noting however, that if the unit is operated in the open-loop configuration, then Eqs (2.9) and (2.10) do not apply. In this case, x_3 can be equal to x_2 , which according to Eq. (2.8) occurs only on the diagonal of the (m_2, m_3) plane where $Q_F = 0$.

2.5.2 Complete separation region for a fixed value of x_2

Let us now vary x_3 , while keeping x_2 constant. The effect of increasing x_3 when $x_2 = 0.2$ is illustrated in Figure 2.5; four different intersecting segments corresponding to $x_3 = 0.4$,

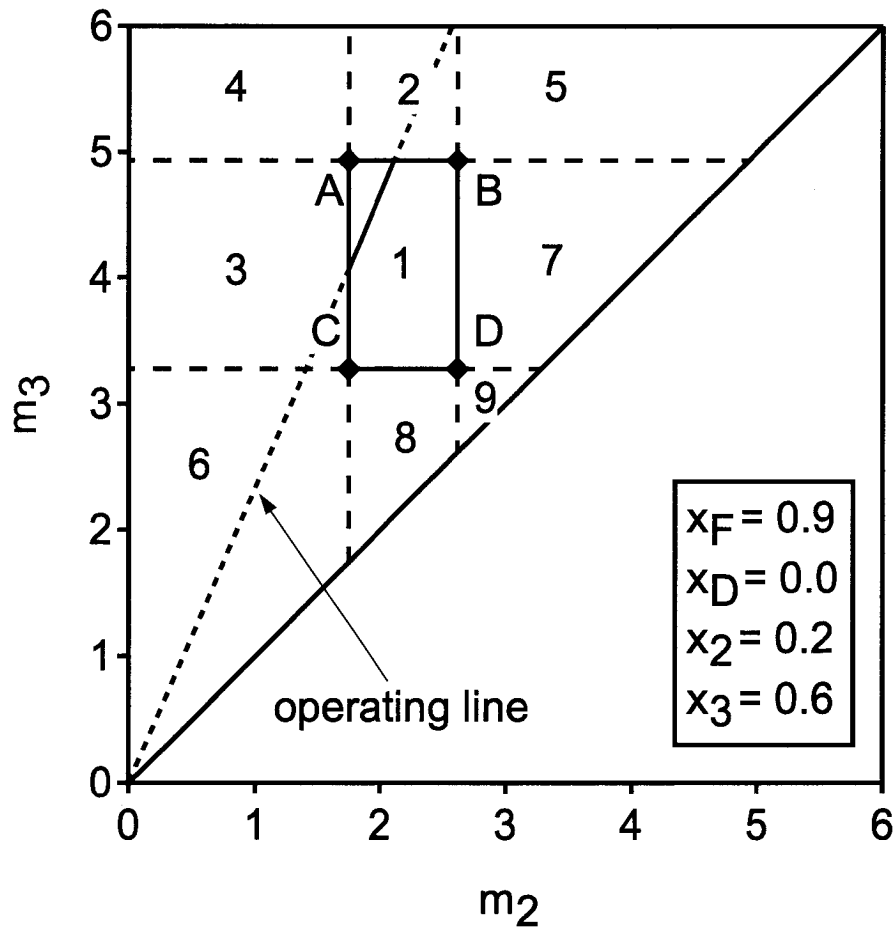


Figure 2.4: Complete separation region in the (m_2, m_3) plane for a fixed pair (x_2, x_3) , and operating line given by Eq. (2.8) for the solvent gradient mode operation. The regions are calculated for the model system with the following retention parameters: $H_A^0 = 2.12$, $H_B^0 = 1.41$, $k_A = k_B = 0.95$, and $n_A = n_B = 1$. Mobile phase composition values are reported in the box. Classification: region 1, complete separation; 2, pure extract and raffinate polluted with component A; 3, pure raffinate and extract polluted with component B; 4, both extract and raffinate containing both A and B; 5, extract flooded with pure desorbent, both A and B entirely collected in the raffinate; 6: raffinate flooded with pure desorbent, both A and B entirely collected in the extract; 7: extract flooded with pure desorbent, pure raffinate, and A accumulating in the unit; 8: raffinate flooded with pure desorbent, pure extract, and B accumulating in the unit; 9: both raffinate and extract flooded with pure desorbent, both A and B accumulating in the unit.

0.5, 0.6, 0.7, are highlighted. It is rather clear that when further increasing x_3 , a value is eventually reached where the operating line and the corresponding rectangle do not intersect any more; this occurrence indicates that the selected pair (x_2, x_3) does not allow for complete separation. These considerations show that there exists a maximum x_3 value, which is defined as that where the intersection between operating line and rectangle in the (m_2, m_3) plane reduces to a point.

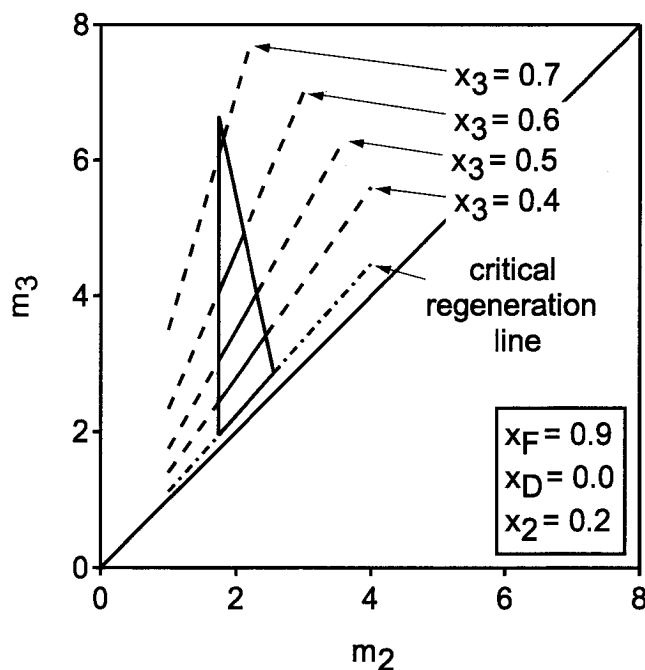


Figure 2.5: Operating lines for constant $x_2 = 0.2$, and $x_3 = 0.4, 0.5, 0.6, 0.7$, for the model system. The solid parts, but not the dashed parts, of the operating lines belong to the complete separation region for $x_2 = 0.2$; this is obtained by combining all the solid segments. The dashed-dotted line represents the critical regeneration line.

Thus summarizing, for a fixed value of x_2 there is a minimum value of x_3 defined by Eq. (2.10) which guarantees proper operation of sections 1 and 4 and a maximum x_3 value beyond which sections 2 and 3 do not separate components A and B any more. Thus, *the complete separation region for the given x_2 value* in the (m_2, m_3) plane is obtained by putting together the intersecting segments for all the feasible x_3 values. This is illustrated in Figure 2.5 for the model system, where the obtained region has a triangular shape, and its basis is the critical regeneration line, i.e. the operating line corresponding to the minimum x_3 value.

The complete separation region for $x_2 = 0.5$ is drawn in Figure 2.6, together with the regions where a different regime is attained; this is identified by a number, with a mean-

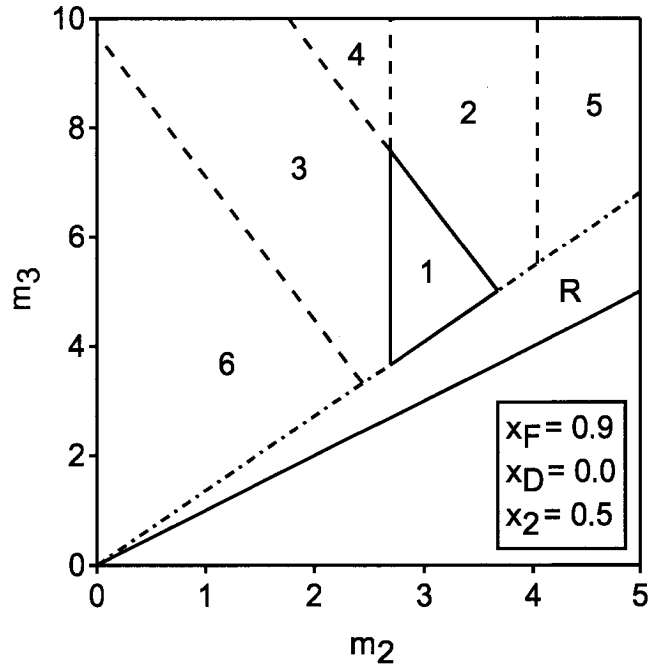


Figure 2.6: Complete separation region for $x_2 = 0.5$ for the model system with $x_F = 0.9$, and $x_D = 0.0$. The same classification of the regions as in Figure 2.4 applies. The region R is below the critical regeneration, hence extract and raffinate are polluted due to incomplete regeneration in sections 1 and 4.

ing identical to that used in Figure 2.4. It is worth noting that in this particular case the unfeasible regions 7, 8, and 9 are missing, whereas the region R below the critical regeneration line is present. The boundaries of region 1 (solid lines), and the boundaries between the other regions (broken lines) in Figure 2.6, as well as in Figure 2.7 discussed in section 2.5.4 below, are given by the following relationships. These are obtained by tracking the intersections between the operating line (2.8) and all the region boundaries shown in Figure 2.4, as x_3 is varied at constant x_2 . In addition, the straight line that constitutes the upper boundary of region R is obtained using Eq. (2.9) and the minimum m_3 value obtained by solving Eq. (2.10).

- Vertical line separating regions 2-5, 1-7, and 8-9:

$$m_2 = H_A(x_2) . \quad (2.11)$$

- Vertical line separating regions 1-3, 2-4, and 6-8:

$$m_2 = H_B(x_2) . \quad (2.12)$$

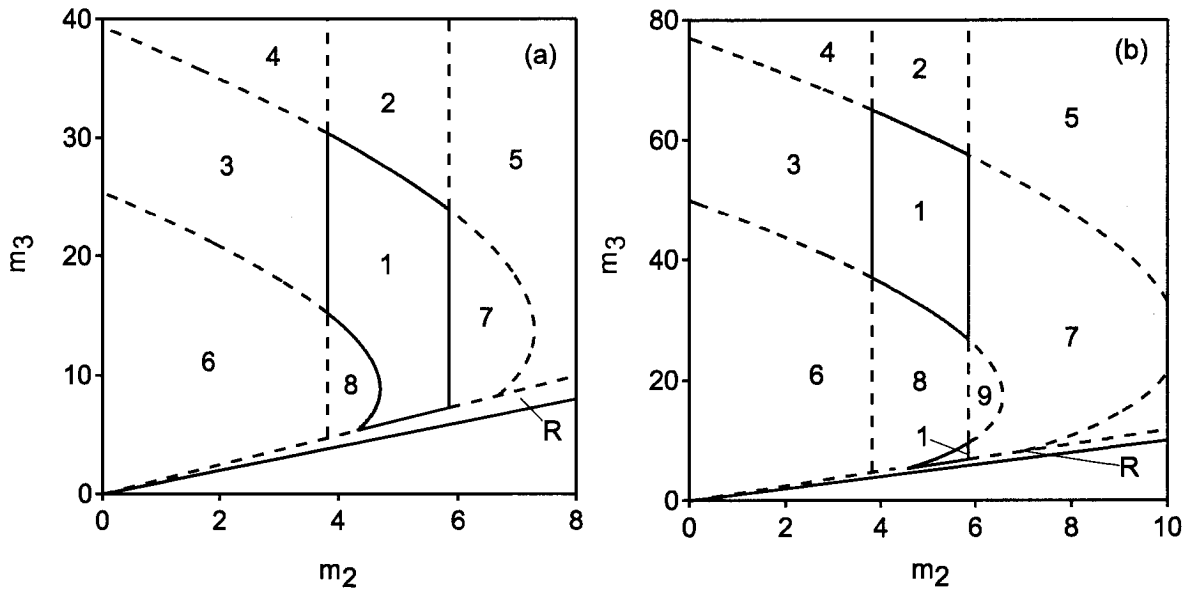


Figure 2.7: Complete separation regions for a given x_2 value for the system α -ionone in water/methanol with: (a) $x_2 = 0.34$, $x_F = 0.5$ and $x_D = 0.0$; (b) $x_2 = 0.34$, $x_F = 0.55$ and $x_D = 0.0$. The same classification of the regions as in Figure 2.6 applies.

- Curve separating regions 1-2, 3-4, and 5-7:

$$m_2 = \frac{m_3^{\frac{n_A-1}{n_A}}}{k_A(x_F - x_2)} \left[m_3^{\frac{1}{n_A}} (k_A x_F - 1) + (H_A^0)^{\frac{1}{n_A}} \right]. \quad (2.13)$$

- Curve separating regions 1-8, 3-6, and 7-9:

$$m_2 = \frac{m_3^{\frac{n_B-1}{n_B}}}{k_B(x_F - x_2)} \left[m_3^{\frac{1}{n_B}} (k_B x_F - 1) + (H_B^0)^{\frac{1}{n_B}} \right]. \quad (2.14)$$

When $n_i = 1$ for either $i = A$ or $i = B$ as in the case of the model system, then a straight line is obtained using either Eq. (2.13) or Eq. (2.14), respectively.

2.5.3 Complete separation region

Let us now vary x_2 as well. As illustrated in Figure 2.8, the complete separation regions for each individual x_2 value move to the upper right corner of the diagram and shrink while x_2 increases. It is found that when further increasing x_2 , a maximum value is eventually achieved where there are no more feasible operating points. On the other hand, x_2 cannot be smaller than x_D .

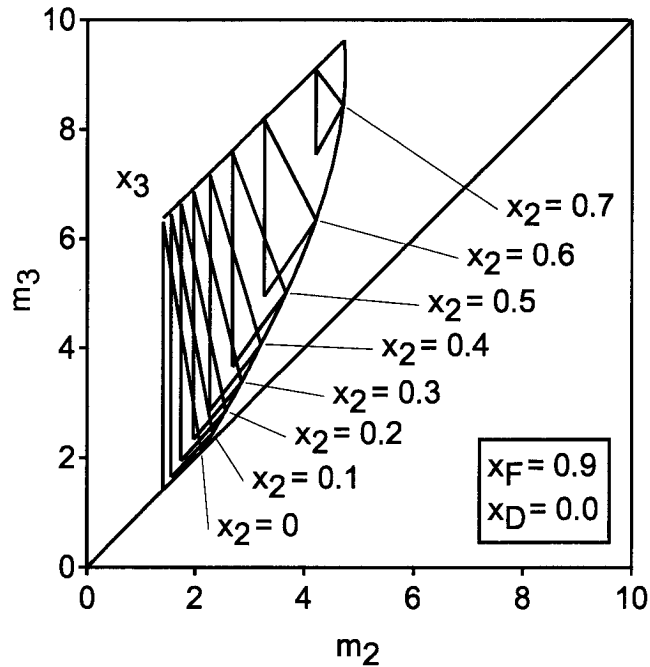


Figure 2.8: Complete separation regions for different values of x_2 for the model system with $x_F = 0.9$, and $x_D = 0.0$. The complete separation region for the given pair (x_D, x_F) is obtained by combining all these. The leftmost region, whose basis is on the diagonal, applies to the open-loop unit where $x_2 = x_D$.

Where $x_2 = x_D$, either $m_4 = 0$ to fulfill Eq. (2.9) or the SG-SMB unit is operated in the open-loop configuration; in both cases, the corresponding critical regeneration line coincides with the diagonal. Thus, *the complete separation region* is finally obtained by putting together all the complete separation regions for the x_2 values between the minimum and the maximum ones. This depends only on the mobile phase composition in the external streams, i.e. on x_D and x_F ; as a matter of fact Figure 2.8 provides a geometrical representation of the solution of the mathematical problem stated in section 2.4. It is worth underlying that for the operating points in the complete separation region all flow rates, both external and internal, may be different, whereas only x_D and x_F are constant.

2.5.4 Effect of retention model parameters

In this section the effect of the parameters describing the retention behavior of the solutes as a function of the mobile phase composition, i.e. those in Eq. (2.1), is considered. When applying Eqs (2.11) to (2.14) to systems with n_i values larger or smaller than 1 and with k_i values different from each other, the shape of the complete separation region for a fixed x_2

value can be rather different from that obtained for the model system and shown in Figure 2.5. Two examples for two different values of x_F are given in Figure 2.7, which applies to the α -ionone system whose retention behavior is illustrated in Figure 2.1. It can be readily observed that all types of separation regime discussed with reference to Figure 2.4 can be observed also in this case, i.e. regions 1 to 9. Moreover, the interaction between solvent balances and separation conditions may be such that the complete separation region for a fixed x_2 value may be constituted of two disjoint parts, as in Figure 2.7b.

Also when considering the complete separation region the effect of the retention model parameters is rather significant. This is illustrated in Figure 2.9 where four different cases are considered. It is worth noting that the complete separation region can be either convex as in Figures 2.9a and 2.9d, or concave as in Figures 2.9b and 2.9c. Moreover, the curve that constitutes the upper boundary of the complete separation region is given by the following equation, which is obtained by intersecting curves (2.12) and (2.13):

$$k_B m_3^{\frac{n_A-1}{n_A}} \left[m_3^{\frac{1}{n_A}} (k_A x_F - 1) + (H_A^0)^{\frac{1}{n_A}} \right] = k_A m_2^{\frac{n_B-1}{n_B}} \left[m_2^{\frac{1}{n_B}} (k_B x_F - 1) + (H_B^0)^{\frac{1}{n_B}} \right]. \quad (2.15)$$

This represents a straight line only where $n_A = n_B = 1$, i.e. in the cases illustrated in Figures 2.8, 2.9a, and 2.9b.

2.5.5 Effect of mobile phase composition

In this section the role of the mobile phase composition of the external streams, i.e. x_D and x_F , on the shape and position of the complete separation region is analyzed. This is of course worth investigating, since these two parameters are of key importance for the overall optimization of the SG-SMB separation. Here, we consider the effect of mobile phase composition on the retention behavior of the two components to be separated only, while neglecting any effect on solubility, density, and viscosity. As a consequence, the whole range of mobile phase composition from pure S solvent to pure W solvent is considered, even though in most real cases only a limited range of composition is practically accessible. Sometimes, for instance, the stationary phase itself is stable only below a certain relative concentration of one of the two solvents, hence this upper limit cannot be overcome in practice.

With reference to the model system, whose complete separation region for $x_D = 0$ and $x_F = 0.9$ is shown in Figure 2.8, the effect of changing the mobile phase composition in the feed x_F at constant $x_D = 0$ is illustrated in Figure 2.10a, whereas the effect of

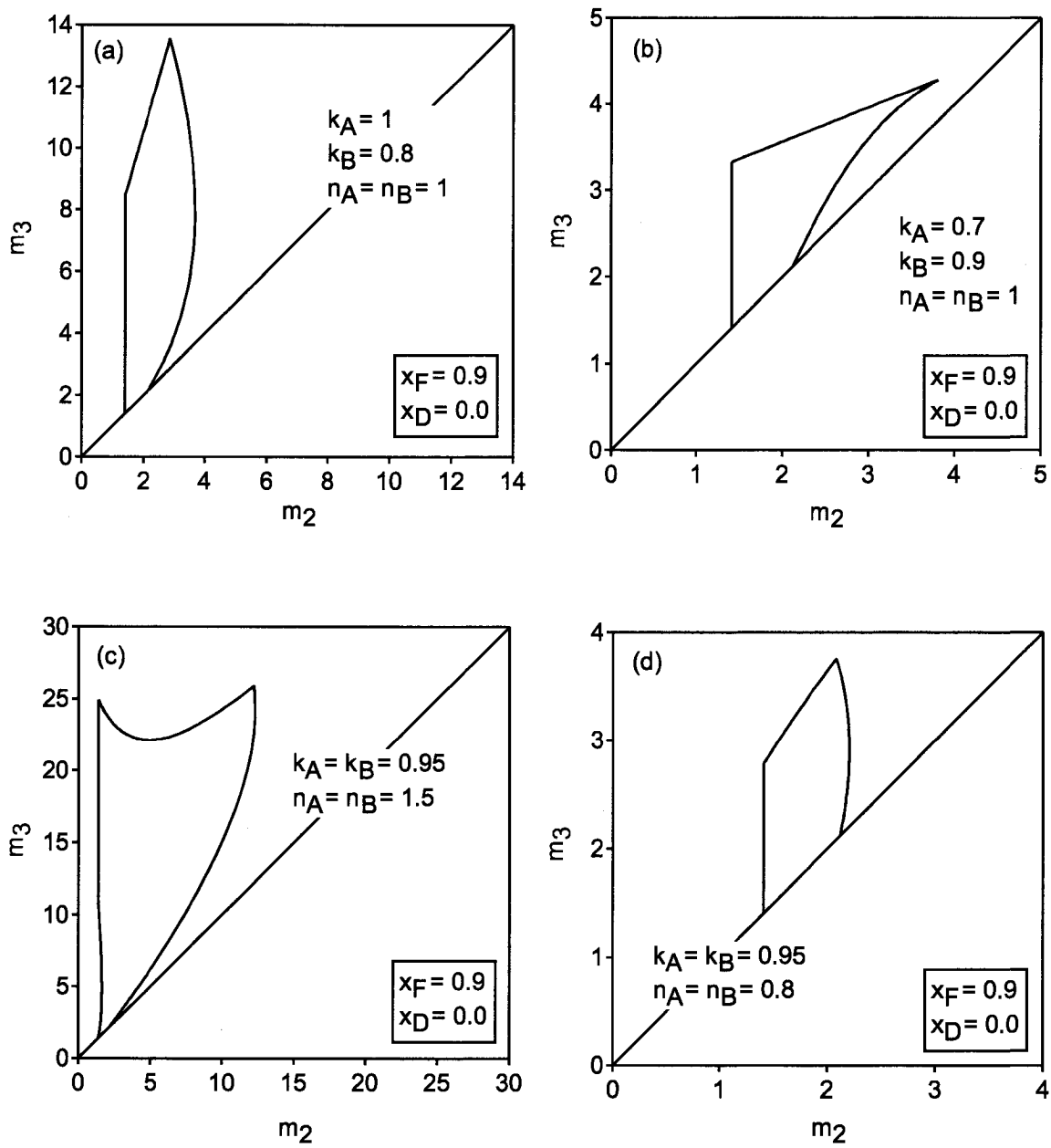


Figure 2.9: Complete separation regions for different systems with $x_F = 0.9$ and $x_D = 0.0$. Retention parameters: $H_A^0 = 2.12$, $H_B^0 = 1.41$; (a) $k_A = 1$, $k_B = 0.8$, $n_A = n_B = 1$; (b) $k_A = 0.7$, $k_B = 0.9$, $n_A = n_B = 1$; (c) $k_A = k_B = 0.95$, $n_A = n_B = 1.5$; (d) $k_A = k_B = 0.95$, $n_A = n_B = 0.8$.

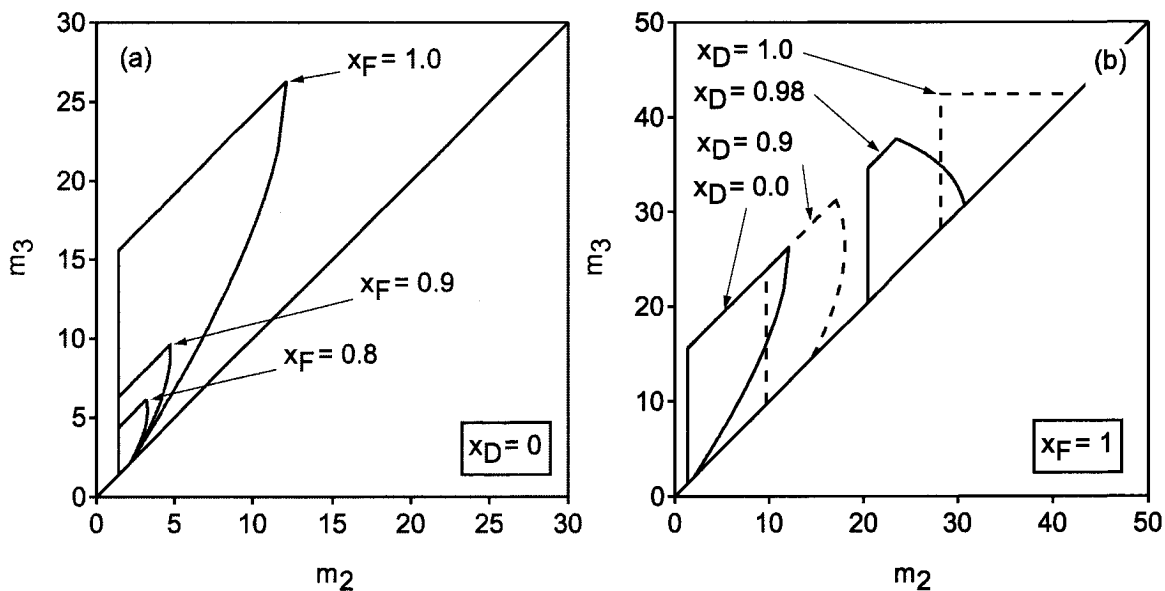


Figure 2.10: Complete separation regions for the model system for different external mobile phase compositions. (a) Effect of changing x_F at constant $x_D = 0$. (b) Effect of changing x_D at constant $x_F = 1$.

changing that in the desorbent stream at constant $x_F = 1$ is shown in Figure 2.10b. It can be observed that in the former case (Figure 2.10a) the complete separation region becomes larger as x_F increases. The largest region is obtained when pure solvent S is fed as desorbent, and pure solvent W is fed with the feed. However, it is worth noting that these are precisely the conditions that are typically difficult to apply in practice for the reasons mentioned above. In the latter case on the contrary (Figure 2.10b), the complete separation region shifts along the diagonal towards the upper right corner of the diagram as x_D increases without significantly changing its size; of course when x_D becomes equal to x_F the complete separation region reduces to the well known linear triangle for isocratic operation. Although, the change of the complete separation region with the composition of the feed and desorbent streams is affected by the values of the retention model parameters, the trends observed are quite general.

2.6 SG-SMB Design and Operation

In this section we discuss how an existing SG-SMB can be operated to achieve the desired separation performance, i.e. complete separation of the two solutes A and B. In the following we assume that the external mobile phase composition is fixed, i.e. that x_D and

x_F have already been selected. In this context, we can assume that this choice is based on considerations, which do not depend only on the retention behavior of the two solutes, but also on the other properties such as solubility, viscosity, and density. In general, it can be said that the maximum possible difference between x_F and x_D should be adopted. To illustrate the discussion, the model system introduced in section 2.5 will be considered once more.

2.6.1 Choosing an operating point

Choosing an operating point for an SG-SMB separation with a given pair of values x_D and x_F requires that all internal flow rates, Q_j , $j = 1, \dots, 4$, and the switch time are selected. In the operating parameter space, an operating point that allows achieving complete separation must belong to the corresponding complete separation region drawn in Figure 2.11; in this particular case $x_D = 0$, and $x_F = 0.9$. For each point in such a region a suitable combination of m_j ($j = 1, \dots, 4$) values can be found that fulfills the solvent mass balances (2.8) and (2.9), and the constraints to achieve complete separation (2.4) to (2.7).

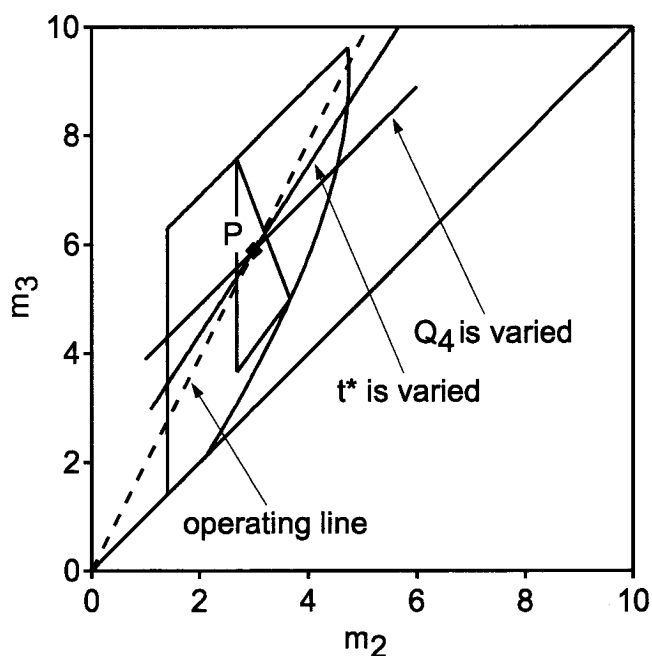


Figure 2.11: Design and operation of a SG-SMB unit, in the case of the model system with $x_F = 0.9$, and $x_D = 0.0$. Operating point P within the complete separation region for $x_2 = 0.5$. The dashed line is the operating line of Eq. (2.8), whereas the two solid lines are given by Eqs (2.16) and (2.17).

The exact location of the point is chosen based on performance and robustness considerations [12, 10]. These will involve an evaluation about the productivity, the solvent consumption, and the robustness of the separation, which means that small disturbances do not significantly modify the separation performance of the unit. These aspects would define which specific point in the complete separation region leads to the best performance. As discussed above, we do not consider this issue here, which most likely would also depend on the specificity of the particular separation under consideration, and simply select one point within the complete separation region, say point P in Figure 2.11, and develop further the SG-SMB design procedure. Note that the selected point is rather far from the boundaries, so as to guarantee that all the nonideal effects, which are neglected in the theoretical analysis based on the equilibrium theory analysis of the equivalent SG-TMB configuration, are not going to hinder the separation performance significantly. The choice of P assigns the values of m_2 and m_3 .

By considering again Figure 2.8, it is observed that the chosen point P belongs to a whole set of complete separation regions for given values of x_2 in a well defined range. In principle any x_2 value among these can be selected; in practice, x_2 is chosen in such a way that P is located in a balanced position within the corresponding complete separation region, as illustrated in Figure 2.11. In other words, the complete separation region for the selected x_2 value should be such that P is not too close to any of its boundaries.

Given m_2, m_3 and x_2 , the solvent balance (2.8) is solved for x_3 , and then the ratio m_1/m_4 is calculated through the second solvent balance (2.9). Since point P is in the complete separation region, i.e. above the critical regeneration line, there is certainly a range of values of m_1 and m_4 , which fulfill Eq. (2.9), as well as the constraints (2.4) and (2.7). Values of these two parameters within this range are chosen in order to keep both of them at the largest possible distance from the corresponding lower and upper bounds given by Eqs (2.4) and (2.7).

Finally, a value for t^* is chosen based on usual pressure drop and efficiency considerations [28]. Once t^* is selected, for every section the internal flow rate Q_j is calculated using the known value of m_j and Eq. (1.1). From the overall material balances at the inlet and outlet nodes of the unit the external flow rates are eventually calculated.

2.6.2 Tuning the separation performance

When running experiments on an SMB unit in a given operating point, e.g. P of coordinates (m_2^P, m_3^P) in Figure 2.11, there is often the need to adjust the operating conditions either to improve the separation performance or to analyse significant effects. If only a fine tuning is required, the operating point is moved in such a way to minimize the number of operating parameters to be actually changed. In practice this is done by changing only either the switch time t^* or the recycle flow rate Q_4 in closed-loop SMBs (the desorbent flow rate Q_1 in open loop SMBs). In the former case all internal and external flow rates are left unchanged, but all flow rate ratios m_j change linearly with t^* . In the latter case, the switch time and all external flow rates are constant, but the internal flow rates increase or decrease following Q_4 , and so do also the m_j values according to Eq. (1.1).

It is rather straightforward to show that following one or the other of the two experimental strategies above, the new operating point belongs to two different straight lines intersecting in point P (see Figure 2.11). The following are the corresponding equations:

$$m_3 = \frac{Q_3}{Q_2} m_2 + \left[m_3^P - m_2^P \frac{Q_3}{Q_2} \right], \quad (2.16)$$

$$m_3 = m_2 + m_3^P - m_2^P, \quad (2.17)$$

which apply to the changes in switch time and in recycle flow rate, respectively. It is worth noting that in Eq. (2.16) the symbols Q_2 and Q_3 are not ambiguous, since these two parameters remain constant along the corresponding straight line. Increasing either t^* or Q_4 moves the operating point along the corresponding line towards larger values of m_2 and m_3 .

It can be readily observed that neither straight line coincides with the operating line given by Eq. (2.8), along which the internal mobile phase composition levels x_2 and x_3 , that are calculated for the equivalent SG-TMB unit and represent average values of the actual mobile phase composition profile in the SG-SMB unit, remain constant. The new x_2 and x_3 are in fact given by solving Eqs (2.8) and (2.9) for the new set of m_j values. Therefore, both the above mentioned strategies yield changes in the values of x_2 and x_3 . Thus, the position of the new operating point should be evaluated with respect to the complete separation region for the new x_2 value and not with respect to the one drawn in Figure 2.11. In principle, this makes things more complicated than in the isocratic case. In practice, the key trends observed in the isocratic case are observed also in the solvent gradient case, and can be summarized as follows. When increasing either t^* or

Q_4 , the operating point moves towards the region where the raffinate gets polluted with component A, and accordingly raffinate purity decreases and extract purity increases if it is not already 100%. On the contrary, when decreasing either t^* or Q_4 , the operating point moves towards the region where the extract gets polluted with component B, and accordingly extract purity decreases and raffinate purity increases, if not already 100%. In other words, increasing either parameter moves the concentration fronts towards the raffinate outlet, whereas the opposite occurs when either t^* or Q_4 decreases.

2.7 Discussion and Conclusions

The conclusions drawn through the theoretical analysis developed above are based on an ideal description of the SG-SMB process, where a number of important assumptions have been made. First, nonideal effects, i.e. axial dispersion and mass transfer resistance, are neglected in the description of the column dynamics. The equilibrium theory model is in fact adopted. Secondly, it is assumed that the separation performance of the SG-TMB unit is the same as that of the SG-SMB, which is equivalent to it according to the definition imbedded in Eqs (1.2) and (1.3); this is assumed despite the evident differences exhibited by the mobile phase composition profiles in the two unit configurations, as illustrated in Figure 2.3. Finally, the complex interaction among the two solutes, the two solvents, and the stationary phase is described through the linear adsorption isotherm (1.4), where the Henry's constants depend on the mobile phase composition through Eq. (2.1).

Whereas the third assumption can be verified only through experiments and represents anyhow a realistic possibility in chromatography, the first two can be easily verified through numerical simulations of the SG-SMB behavior. Thus, simulations have been carried out using a detailed description of the SMB process, which is based on the lumped solid diffusion model to describe each individual chromatographic column [14]. Thus, the column model is constituted of two material balance equations for each component A and B, and of a balance equation for the weak solvent W. The former are written in terms of molar concentrations, whereas the latter in terms of volume fraction, under the

assumption of negligible volume effects upon mixing:

$$\varepsilon^* \frac{\partial c_i}{\partial t} + (1 - \varepsilon^*) \frac{\partial q_i}{\partial t} + u \frac{\partial c_i}{\partial z} = \varepsilon D_i \frac{\partial^2 c_i}{\partial z^2} \quad (i = A, B) \quad (2.18)$$

$$\frac{\partial q_i}{\partial t} = k_{q,i} a_p [H_i(x) c_i - q_i] \quad (i = A, B) \quad (2.19)$$

$$\varepsilon^* \frac{\partial x}{\partial t} + u \frac{\partial x}{\partial z} = \varepsilon D_W \frac{\partial^2 x}{\partial z^2} \quad (2.20)$$

Here k_i and D_i are the overall mass-transfer coefficient and the axial dispersion coefficient of component i , respectively, and a_p is the specific surface area for adsorption. The last equation is coupled to the others through the equilibrium adsorbed concentration, which appears in the linear driving force model on the right hand side of Eq. (2.19).

The many simulations that have been carried out with such a model confirm the validity of the theoretical analysis presented above, particularly in identifying the typical separation regimes and in locating with a rather good approximation the corresponding separation regions in the operating parameter space (cf. [14, 28] for a quantitative comparison between equilibrium theory results and detailed simulations in the case of isocratic SMBs).

In the following, this conclusion is supported by the discussion of the simulation results obtained for the α -ionone system mentioned above. In all simulations, $x_D = 0$ and $x_F = 0.5$, and the operating conditions are tuned in such a way that x_2 would always be equal to 0.34 in the equivalent SG-TMB unit. Accordingly, the topology of the separation regions shown in Figure 2.7a and redrawn for the sake of convenience in a different scale in Figure 2.12 applies. The SG-SMB unit is constituted of eight columns, arranged in a closed-loop 2-2-2-2 configuration. A complete set of the equations (2.18) to (2.20) above is used to describe each column, and the eight sets of partial differential equations are coupled through algebraic equations enforcing fulfilment of the overall and of the component material balances at the nodes of the unit. The following transport and column parameters have been adopted: $D_A = D_B = D_W = 0.001$ cm²/sec; $a_p k_{q,A} = a_p k_{q,B} = 10$ sec⁻¹; $\varepsilon = 0.7$, and $\varepsilon_p = 0$. A switch time $t^* = 200$ sec has been adopted in all simulations, whereas internal and external flow rates have been adjusted so as to obtain different sets of m_j values.

In Table 2.1, the operating conditions and the simulation results obtained for the operating points A to I in Figure 2.12 are shown. The first two columns report the values of x_2 and x_3 that have been calculated for the equivalent TMB unit. Then the m_j values ($j = 1, \dots, 4$) are given, and finally the calculated extract and raffinate purities are indicated; these are

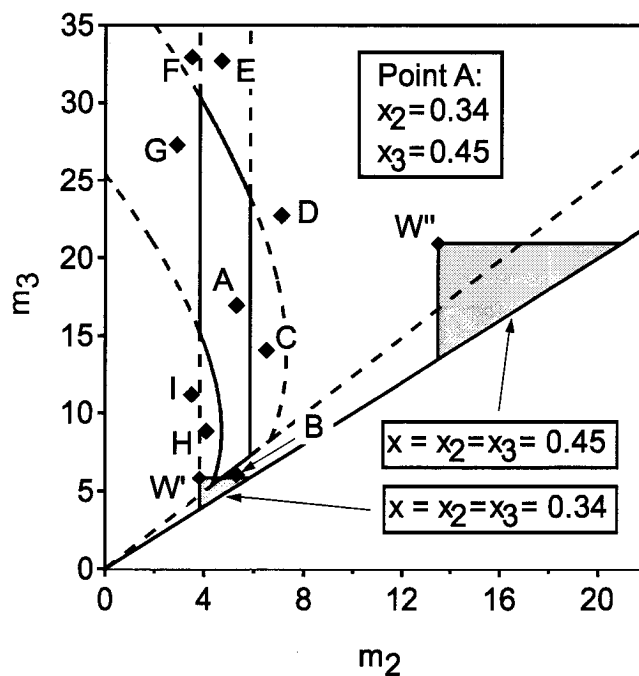


Figure 2.12: SMB separation of the α -ionone enantiomers in methanol/water. Solvent gradient mode complete separation region for $x_2 = 0.34$, with $x_F = 0.5$ and $x_D = 0$; the broken lines define the regions attaining different separation regimes as illustrated in Figure 2.7a. The hatched triangles are the isocratic complete separation regions for the mobile phase compositions as indicated in the figure. The operating points of the simulation runs in Tables 2.1 and 2.2 are also drawn.

RUN	x_2	x_3	m_1	m_2	m_3	m_4	P_E	P_R
A	0.340	0.450	11.9	5.3	17.0	9.0	100	100
B	0.340	0.360	6.0	5.3	6.1	5.7	95	66
C	0.340	0.426	9.3	6.5	14.1	7.4	-	100
D	0.340	0.450	11.9	7.1	22.7	8.9	-	50
E	0.340	0.477	19.5	4.7	32.7	13.9	100	79
F	0.340	0.483	11.4	3.5	32.9	8.0	93	92
G	0.340	0.483	8.5	2.9	27.3	6.0	78	100
H	0.340	0.426	9.3	4.1	8.9	7.4	100	-
I	0.340	0.450	11.9	3.5	11.2	9.0	50	-

Table 2.1: Solvent gradient SMB separation of the α -ionone enantiomers in methanol/water. Operating conditions and calculated purity performance.

RUN	$x_2 = x_3$	m_1	m_2	m_3	m_4	P_E	P_R
A'	0.340	9.4	5.3	17.0	3.0	100	51
A''	0.450	26.0	5.3	17.0	10.0	59	100
B'	0.340	9.4	5.3	6.1	3.0	100	79
C'	0.340	9.4	6.5	14.1	3.0	-	50
H'	0.340	9.4	4.1	8.9	3.0	100	61
W'	0.340	9.4	3.8	5.9	3.0	100*	100*
W''	0.450	26.0	13.5	20.9	10.0	100*	100*

(*) assumed value, not calculated.

Table 2.2: Isocratic SMB separation of the α -ionone enantiomers in methanol/water. Operating conditions and calculated purity performance.

defined as the solvent free average purity (in per cent) of A in the extract and of B in the raffinate, when the SMB cyclic steady state is achieved. If no purity value is indicated, this means that no solute is present in the corresponding outlet stream, i.e. that stream is flooded with mobile phase containing no solute. It can be readily observed that the calculated separation performance is fully consistent with the position of the operating point in the diagram. In particular, it is worth noting that in run C component A indeed accumulates in the unit, as predicted by our theoretical analysis, and that the same happens with component B in point H. Of course, this can happen since in the model the saturation either of the stationary phase or of the fluid phase is not accounted for, hence the solutes can indeed accumulate indefinitely in the unit.

Let us focus on the operating point A, where the theoretical internal mobile phase composition levels are $x_2 = 0.34$ and $x_3 = 0.45$, and complete separation of the two enantiomers has been achieved. In Figure 2.12 also the two isocratic complete separation regions are drawn, which correspond to the two cases $x_D = x_F = x_2 = x_3 = 0.34$ (smaller hatched triangle below the SG-SMB complete separation region) and $x_D = x_F = x_2 = x_3 = 0.45$ (larger hatched triangle on the right hand side of the SG-SMB complete separation region). The operating conditions and the results of a few isocratic simulations are reported in Table 2.2; each run is identified by a letter, referring to the corresponding operating point in Figure 2.12, and by either a prime or a double prime, indicating whether the mobile phase composition is $x = 0.34$ or $x = 0.45$, respectively. The m_1 and m_4 values have been chosen in such a way to fulfill the relevant constraints (2.4) and (2.7), respectively, namely $m_1 > H_A(0.34) = 5.85$ and $m_4 < H_B(0.34) = 3.82$ in runs A', B', C', and H', and $m_1 > H_A(0.45) = 20.9$ and $m_4 < H_B(0.45) = 13.5$ in run A''.

In run A' only the extract is pure, but almost the whole feed is collected in the raffinate,

where purity is only slightly larger than 51%. On the contrary, in run A'' only the raffinate is pure. In both cases the behavior is fully consistent with the relative position of point A in the (m_2, m_3) plane with respect to the small isocratic triangle at $x = 0.34$ in the case of run A', and to the large isocratic triangle at $x = 0.45$ in the case of run A''. This proves that the solvent gradient operation makes indeed available for complete separation zones of the operating parameter space, which do not achieve complete separation in the isocratic case. Now, let us consider runs B', and H', where only the extract is pure, and run C' where all the feed ends up in the raffinate product. The calculated behavior is again consistent with the relative position of the relevant operating points with respect to the isocratic triangle for $x = 0.34$. On the one hand, run B' improves the performance of run B, since point B is below the critical regeneration line in the (m_2, m_3) plane in the solvent gradient mode, whereas in the isocratic mode there is no solvent balance constraint (2.9) on m_1 and m_4 , and then these can be properly chosen to fulfill the corresponding separation constraints (2.4) and (2.7). On the other hand, runs C' and H' do not lead to accumulation of any component in the unit as it happens in the solvent gradient runs C and H; this is because this accumulation effect cannot occur in the isocratic mode. However, since $m_2 > H_A(0.34)$ in run C', both components are collected only in the raffinate outlet and the extract is flooded with desorbent.

Thus, it has been shown how different the separation performance can be in the solvent gradient mode with respect to the isocratic mode for the same operating point in the (m_2, m_3) plane. Let us now evaluate the benefit in terms of separation performance that can be gained when operating a SG-SMB unit in the operating point corresponding to run A in Table 2.1, with respect to operating an isocratic SMB in the optimal vertices of the two isocratic triangles in Figure 2.12, which are identified as runs W' and W'' in Table 2.2. For the sake of simplicity, we assume that these two runs achieve 100% purity in both extract and raffinate, i.e. the same separation quality as in run A. Two performance parameters are considered, namely desorbent requirement and productivity [10, 28]. The former is calculated as the ratio $(m_1 - m_4)/(m_3 - m_2)$. The latter is not very significant here since it is proportional to the feed concentration, which plays no role under the linear adsorption conditions studied in this work; a measure of productivity that can be used for comparison is provided by the difference $(m_3 - m_2)$, which is proportional to the feed flow rate. First, it must be observed that both performance parameters are better in run W'' than in W'; in fact the productivity measure $(m_3 - m_2)$ is 7.4 and 2.1, respectively, whereas desorbent requirement is 2.2 and 3.0, respectively. However, it should be observed

that the very large value of m_1 in run W'' calls for a smaller switch time than in run W' to keep pressure drop under control (or for a larger column cross section to have the same linear velocity in the two cases); this has a negative effect on productivity that may compensate the difference in the figures given above. In run A the solvent gradient mode allows for a productivity, i.e. a value of $(m_3 - m_2)$, equal to 11.7, i.e. more than 50% larger than in run W'' ; at the same time desorbent requirement drops to 0.25, i.e. almost ten times less than in the same run W'' . This high performance is achieved with an m_1 value, which is only 25% larger than in run W' . It should be noted that as far as pressure drop is considered in the solvent gradient mode operation section 3 is limiting rather than section 1, since most often $m_3 > m_1$. These figures provide a quantitative assessment of the arguments that were used in the Introduction to motivate the implementation of the solvent gradient strategy.

It is worth underlying once more that the gradient mode operation has not been optimized at all; in fact point A may well be non-optimal, and the external mobile phase compositions that have been selected may well be not appropriate when the dependence of solubility, density, and viscosity on mobile phase composition is considered. However, the results reported above indicate that really significant performance improvements can be achieved when a SMB separation is operated in the solvent gradient mode. This possibility certainly deserves careful consideration and further investigation.

One limitation to this rather optimistic picture comes from the observation that the use of the solvent gradient operation mode may make the constraints coming from the solubilities of the solutes more strict, which is investigated in more detail in chapter 3. In fact, the condition $x_F > x_D$ implies that the feed, where the solute concentration is larger, is richer in the weak solvent, and therefore the solute solubility is lower. This limitation depends of course on the specific separation under examination, and is of course absent in all those cases where solute solubility is not limiting.

3 Solvent Gradient SMB (SG-SMB) for Langmuir isotherms

3.1 Introduction

In chapter 2 design and optimization criteria have been developed for the SG-SMB in the case where the species to be separated, the more retained component A and the less retained solute B, follow a linear chromatographic behavior, i.e. their adsorption isotherms are linear (see Equ. 1.4). Such analysis was carried out in the frame of the so called Triangle Theory, whereby two basic assumptions are made. First, the SMB unit is considered equivalent to the TMB unit; the TMB unit achieves a steady state regime, which is not accessible to the SMB unit that can attain only a cyclic steady state behavior due to its port switch mechanism.

In this chapter, the linear analysis of chapter 2 is extended to the case of systems following the nonlinear, competitive Langmuir isotherm. This extension is needed because in SMB practice it is necessary to operate at high feed concentration in order to increase throughput, i.e. under overload conditions where the assumption of linear, decoupled isotherms does not apply. The chiral separation of α -ionone enantiomers has been selected to illustrate the developed concepts and methods [29, 30]. These enantiomers are separated on a cyclodextrin based chiral stationary phase using methanol as main solvent and water as modifier. Since α -ionone enantiomers are more soluble in methanol than in water, increasing the water fraction in the mobile phase leads to longer retention times, as implied in Fig. 2.2 in chapter 2.

3.2 Solubilities and adsorption isotherms

In general, changing the mobile phase composition, i.e. the modifier concentration or the pH of the solution or its ionic strength, has a major effect both on the competitive, nonlinear adsorption behavior of the solutes under overload conditions and on their solubility. In principle, when varying the mobile phase composition, one should expect different patterns of behavior obtained by combining opposite trends in the two properties above, i.e. increasing or decreasing retention and increasing or decreasing solubility. In practice, retention and solubility are related, even though such relationship may be difficult to describe quantitatively. In the following we consider the case of the enantiomers of α -ionone in a mixed methanol/water mobile phase, to be separated on a cyclodextrin

based Nucleodex- β -PM column (Macherey-Nagel, Düren, Germany) at 20°C. This system is representative of a rather large class of systems, where increasing solubility (in methanol-rich mobile phases) implies decreasing retention, and vice versa.

3.2.1 Solubility

The solubility of the α -ionone racemate as a function of the mobile phase composition has been measured at 20°C. This was done by preparing solvent mixtures with different water content, and saturating them with α -ionone. Pure α -ionone is liquid at 20°C, thus in order to provide a large interface for mass transfer, the samples were shaken until a raw emulsion was formed and left for 24 hours at 20°C in a water quench. To break the emulsion into a two-phase-system, centrifugation was applied if necessary, and the α -ionone concentration in the solution could be determined by HPLC measurement. From the results illustrated in Fig. 3.1 it is clear that solubility is quite high in methanol and decreases sharply when adding water to the solution; α -ionone is practically insoluble for $x \geq 0.7$.



Figure 3.1: Solubility of the racemate of α -ionone in methanol/water at 20°C depending on the solvent composition.

3.2.2 Nonlinear competitive adsorption isotherms

In order to characterize the nonlinear competitive retention behavior of the α -ionone enantiomers as a function of the mobile phase composition, a series of pulse chromatograms of the α -ionone racemate has been measured at 20°C. These have been performed at various water (modifier) volume fraction values in the mobile phase, i.e. $x = 0.2, 0.3, 0.4$ and 0.5 , and at various solute concentrations and amounts injected. The obtained chromatograms show that the retention times of the peak maxima decrease when the amount injected increases, as expected for a Langmuir-type isotherm, whereas the shape of the peaks deviates from the standard Langmuirian behavior. In the following we do not try to capture the detailed behavior of this system, which most likely is rather complex, and we proceed instead by using a standard competitive langmuir isotherm, also based on previous results [20]. In order to highlight the dependence of the adsorption isotherm parameters on the mobile phase composition the following isotherm has been used:

$$q_i(x) = \frac{H_i(x)c_i}{1 + k_A(x)c_A + k_B(x)c_B} \quad (i = A, B), \quad (3.1)$$

where H_i and k_i are the Henry's constant and the adsorption equilibrium constant, respectively, while A and B refer to (R)-(+)- α -ionone and to (S)-(-)- α -ionone, respectively. The dependence of H_i and k_i on the mobile phase composition can be described in the range of $x \leq 0.85$ through the following equations:

$$H_i(x) = \frac{H_i(0)}{(1 + h_i x)^{n_i}} \quad (i = A, B) \quad (3.2)$$

$$k_i(x) = k_i(0) \exp\left(\frac{x}{a_i}\right) \quad (i = A, B) \quad (3.3)$$

where $H_A(0) = 0.32$, $H_B(0) = 0.26$, $h_A = -1.13$, $h_B = -1.17$, $n_A = 5.80$, $n_B = 5.33$, $k_A(0) = 1.48 \times 10^{-5}$ ml/g, $k_B(0) = 2.96 \times 10^{-5}$ ml/g, $a_A = 4.38 \times 10^{-2}$ and $a_B = 4.93 \times 10^{-2}$.

The relationships above indicate that as the water content in the mobile phase increases, the solutes are adsorbed more strongly, the maximum loading capacities (H_i/k_i) decrease, and therefore the nonlinear character of the adsorption isotherm increases.

3.3 Operating conditions for complete separation in nonlinear SG-SMBs

The temperature or pressure levels in a temperature gradient or pressure gradient simulated moving bed unit can be controlled independently through a device, either a heat exchanger or a back pressure regulator, that does not affect directly the SMB internal flow rates. On the contrary, the mobile phase composition in the solvent gradient SMB unit, e.g. the modifier concentrations x_2 and x_3 in Fig. 2.2, depend not only on the composition of the external streams, i.e. desorbent and feed, but also on the internal flow rates. To clarify this, let us first consider the closed loop TMB unit illustrated in Fig. 2.2. Given the modifier concentrations x_D and x_F in the desorbent and feed streams, respectively, the modifier levels x_2 and x_3 are related to the external flow streams through the following material balances at the desorbent and feed nodes:

$$x_2 Q_1^{TMB} = x_D Q_D + x_4 Q_4^{TMB} \quad (3.4)$$

$$x_3 Q_3^{TMB} = x_F Q_F + x_2 Q_2^{TMB} \quad (3.5)$$

where Q represents volume flow rates, and for the sake of simplicity volume changes upon mixing are neglected. Let us now consider an open loop unit, where the flow stream leaving section 4 is discarded and not recycled to section I. In this configuration, the mobile phase composition in sections 1 and 2 is the same as that in the desorbent stream. Accordingly, $x_2 = x_D$ replaces Eq. (3.4), whereas Eq. (3.5) still applies to describe the mass balance at the feed node. It is worth noting that the modifier concentration profiles drawn in Fig. 2.2 apply only to TMB units, whereas in a SMB unit such concentration values undergo variations due to port switching (see chapter 2). In this section we derive criteria for the choice of complete separation operating conditions in the frame of equilibrium theory with reference to a TMB unit, i.e. following a similar approach as in chapter 2, but for the more realistic case of nonlinear isotherms.

3.3.1 The 'open loop'-configuration

For a nonlinear system a similar procedure can be followed to construct the complete separation region in the (m_2, m_3) plane as in the linear case (see chapter 2). For a given pair of (x_2, x_3) modifier concentration values, a triangle-shaped region such as the one drawn in Fig. 3.2 can be obtained, by considering that different isotherms apply in the different sections of the unit. The specific example considered in Fig. 3.2 refers to the

separation of the α -ionone enantiomers with $x_2 = 0.3$ and $x_3 = 0.34$, and a total racemate feed concentration, $c_T^F = 6$ g/l. By considering an open loop configuration, $x_D = x_2 = 0.3$, and only the points in the triangle-shaped region fulfilling the feed node material balance (3.5) for the given feed concentration, $x_F = 0.5$ in Fig. 3.2, are to be considered. These belong to the broken operating line in Fig. 3.2, obtained by combining Eqs. (1.1) and (3.5):

$$m_3(x_F - x_3) = m_2(x_F - x_2), \quad (3.6)$$

whose intersecting segment (see Fig. 3.2) with the complete separation area comprises all points that guarantee complete separation, and are also compatible with the solvent gradient mode operation for the given values x_D , x_3 and x_F .

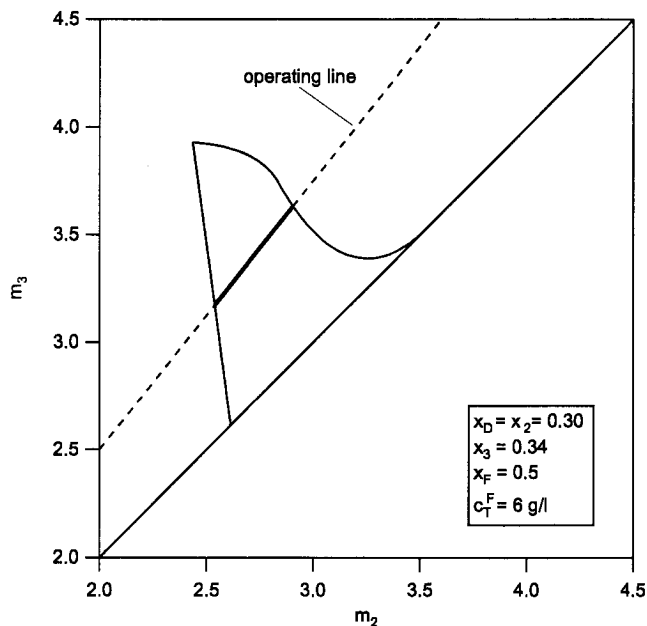


Figure 3.2: Nonlinear complete separation region in the (m_2, m_3) plane for a fixed pair (x_2, x_3) for an open-loop configuration, and the operating line given by Eq. (3.6). Only the segment of the operating line which lies inside the separation area provides accessible operating points for the solvent gradient separation.

By repeating this procedure for various values of x_3 , while keeping x_D and x_F constant, we get a set of segments for all feasible x_3 values, which can be assembled to form the complete separation region for the given x_D and x_F values in the (m_2, m_3) plane, shown in Fig. 3.3.

Contrary to the linear case, such a region depends on the concentration of the components to be separated in the feed stream, and therefore on the total racemate concentration c_T^F .

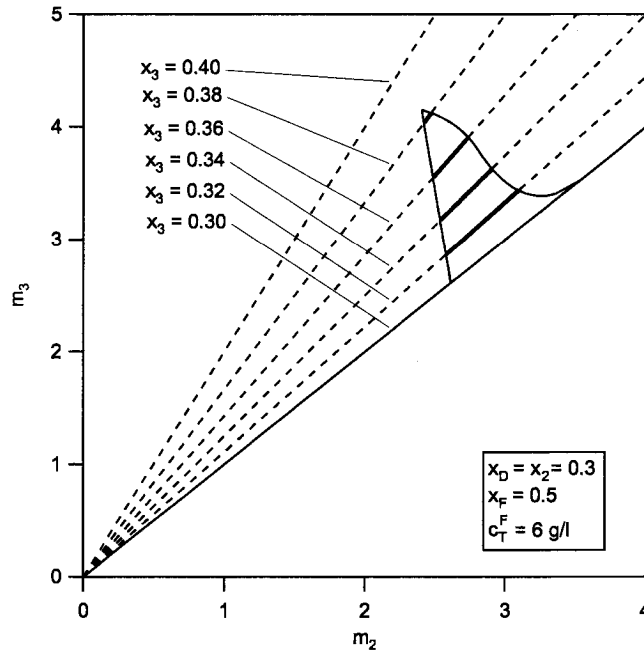


Figure 3.3: Operating lines (Eq. (3.6)) for constant $x_2 = 0.3$, and $x_3 = 0.3, 0.32, 0.34, \dots, 0.4$. Only the solid sections of the operating lines belong to the complete separation region for $x_2 = 0.2$. Same for both linear and nonlinear isotherm, it is obtained by combining all the solid segments.

The effect of c_T^F on the shape and position of the complete separation region, for the given x_D and x_F values, is illustrated in Fig. 3.4. It can be seen that the area of complete separation shrinks as the feed concentration increases, and the vertex shifts to the left towards lower m_2 values, whereas the intersections with the diagonal do not change.

Let us consider Fig. 3.4 in view of the following generally accepted definition of productivity for an SMB achieving complete separation of the components in the feed mixture [10]:

$$PR = \frac{Q_F c_T^F}{n_{col} V} = \frac{(m_3 - m_2)(1 - \varepsilon^*) c_T^F}{n_{col} t^*} \quad (3.7)$$

It is seen that the productivity is proportional to the product of the total feed concentration, c_T^F , by the distance of the operating point from the diagonal of the (m_2, m_3) plane. In the particular case under examination in Fig. 3.4, it can be shown that the maximum productivity increases with c_T^F , under the combined effect of an increasing value of c_T^F and a decreasing value of $(m_3 - m_2)$ [10].

It is worth recalling that the triangle-shaped regions in the (m_2, m_3) plane shown in Figs. 3.2 to 3.4 represent a region of complete separation only under the assumption that a

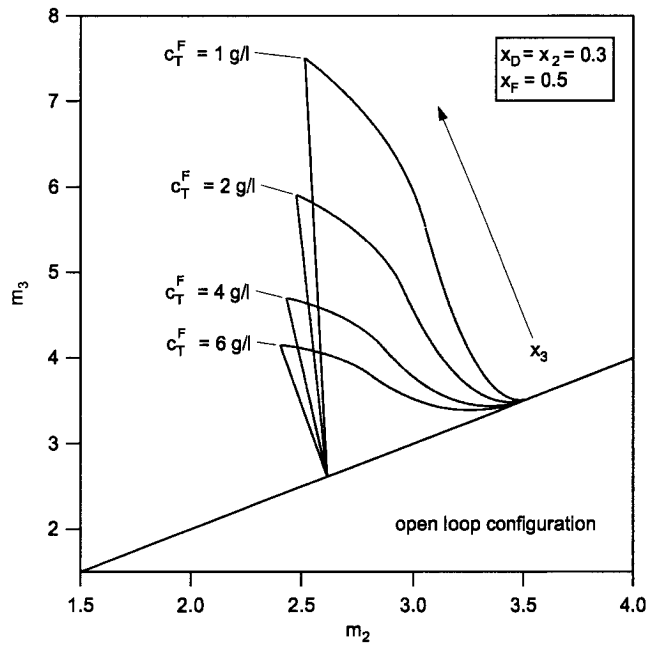


Figure 3.4: In case of a nonlinear isotherm, the complete separation region for fixed x_2 depends on the feed concentration c_T^F . The area decreases with increasing feed concentration.

complete regeneration of the solid and the fluid phase in sections 1 and 4, respectively, is achieved. This is guaranteed when the following conditions on m_1 and m_4 are fulfilled:

$$m_1 > m_1^{cr}(x_2) = H_A(x_2) \quad (3.8)$$

$$m_4 < m_4^{cr}(m_2, m_3, x_2, x_3) = \frac{1}{2} [H_B(x_3) + m_3 + k_B(x_3)c_B^F(m_3 - m_2) + \sqrt{(H_B(x_3) + m_3 + k_B(x_3)c_B^F(m_3 - m_2))^2 - 4H_B(x_3)m_3}] \quad (3.9)$$

It is worth noting that the former constraint on m_1 is the same as in the linear case, whereas the latter depends on the operating point (m_2, m_3) [10].

3.3.2 The 'closed loop'-configuration

In the case of an open loop configuration x_2 equals x_D , and the complete separation regions in Figs. 3.3 and 3.4 are constituted of points at constant x_F value, which fulfil Eq. (3.6). For a closed loop configuration, however, x_2 is usually larger than x_D , except for

the limiting cases where either the recycle flow Q_4 or the feed flow Q_F approaches zero. Following the same approach as for the open loop configuration, a complete separation region can be determined for the chosen value of x_2 . However, in this case, in addition to the solvent balance at the feed node (3.6) also the balance at the desorbent node, i.e. Eq. (3.4), must be fulfilled, which can be recast in terms of m_j values as follows:

$$m_1(x_2 - x_D) = m_4(x_3 - x_D) \quad (3.10)$$

At the same time m_1 and m_4 must comply with the constraints given by Eqs. (3.8) and (3.9). This implies that among the operating points in the (m_2, m_3) plane associated to a given pair of modifier concentrations (x_2, x_3) only those are feasible, for which two values m_1 and m_4 can be found that fulfill Eq. (3.10) and at the same time Eqs. (3.8) and (3.9). Such requirement defines implicitly a line in the (m_2, m_3) plane such that the operating points below it are not acceptable, because they violate the regeneration specifications in either section 1 or section 4. This line depends on the chosen values of x_F and x_D as illustrated in Fig. 3.5, for the case of $c_T^F = 6$ g/l, $x_F = 0.5$, and various x_D values between 0 and 0.3. Such lines identify a feasible upper region in the triangle-shaped complete separation region associated to $x_2 = 0.3$.

The ultimate result, i.e. the final complete separation region for a given set of external mobile phase compositions, i.e. for a given pair x_F and x_D , and for a given total feed concentration c_T^F , is obtained by combining the separation regions obtained for different values of x_2 . This is illustrated in Fig. 3.6, for $c_T^F = 6$ g/l, $x_F = 0.5$ and $x_D = 0.25$. The complete separation region is identified by a thick boundary, and is constituted of a series of triangle-shaped regions (with thinner boundaries) associated to x_2 values between 0.25 (the leftmost region) and about 0.36. Beyond this last x_2 value, the intersection between the region calculated for the chosen x_2 value and the feasible region complying with constraints (3.8), (3.9) and (3.10) is void. In the case shown in Fig. 3.6, the highest productivity and lowest desorbent requirement are achieved in the vertex of the triangle with the lowest x_2 value where the recycle flow goes to zero.

3.4 Discussion and conclusion

Tools to understand the behavior of SG-SMBs and to design their operating conditions have been introduced in this chapter. Next, we evaluate critically the potential of the solvent gradient operation of SMBs for practical applications. Our discussion will focus

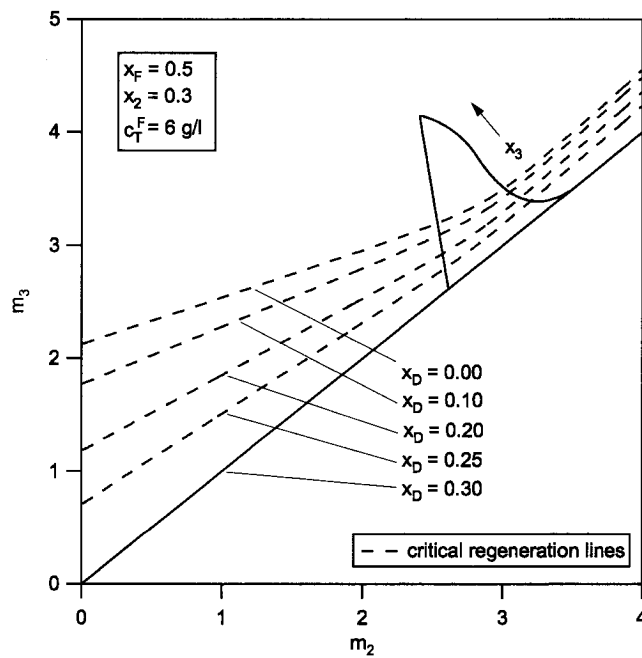


Figure 3.5: Nonlinear complete separation region for fixed x_2 . The dashed lines represent the critical regeneration lines for different desorbent compositions in a closed loop configuration. Only above the lines, a set of m_1 and m_4 fulfilling the regeneration constraints (Eqs. (3.8), (3.9)) can be found. Hence, the critical regeneration line cuts off the complete separation area and detaches it from the diagonal.

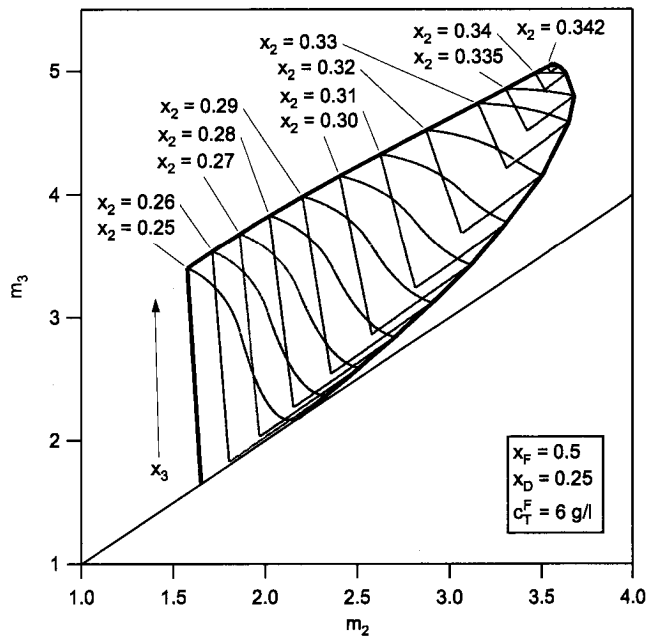


Figure 3.6: Nonlinear complete separation region for different values of x_2 . The complete separation region for the given pair (x_D, x_F) is obtained by combining all of them. The leftmost region, whose basis is on the diagonal, applies to the open loop configuration where $x_2 = x_D$.

on the issue of solubility, and we will refer to the α -ionone system and the corresponding data presented in section 2.2 and in Fig. 3.1.

For the sake of simplicity, but without loss of generality, let us consider the open-loop SG-SMB where the composition of the desorbent stream, i.e. x_D , and x_2 are the same and fixed. By fixing the composition of the solvent used in the feed stream, the maximum feed concentration, c_T^F , can be obtained from the curve in Fig. 3.1. For $x_F \geq x_D$, where $x_F = x_D$ identifies the isocratic SMB operation, the maximum solubility decreases with increasing x_F . Assuming as a reference for the analysis that c_T^F coincides with the racemate solubility, it is then possible for every pair x_F and c_T^F to determine the corresponding complete separation region in the (m_2, m_3) plane. A few such regions are drawn in Fig. 3.7. It can readily be observed that increasing x_F , and decreasing c_T^F accordingly, leads to larger regions, whereas values of x_F close to x_D leads to very high feed concentrations and very thin complete separation regions. The thinnest triangle in Fig. 3.7 corresponds to isocratic SMB operation, i.e. no gradient. With reference to the definition of productivity (3.7), changing x_F yields conflicting trends in the two key parameters controlling productivity, i.e. $(m_3 - m_2)$ and c_T^F . In the case under examination

the effect of the feed concentration prevails and a five-fold increase of productivity in going from $x_F = 0.7$, i.e. maximum gradient, to $x_F = 0.3$, i.e. isocratic SMB, can be observed (see Table 1). This indicates that SG-SMB operation does not improve on isocratic SMB in this case, and we suspect that this might be a general trend.

However, this first result has to be considered also in view of robustness considerations. It is well known that the thinner the complete separation region the less robust the SMB operation is [10]. This implies that decreasing x_F in Fig. 3.7 leads to less robust operation from the point of view of the feasible region of separation. This should lead to the conclusion that there might be an optimal gradient operation, i.e. a value of x_F that allows for the best trade-off between productivity and robustness. This could be determined only through detailed optimization, based on a proper measure of robustness. This measure should include another important aspect of SMB operation, particularly

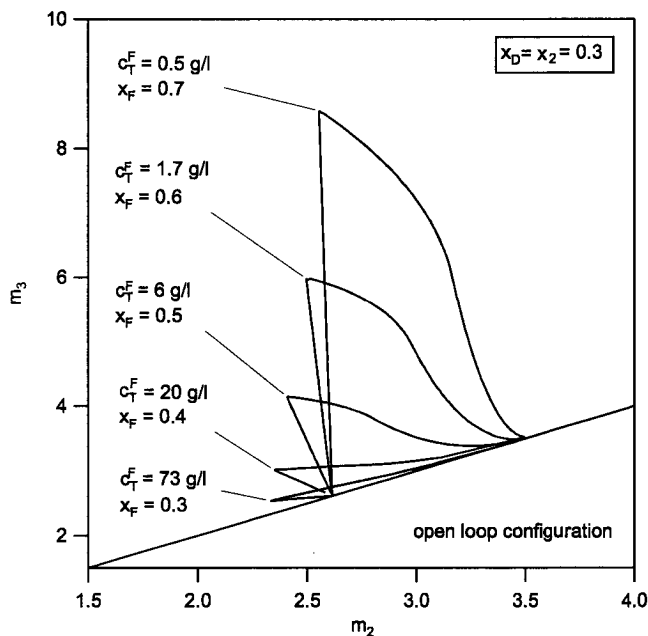


Figure 3.7: Nonlinear complete separation regions at fixed $x_2 = 0.3$ for $x_F = 0.3, 0.4, 0.5, 0.6, 0.7$, each with the racemic feed concentration slightly below the corresponding solubility limit.

of SG-SMB operation, namely the internal concentration profiles. It has in fact been observed that solvent gradient operation of SMBs may lead to an enrichment in the fluid phase beyond the feed concentration, as already described in chapter 2. An example of this is shown in Fig. 3.8a where the internal concentration profiles are shown, as computed with a detailed SMB model including the modifier mass balance equation (Eqs. (2.18)

to (2.20) of chapter 2, modified to account for the Langmuir adsorption isotherm of Eq. (3.1)). The nominal modifier concentrations x_2 and x_3 that are calculated using the TMB model and are used for the design of the separation are $x_2 = 0.3$ and $x_3 = 0.457$. The former coincides with the correct value for the SMB unit, whereas the latter is only an approximation of the real water concentration profile, which is shown in Fig. 3.8b. The solubility value corresponding to x_2 is extremely high, whereas that corresponding to the nominal x_3 value, i.e. 10 g/l, is very close to the actual c_B concentration in section 3. This raises the question whether there might be solubility problems within the SMB columns in the gradient mode operation, that might completely spoil the separation. It is difficult to answer this question in general terms since this is very much system-specific, and depends also on the detailed solid/liquid equilibrium of the two enantiomers in the mixed solvent system. In general in fact pure enantiomers have a different solubility, either higher or lower than the racemate.

The general conclusion to be drawn based on the analysis above is that the technical feasibility and attractiveness of solvent gradient SMBs depend on a rather delicate compromise between conflicting requirements and constraints. Feasibility should be assessed through detailed optimization. However, such optimization requires an amount of rather detailed information about retention and solubility at different mobile phase compositions, that goes beyond what is normally required for isocratic SMB design.

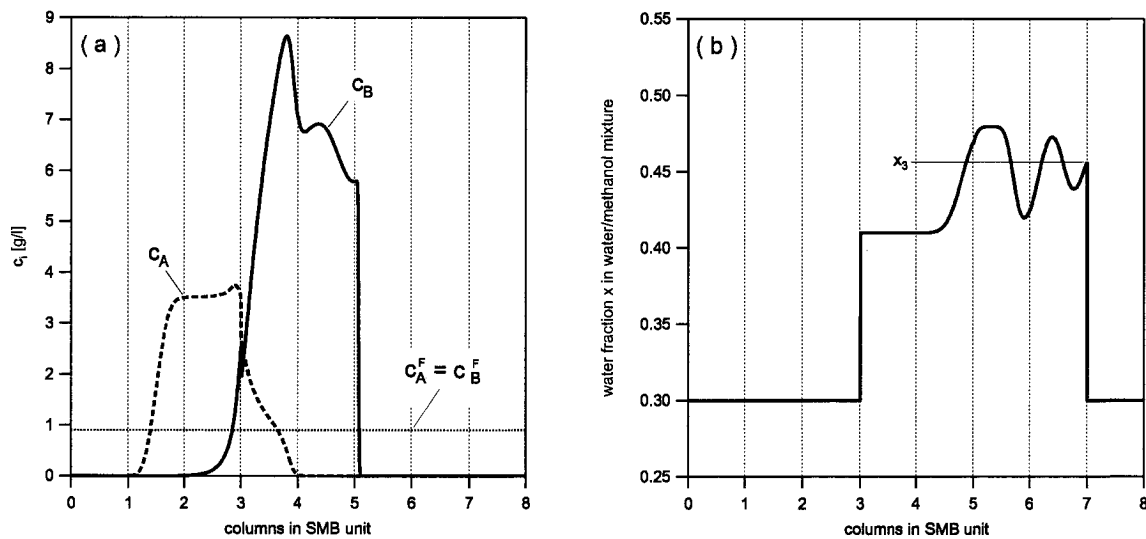


Figure 3.8: Detailed simulation of an open loop SMB with $x_2 = x_D = 0.3$, $x_F = 0.6$, $m_1 = 4.3$, $m_2 = 2.63$, $m_3 = 5.5$, $m_4 = 1.8$, $\varepsilon_p = 0$, $\varepsilon^* = 0.7$, $D_A = D_B = D_W = 0.001 \text{ cm}^2/\text{s}$, $a_p k_{q,A} = a_p k_{q,B} = 10 \text{ s}^{-1}$, $V = 0.785 \text{ ml}$, $t^* = 200 \text{ s}$, $c_T^F = 1.8 \text{ g/l}$ (slightly below solubility limit for x_F), adsorption isotherms according to Eqs. (3.2) and (3.3). Internal profile just after the switch versus the position of the 8 columns inside the SMB unit of: (a) concentration of A and B; (b) water fraction x .

4 Experimental implementation of the SG-SMB concept

4.1 Experimental setup

For the experimental implementation of the solvent gradient approach the separation of the enantiomers of the flavor norterpeneoid α -ionone (Fluka) on the stationary phase Nucleodex- β -PM (Macharay Nagel) using mixtures of water and methanol has been considered. The identical columns and plant setup have been used previously to perform a standard SMB separation of the enantiomers of α -ionone [30]. The experimental SMB unit is shown in Fig. 4.1, whereas the complete scheme of the pilot SMB unit can be found in [31]. The plant consists of eight HPLC columns (12.5 cm x 1 cm i.d., particle diameter 10 μ m) with two columns in each section (2-2-2-2 configuration). The columns are located in a thermostatic chamber to guarantee isothermal operations. The unit is operated in the open loop mode, that means the fluid phase is withdrawn at the end of section 4 and not recycled to section I. Instead, fresh solvent is fed to section I. Four inlet and outlet streams, i.e. desorbent inlet, extract, feed and raffinate, are controlled by HPLC pumps (Jasco, PU-987). The desorbent outlet after section 4 is not controlled and open to atmospheric pressure, whereas the flow rate is determined by the material balance. Five (12+1) port multi-position valves (Vici-Valco EMT-6-CSD12UW), one connected to each inlet- or outlet flow, implement the periodic port switching mechanism. The flow direction is determined by eight check valves (SS-CHS2-CH4, Swagelok), always one in the line between two columns. The outlet ports of each column and the inlet ports of the following one are respectively located before and after the check valve in order to establish the liquid flow in the unit and to avoid cross-contamination. The pressure after each column as well as the temperature in the unit is monitored. The plant is automated by a program using the software package LabView (National Instruments).

4.2 SG-SMB separation of α -ionone enantiomers

In the following the two enantiomers, i.e. (R)-(+) α -ionone and (S)-(-) α -ionone, will be referred to as enantiomer 1 and 2, respectively. The operating conditions for the experimental implementation of the SG-SMB concept and the achieved performances are summarized in table 4.1. The feed concentration was low enough to assume linear adsorption conditions. To establish the solvent gradient in the unit, different solvent compositions

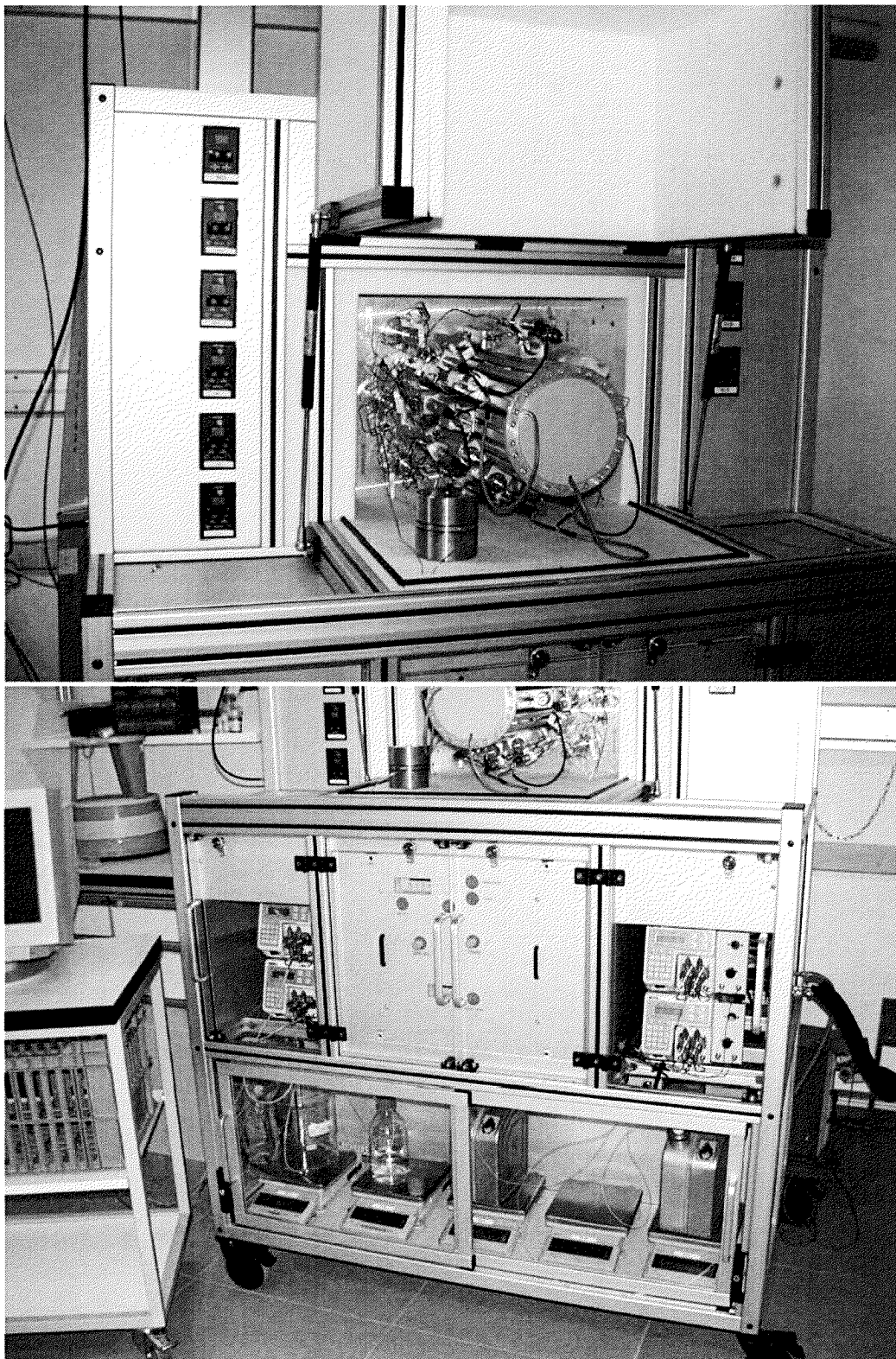


Figure 4.1: Experimental lab-scale SMB plant.

in desorbent and feed were chosen, i.e. $x_D = 0.2$ and $x_F = 0.4$. This leads to a solvent composition of $x_D = x_2$ in sections 1 and 2, since an open loop configuration was used. In sections 3 and 4, the solvent composition establishes by mixing of the feed with the outlet of section 2 with an average value of $x_3 = 0.36$. It can be calculated by a mass balance at the feed point assuming a TMB. Based on this data the region of complete separation is calculated and shown in Fig. 4.2b together with the operating points of the experiments.

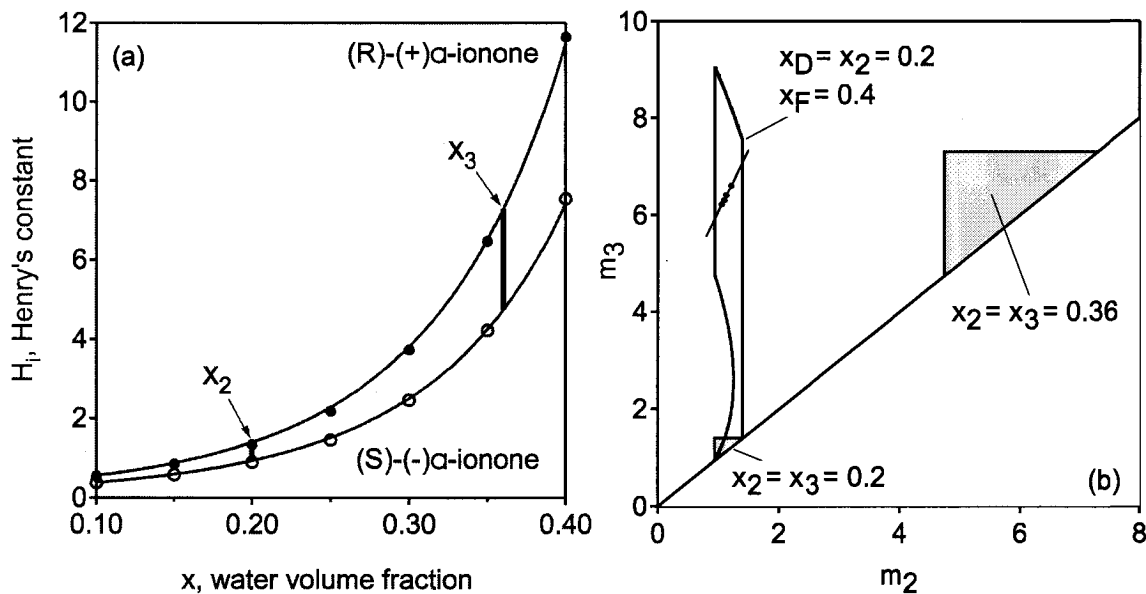


Figure 4.2: Experimental separation of the enantiomers of α -ionone: (a) Henry's constants with indicated gradient step levels; (b) region of complete separation for the SG-SMB including experimental operating points and isocratic separation regions for solvent compositions present in each of the two gradient steps.

As a comparison Fig. 4.2b shows also the two separation triangles for an isocratic SMB separation of both solvent compositions present in the gradient step of the SG-SMB. It can be readily observed that in the gradient region of complete separation the highest difference between m_3 and m_2 can be achieved, which indicates a high productivity. Since Eq. (2.4) applies, a lot of solvent can be saved in comparison to the isocratic mode of $x = 0.36$, which would achieve a similar high productivity. The gain of the SG-SMB is in the exploitation of the effective selectivity, i.e. $S_{SG} = H_1(x_3)/H_2(x_2)$, which is much higher as the one in either of the shown isocratic cases.

The results in table 4.1 show that high purity above 99% could be achieved for both extract and raffinate. In Fig. 4.3 the measured concentrations for both enantiomers in

t^* [s]	410	415	420	430
m_2	1.05	1.09	1.13	1.21
m_3	6.22	6.31	6.41	6.61
P_E [%]	98.4	99.4	98.5	96.6
P_R [%]	99.5	94.7	75.8	56.2

Table 4.1: Experimentally achieved purities of the linear separation of the enantiomers of α -ionone in an open loop SG-SMB. Flow rates: $Q_D = 3.634$ ml/min; $Q_E = 1.844$ ml/min; $Q_F = 2.66$ ml/min; $Q_R = 1.826$ ml/min. Racemic feed concentration $c^F = 0.054$ g/l. Average column porosity $\varepsilon^* = 0.62$. Solvent: methanol/water mixture with water fraction x in desorbent and feed: $x_D = 0.2$; $x_F = 0.4$. $T=20^\circ\text{C}$.

extract and raffinate are shown versus the switch time t^* . It can be observed that the concentration of enantiomer 1 goes down in the extract with increasing switch time. The concentration of the impurity, enantiomer 2, is very low but almost constant. Therefore the decrease in purity in the extract can be regarded as a concentration effect due to the decrease of the concentration of target enantiomer 1. In the raffinate the concentration of enantiomer 2 is high and almost constant. With increasing switch time the impurity, enantiomer 1, increases and the purity decreases. This is consistent with the expected trend. It has to be kept in mind that non-idealities and disturbances of the solvent composition in section 3 due to the switching mechanism influence the separation and the real region of complete separation shrinks.

Finally it can be stated that the concept of SG-SMB could be proved experimentally, whereas it has to be mentioned that the process is not as robust as an isocratic SMB separation.

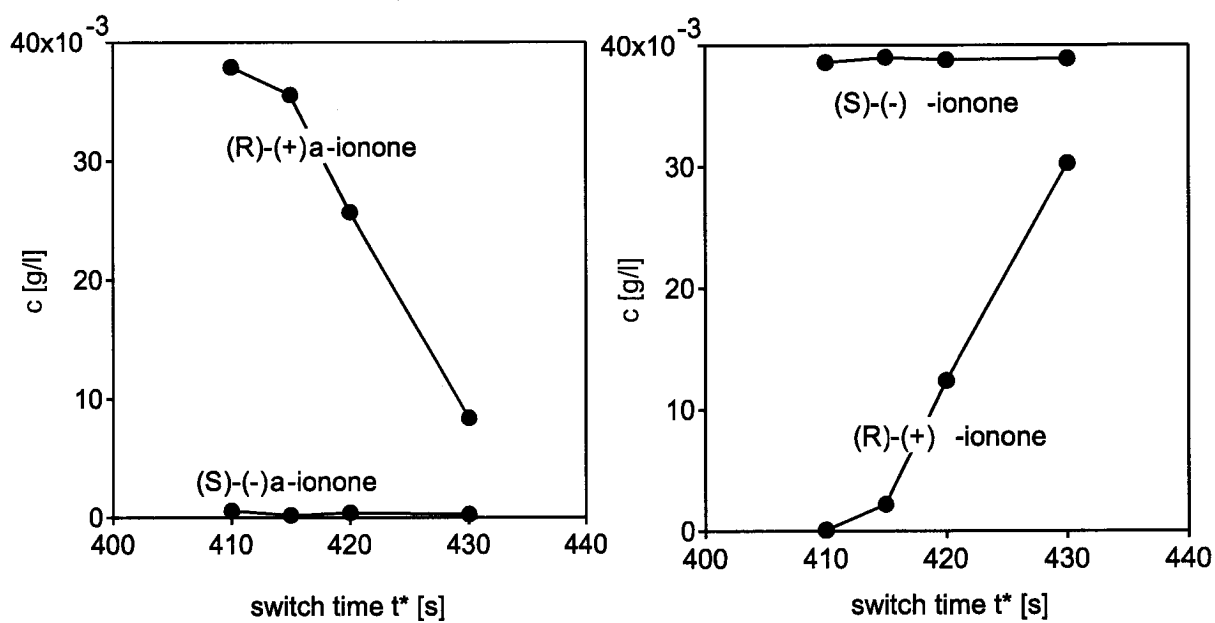


Figure 4.3: Experimental separation of the enantiomers of α -ionone: concentration of both enantiomers (a) in the extract; (b) in the raffinate.

5 Three fraction SMB

In the following a new SMB concept is introduced, which can be especially useful for the separation and the purification of bio-molecules. Such new concept exploits the dynamical characteristics of SMBs, without necessarily being equivalent to a TMB unit. The scheme of the new setup is shown in Fig. 5.1.

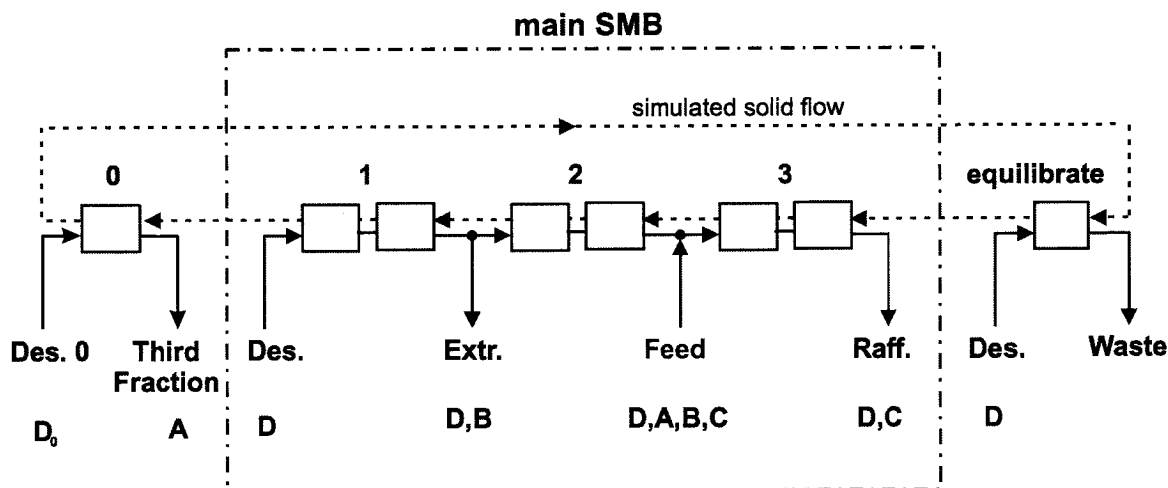


Figure 5.1: Scheme of a 3F-SMB unit, that can be used for a three fraction separation, or to perform CIP continuously.

In the central part of the unit there is the main SMB, here shown as a 2-2-2-0 configuration as used in section 6.3.3. This can be replaced by any other column configuration used in a standard SMB unit. The scheme has a section 0, which can, if necessary, be operated using a different solvent (Des. 0) from that in the main SMB, and a new stream, called the third fraction, can be collected at the end of this section. After passing through section 0, each column is switched to the 'equilibrate' section, which is necessary only if two different solvents are used, in order to re-equilibrate the column using the same solvent as in the main SMB before the column is again included in the main SMB cycle. A separation into three pure fractions is possible for a ternary mixture consisting of three compounds A , B and C with Henry's constants in the sequence $H_A > H_B > H_C$. Under proper operating conditions, the most retained species A will be trapped by the solid phase, eluted in section 0, and collected in the third fraction. The key to obtain both the extract and the third fraction pure is to control the dynamics of the SMB, and how component A propagates. Fig. 5.2 shows the position of the band of component A at different time points during one switching period after the unit has reached cyclic steady

state.

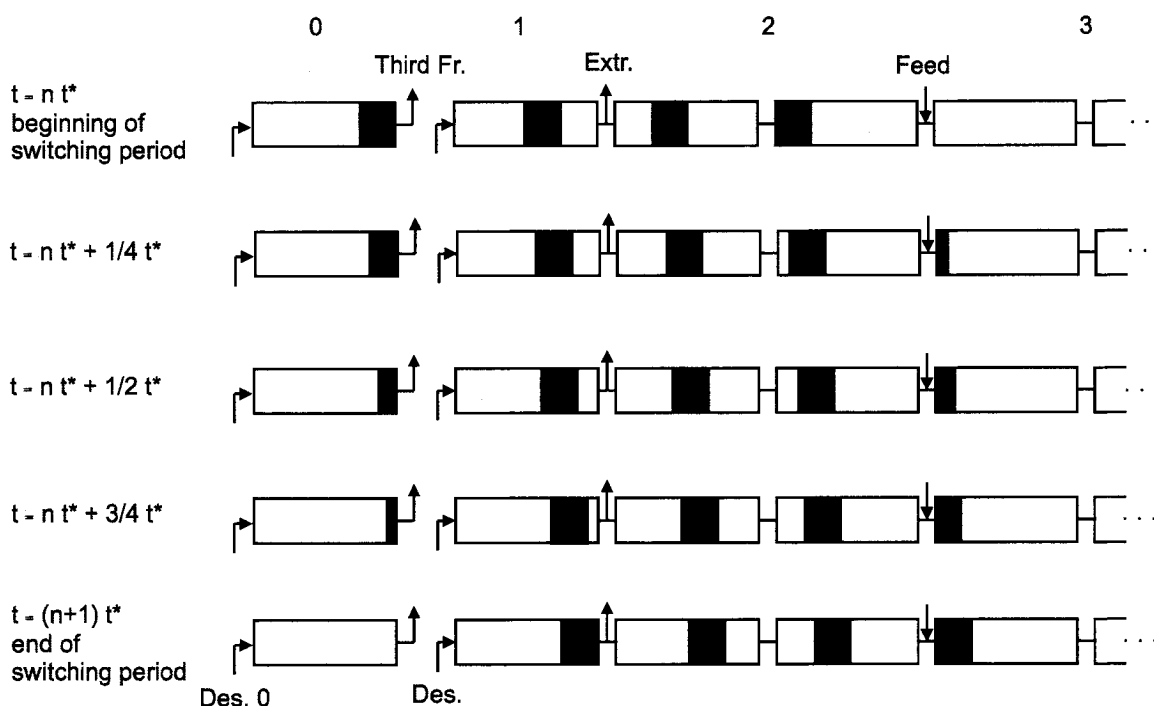


Figure 5.2: Position of successive bands of the most retained component at different times during a switch period. Time increases from the top down.

Component *A* enters the plant with the feed. It advances a bit in the first column of section 3, but is still far away from the column outlet by the time of the switch, when this column is switched to section 2. While the column moves through all positions of section 2, the band advances more, but does not yet reach the end of the column. Then the column is switched to section 1 where compound *B* to be collected in the extract is eluted. This position is critical for this kind of separation, since the extract must not be polluted by compound *A*. This is guaranteed if compound *A* does not reach the end of the column in this position before the switch. After the next switch the column reaches section 0 and all of component *A* can be eluted, if necessary by using a different solvent, and collected in the third fraction. The key feature of this approach is that the band of component *A* can be switched past the extract outlet without ever being in the position to leave the unit with the extract. This is possible in the SMB, due to the simulated nature of the countercurrent solid movement, but would not be possible in a TMB unit. This new operation mode, first proposed in the patent literature [32, 33], is called three-fraction SMB separation, i.e. 3F-SMB in short.

5.1 Design criteria for linear adsorption isotherms

For the 3F-SMB three fraction separation complete separation is regarded as the operation regime where all outlet streams exhibit a purity of 100% with the definition of the purity as:

$$P_T = \frac{c_A^T}{c_A^T + c_B^T + c_C^T} \quad (5.1)$$

$$P_E = \frac{c_B^E}{c_A^E + c_B^E + c_C^E} \quad (5.2)$$

$$P_R = \frac{c_C^R}{c_A^R + c_B^R + c_C^R} \quad (5.3)$$

In the following the constraints on the operating conditions for complete three fraction separation are derived in order to provide a tool for separation design and performance estimation. In addition to the constraints on the binary separation of components B and C according to triangle theory (see chapter 1.2), the band of the most retained component A should not, after being fed to a column, reach the end of that column before it leaves the position in section 1 next to the extract outlet, as it is illustrated in Fig. 5.2. This constraint can be formulated as follows:

$$S_1 + n_2^{col} S_2 + S_3 < L \quad (5.4)$$

where L is the column length, n_2^{col} is the number of columns in section 2 and S_j is the distance component A propagates during a switching period t^* in section j of the SMB unit. For a linear adsorption isotherm, the propagation velocity of component A is independent of the concentration and is given by:

$$w_j = \frac{u_j}{\varepsilon^* + (1 - \varepsilon^*)H_A} \quad (5.5)$$

with u_j being the superficial fluid velocity in section j :

$$u_j = \frac{Q_j}{A} \quad (5.6)$$

Eq. (5.4) can be rewritten using the definition of the distance $S_j = w_j t^*$:

$$w_1 t^* + n_2^{col} w_2 t^* + w_3 t^* < L \quad (5.7)$$

Eq. (1.1) and (5.6) can be combined with Eq. (5.5):

$$w_j = \frac{m_j(1 - \varepsilon^*)V + \varepsilon^*V}{t^*A(\varepsilon^* + (1 - \varepsilon^*)H_A)} \quad (5.8)$$

and to be able to conveniently use the constraint given by Eq. (5.4), it can now be expressed as a function of the flow rate ratios m_j of the sections by combining Eq. (5.7) and (5.8):

$$m_1 < H_A - \frac{\varepsilon^*}{1 - \varepsilon^*} (1 + n_2^{col}) - n_2^{col} m_2 - m_3 \quad (5.9)$$

The obtained relationship can be regarded as an upper bound on m_1 , that still depends on the actual operating point in the (m_2, m_3) plane.

In the presence of significant extra-column dead volume between the chromatographic columns of the SMB unit, two modifications to the equations should be made. First, the modified flow rate ratios should be used, which are obtained from those in Eq. (1.1) by subtracting V_j^D in the numerator of the right hand side, where V_j^D is the dead volume of section j , whereas a detailed description how to account for extra-column dead volume in SMB units can be found in [11]. Second, the upper bound of m_1 in Eq. (5.9) is modified by subtracting on the right hand side the term ϕ , which is defined as follows:

$$\phi = \frac{V_1^D + n_2^{col} V_2^D + V_3^D - (V_{in}^D + V_{out}^D)}{V(1 - \varepsilon)} \quad (5.10)$$

where V_{in}^D and V_{out}^D are the extra-column dead volumes between the inlet port and the column inlet, and between the column outlet and the outlet port, respectively.

Finally, the complete separation conditions for the 3F-SMB separation in case of linear adsorption isotherms can be given by the following relationships:

$$m_1^L = H_B \leq m_1 \leq m_1^U = H_A - \frac{\varepsilon^*}{1 - \varepsilon^*} (1 + n_2^{col}) - \phi - n_2^{col} m_2 - m_3 \quad (5.11)$$

$$H_C \leq m_2 \leq m_3 \leq H_B \quad (5.12)$$

$$\frac{-\varepsilon_P}{1 - \varepsilon_P} \leq m_4 \leq H_C \quad (5.13)$$

Proper conditions to operate section 0 and the equilibration section, if needed, are easy to derive:

$$H_{A,0} \leq m_0 \quad (5.14)$$

whereas $H_{A,0}$ is the Henry's constant of A depending on the solvent used in section 0; and the flow rate in the equilibration section has to be large enough to flush the column completely:

$$0 \leq m_{eq} \quad (5.15)$$

If the time needed to equilibrate a column is larger than t^* , the number of columns in this section should be increased, since $t_{eq} = n_{eq}^{col} t^*$.

The upper bound on m_1 , Eq. (5.11), depends on m_2 and m_3 . As a matter of fact, this enforces a constraint on the values of m_2 and m_3 that allow for the existence of a finite range of feasible m_1 values. This can be obtained by imposing the conditions that the upper bound is larger than the lower one in Eq. (5.11), and leads to a critical line in the (m_2, m_3) plane:

$$m_3 = H_A - \frac{\varepsilon^*}{1 - \varepsilon^*} (1 + n_2^{col}) - \phi - H_B - n_2^{col} m_2 \quad (5.16)$$

Below this line it is possible to find values for m_1 that fulfill Eq. (5.11), that means the third fraction can be collected pure and the extract is not polluted by compound A of the third fraction.

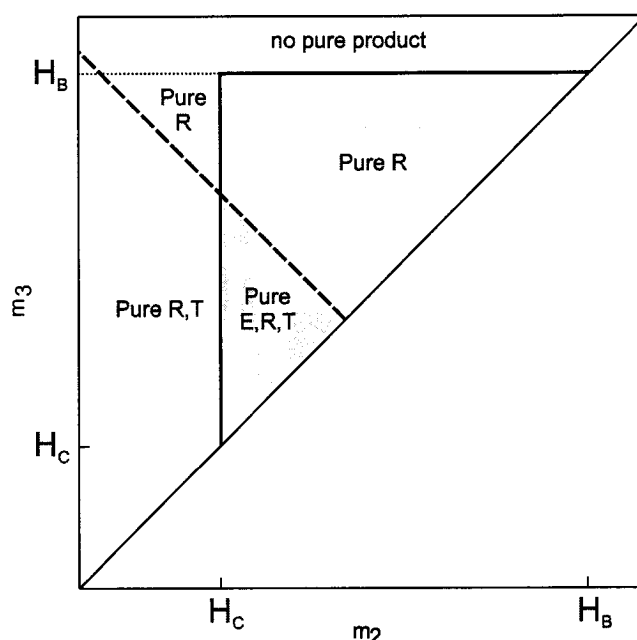


Figure 5.3: Region of complete three fraction separation in the (m_2, m_3) plane.

In Fig. 5.3 the critical line is represented by the broken line, that intersects the binary separation triangle of components B and C . The area below the line which is still part of the triangle is the region of complete separation of all three fractions, provided that suitable values for m_1 and m_4 are chosen. Above the critical line, no suitable value for m_1 , i.e. fulfilling Eq. (5.11), exists, so the constraint has to be violated and neither the purity of the third fraction nor of the extract can be guaranteed. Still there might exist values for m_1 that allow one of the mentioned outlet streams to be pure.

It has to be kept in mind that the position of the critical line with respect to the corresponding binary separation triangle depends on the separation system. Not for all systems

a critical line above or intersecting the triangle and thus creating a region of complete three fraction separation can be found. For a quick check of feasibility the following approach might be useful. Let us consider point $(H_C|H_C)$ in the (m_2, m_3) plane, which is the lower left corner of the binary separation triangle of B and C . In case a region of complete three fraction separation exists, the critical line should be above that point, which is fulfilled if the following inequality holds true:

$$H_A > H_B + (1 + n_2^{col}) \left(H_C + \frac{\varepsilon^*}{(1 - \varepsilon^*)} \right) + \phi \quad (5.17)$$

As it can be readily observed from Eq. (5.17), the number of columns in section 2, n_2^{col} , may be limiting and in many cases the principle of the 3F-SMB, if possible at all, can only work with just one column in section 2. This again might effect the quality of the separation of component B and C in the main part of the SMB. In reality, as the region of complete separation shrinks under the effect of non-idealities [14], also the effective position of the critical line shifts towards smaller values of m_2 and m_3 and thus making the attainment of complete separation conditions in real 3F-SMBs more difficult.

5.2 Performance analysis

In order to investigate the behavior of a 3F-SMB unit and to validate the design criteria derived above, a performance study based on simulations has been carried out. As a model system the separation of the nucleosides thymidine, 2'-deoxyguanosine and 2'-deoxyadenosine (in the following referred to as dT , dG and dA , respectively), on the reversed phase SOURCETM 30RPC, was considered. The Henry's constants of dT , dG and dA have been measured in water containing 5% ethanol as $H_{dA} = 69$, $H_{dT} = 23$ and $H_{dG} = 16.5$ (see chapter 6.2), whereas the axial dispersion coefficient $D_{L,i}$ and the product of the specific surface of the adsorbent particles, a_p , and the overall mass transfer coefficient, k_i , has been measured [34]: $D_L = 0.00375 \text{ cm}^2/\text{sec}$ at $u = 1 \text{ cm/s}$ for all components; $a_p k_{dA} = 0.1 \text{ sec}^{-1}$ and $a_p k_{dG} = a_p k_{dT} = 0.5 \text{ sec}^{-1}$. The columns were $L = 15 \text{ cm}$ long and had an internal diameter of $d = 0.46 \text{ cm}$. The overall bed void fraction was $\varepsilon^* = 0.78$, whereas the porosity of the particles was assumed to be zero. The simulations have been carried out using a detailed one-dimensional model of the SMB unit, the lumped solid diffusion model. This model accounts for all the phenomena taking place in the column: accumulation in the fluid and solid phases, convection and axial dispersion in the fluid phase, and mass transfer assuming that solid diffusion is the rate limiting step [14]. The same detailed column model as described in chapter

1.3 was used. Space discretization is based on finite differences, and 450 grid points per column were used after checking that this practically eliminates the error due to numerical dispersion.

The separation was considered in a 3F-SMB unit, where only the main SMB part in the middle of the unit was simulated, using a 2-1-2-2 column configuration having only one column in section 2. It was assumed that in section 0 all components are completely eluted and the columns are equilibrated before re-entering section 4 of the main SMB loop.

The simulations were carried out moving the operating point along a straight line almost parallel to the diagonal going through different regions in the (m_2, m_3) plane by changing the switch time t^* and keeping all other parameters constant (see Fig. 5.4). This is, among others, a common strategy to investigate SMB performance and look for the separation region [14].

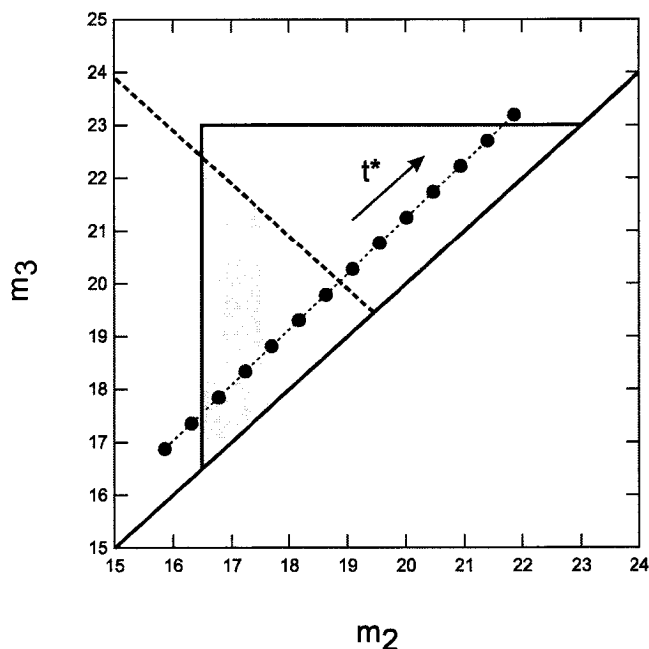


Figure 5.4: Operating points investigated by simulation and region of complete separation of the system of nucleosides in the (m_2, m_3) plane, whereas the large triangular region is the binary separation triangle of dT and dG and the broken line represents the critical line below which dA can be completely separated from dT .

The internal flow rates of the sections 2 to 4 were always kept constant, i.e. $Q_2 = 0.76$ ml/min, $Q_3 = 0.8$ ml/min and $Q_4 = 0.4$ ml/min. The switch time t^* was varied in steps of $\Delta t^* = 20$ s between 840 s and 1100 s. Since section 1 plays a key role for the

three fraction separation, it has been investigated in more detail. Therefore the set of operating points shown in Fig. 5.4 has been repeated with different values for Q_1 , i.e. $Q_1 = 0.8, 0.85, \dots, 1.2$. This can be illustrated in the (m_2, m_1) plane as shown in Fig. 5.5. It has to be kept in mind that each line of operating points in Fig. 5.5 is represented by the same set of operating points in the (m_2, m_3) plane in Fig. 5.4.

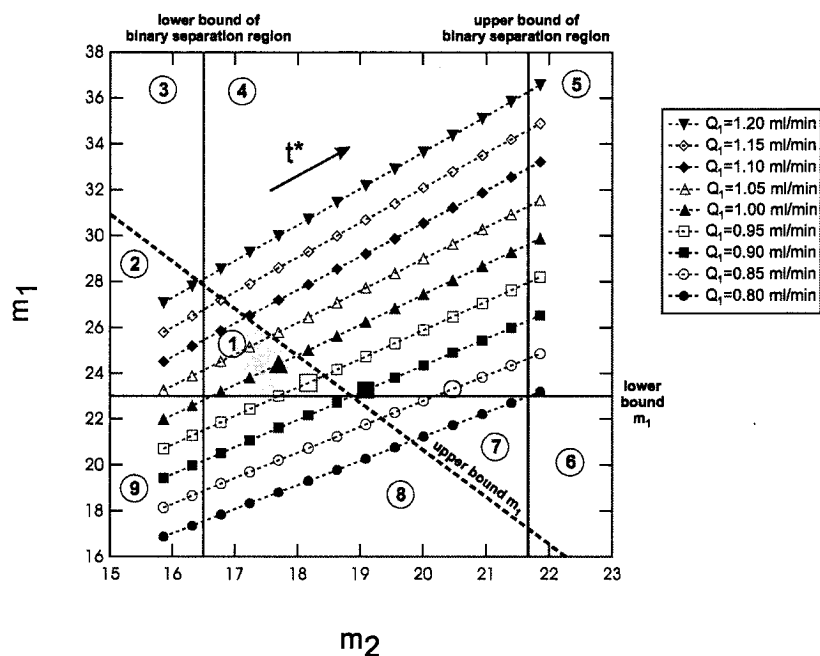


Figure 5.5: Operating points investigated by simulation and region of complete separation of the system of nucleosides in the (m_2, m_1) plane, whereas the two vertical lines are the limits of the binary separation region of dT and dG , the broken line represents the upper limit of m_1 and the horizontal line is the lower limit of m_1 (see Eq. (5.11)). The following outlet streams are expected pure: region 1: E,R,T; region 2: R,T; region 3: R,T; region 4: R,T; region 5: T; region 6: no pure outlet; region 7: R; region 8: E,R; region 9: R.

The simulation results are illustrated in Figs. 5.6,5.7,5.8. As expected, the purity of the raffinate does not depend on Q_1 and only drops below 100% for the operating point in the 'no pure product' region outside the binary separation triangle. From Fig. 5.7 it can be observed that the purity of the third fraction is 100 % for all operating points below the lower bound of m_1 . It only drops if m_1 is not high enough and the third fraction is polluted by dT , which should be collected in the extract. In Fig. 5.8 the behavior of the extract purity, which is less obvious, is illustrated. The shape of the purity surface can be explained as follows. If m_2 is too low and outside the binary separation region, the extract is polluted by dG , which should be collected in the raffinate. This explains the low purity of the two lowest values of m_2 . The operating points below the upper limit for

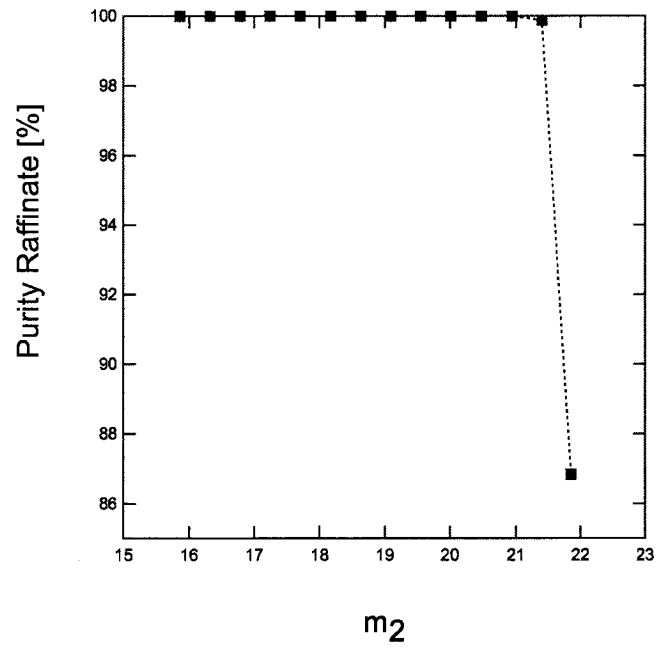


Figure 5.6: Purity of the raffinate for the operating points in Fig. 5.5.

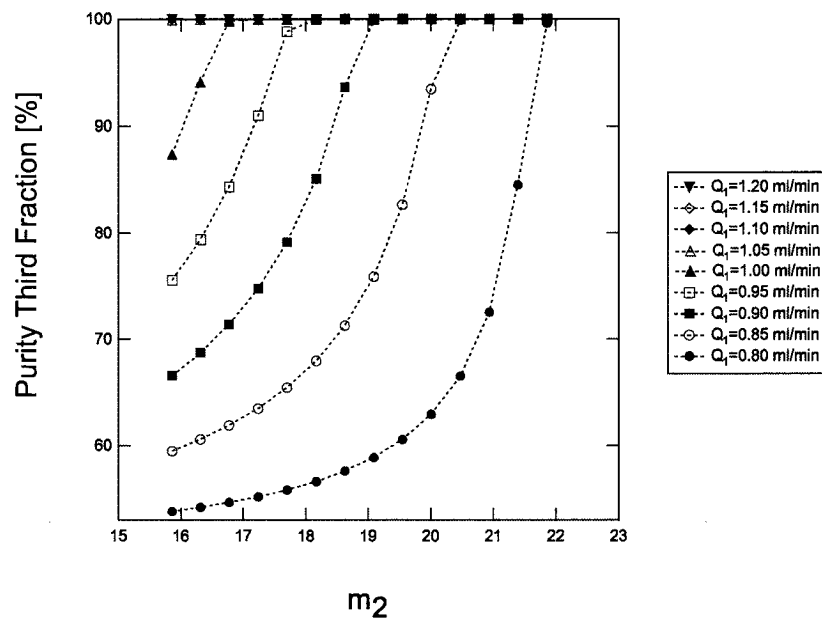


Figure 5.7: Purity of the third fraction for the operating points in Fig. 5.5.

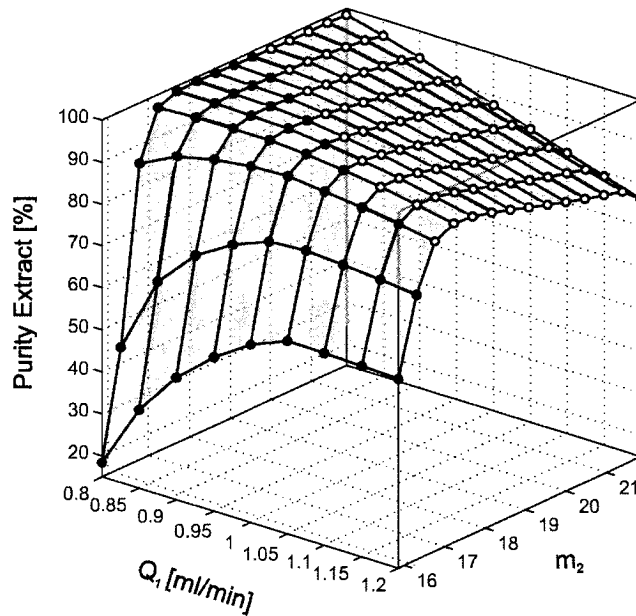


Figure 5.8: Purity of the extract for the operating points in Fig. 5.5, whereas the points indicated by the filled circles are below the upper bound of m_1 .

m_1 are indicated by filled circles. If m_1 is above the upper limit, the extract is polluted by dA , which should be collected in the third fraction. This explains that the extract purity in Fig. 5.8, after reaching a maximum, goes down with increasing values of m_2 . For increasing Q_1 the purity maximum decreases, because the upper limit of m_1 moves closer to the lower boundary of the binary separation region and eventually crosses it, which means that finally the component to be collected in the extract pollutes the third fraction and vice versa. In reality, the size of the complete separation region shrinks due to non-idealities [14], especially when using only one column in section 2. The mentioned effect will increase and it will be even harder to find operating conditions for a good extract purity.

A very interesting effect is that for low values of Q_1 the extract purity decreases very slowly with increasing values of m_2 , whereas it goes down much faster for larger values of Q_1 . This leads to the rather remarkable result, that the operating points leading to the best purities for all three fractions are not necessarily below the critical line. All operating points leading to purities above 97% are summarized in table 5.1 and highlighted using enlarged symbols in Fig. 5.4. This can be explained by a concentration effect caused by the mixed batch/continuous character of the 3F-SMB. Component dA , which should be collected in the third fraction, propagates through the SMB unit like a peak through a

Q_1 [ml/min]	t^*	m_2	m_3	P_{TF}	P_E	P_R
0.85	1040	20.47	21.74	99.93	97.98	100
0.9	980	19.09	20.28	99.87	97.98	100
0.95	940	18.17	19.31	99.99	97.79	100
1.0	920	17.7	18.82	99.99	97.03	100

Table 5.1: Summary of simulation results with purities of all three fractions above 97 %.

batch column, which means that this peak has its maximum height, which depends only on the feed concentration, at the feed point. At the extract point, the concentration of dA will always be lower, for all values of Q_1 . Components dT and dG are separated like in a continuous SMB unit and the characteristic concentration profile is established. That means that the concentration of dT in the extract strongly depends on the extract flow rate Q_E , provided that the third fraction and the raffinate are pure. If Q_E is low, the concentration of dT will be high and vice versa in order to fulfill the material balance in a continuous process, i.e. $c_{dT}^E \propto 1/Q_E$. In contrast to this, the concentration of dA in the extract does not depend on Q_E that way due to the batch character of the separation. The lower the value of Q_1 , the lower is also the extract flow rate Q_E , because in our case Q_2 is kept constant and $Q_E = Q_1 - Q_2$. So the concentration of dT in the extract is increased with decreasing Q_1 , which improves the extract purity with respect to dA and explains the observed effect.

To know about this effect might help the SMB practitioner to find good operating points. Especially if the region of complete separation is small and the extract purity is low, exploiting this effect makes sense.

As an example, Fig. 5.9 shows a concentration profile of the three nucleosides in the main part of the SMB unit. The operating point is in region 4 of Fig. 5.5 just above the lower limit of m_1 . One can observe from the profile in column 1 that at this operating point the third fraction is just not polluted by dT . The profile in column 2 tells us that the extract will be, if only slightly due to the high concentration of dT , polluted by dA . The raffinate is pure.

As a result of this performance study it can be stated that the trends predicted by the design criteria derived from equilibrium theory could be confirmed. In addition to this, it is helpful to keep the character of the mixed batch/continuous process in mind, which can not be completely grasped by the design criteria.

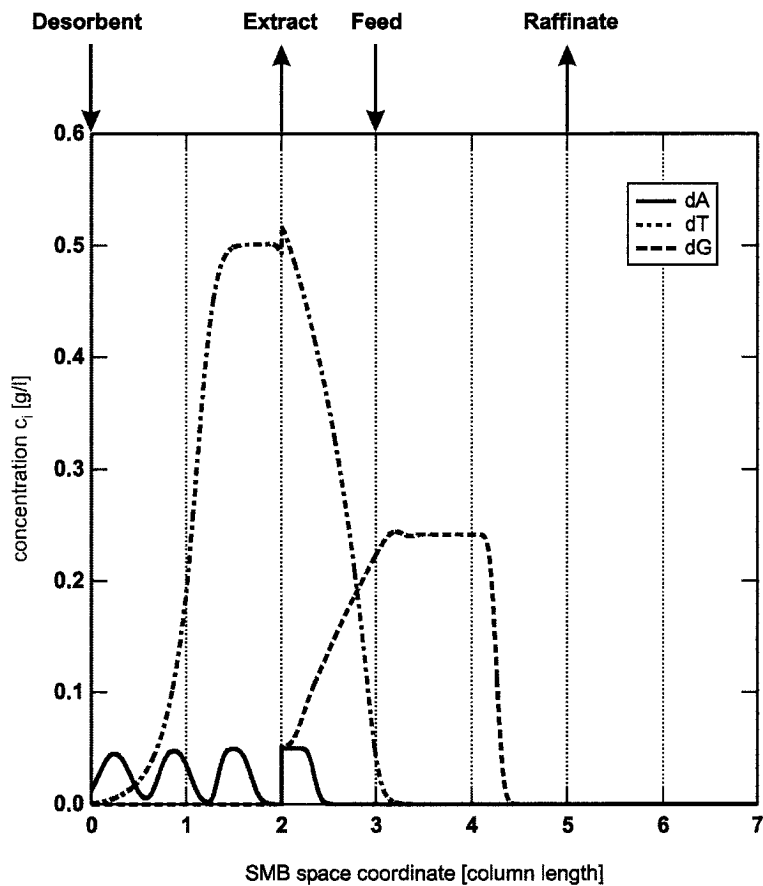


Figure 5.9: Concentration profile in the main SMB part at the beginning of a switch period: $Q_1 = 0.85$ ml/min, $m_2 = 20.47$, $t^* = 1040$ s

6 SMB separation of nucleosides into two fractions and three fractions

6.1 Introduction

In this chapter the use of SMB in the field of bio-separations is considered. The separation of nucleosides, the building blocks of DNA, using different standard and non-standard SMB setups, is investigated. In this context a new SMB setup that allows for continuous CIP is introduced. Also a SMB separation into three fractions is shown, where the non-standard setup benefits from the special dynamics of the SMB and exploits the fact that the SMB is a simulated countercurrent process and not a true countercurrent unit (see chapter 5). This type of separation can no longer be regarded as a technical implementation of the TMB process, as it is the case for the classical binary SMB separation, but it has to be viewed as a new independent multi-column chromatographic process.

Nowadays, the separation of bio-molecules is largely performed using the less efficient batch chromatography, due to the complexity of the mixtures involved in the downstream processing of bio-products. These mixtures usually contain a variety of large molecules and a number of impurities coming from the cell broth. Some of these substances might clog the column due to their size, others might bind very tightly to the stationary phase, precipitate, or denature during the separation process. The target molecules are usually rather dilute. This makes a cleaning in place (CIP) of the column necessary after several uses. CIP is often performed in the reverse flow mode to destroy and remove molecules irreversibly bound to the stationary phase. Applying the classical SMB setup as shown in Fig. 6.1, the columns are used continuously and the scheme does not allow to take out columns for cleaning without shutting down the plant.

6.2 Chromatography of nucleosides

The separation of the nucleosides thymidine, 2'-deoxyguanosine, 2'-deoxyadenosine and 2'-deoxycytidine hydrochloride (in the following referred to as *dT*, *dG*, *dA* and *dC*, respectively), all purchased from Sigma-Aldrich Chemie GmbH (Steinheim, Germany), on the reversed phase SOURCETM 30RPC (Amersham Biosciences AB, Uppsala, Sweden), was considered. This stationary phase is designed for fast, high performance preparative separations of bio-molecules such as proteins, peptides and oligonucleotides and has a matrix based on rigid, polystyrene/divinyl benzene 30 μm mono-sized beads. This material was

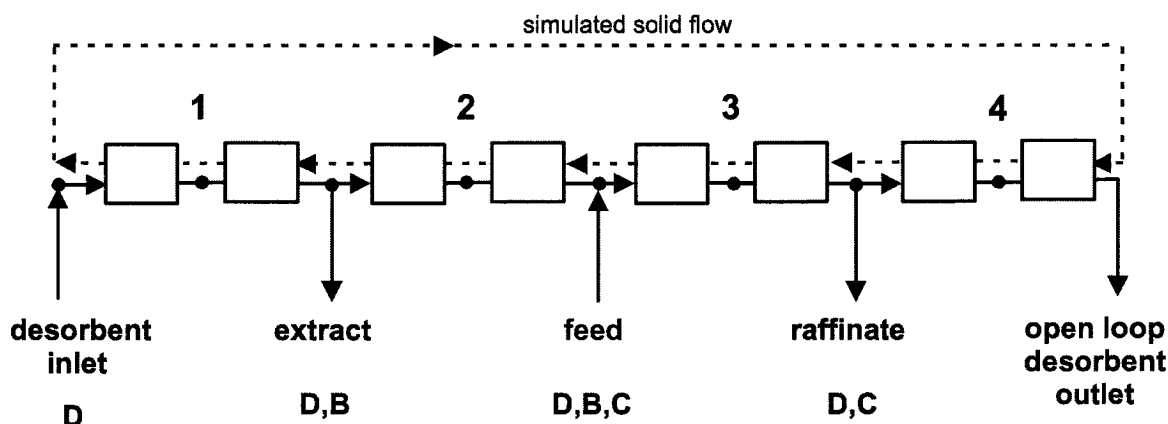


Figure 6.1: Scheme of an open loop four-section SMB unit.

packed into two sets of SMB columns: 6 columns of 10 mm diameter and 10.32 ± 0.3 cm length (column set α) and 7 columns of 4.6 mm diameter and 15 cm length (column set β). For column set α , columns of the type with column plungers for length adjustment and elimination of column dead volume were used, which made it difficult to pack them with identical packing length and/or identical bed porosity. For column set β , standard PEEK columns were used where the bed length is defined by the column length. The porosity was measured by injecting a potassium chloride solution as a non-adsorbing tracer, which is detected at the column outlet by measuring conductivity. The average porosity of both column sets is $\varepsilon = 0.78 \pm 0.02$. As a mobile phase, mixtures of water-ethanol with ethanol fractions between 0 - 12 vol % were used.

The retention behavior of the nucleosides under investigation depends as expected on the composition of the mobile phase, e.g. changing the ratio between a polar and a less polar solvent changes the affinity of the solutes for the solid or the liquid phase. The effect of increasing the ethanol content in the water-ethanol mixture on the Henry's constants of the nucleosides dC , dG , dT and dA at 30°C is illustrated in Fig. 6.2. Nucleosides are detected at the column outlet using a UV detector. Henry's constants are calculated from the retention time in the bed $t_{R,i}$, from which the residence time in the extra column dead volume is subtracted beforehand, using the standard relationship:

$$H_i = \frac{Qt_{R,i} - \varepsilon V}{V(1 - \varepsilon)}, \quad i = dT, dG, dA, dC. \quad (6.1)$$

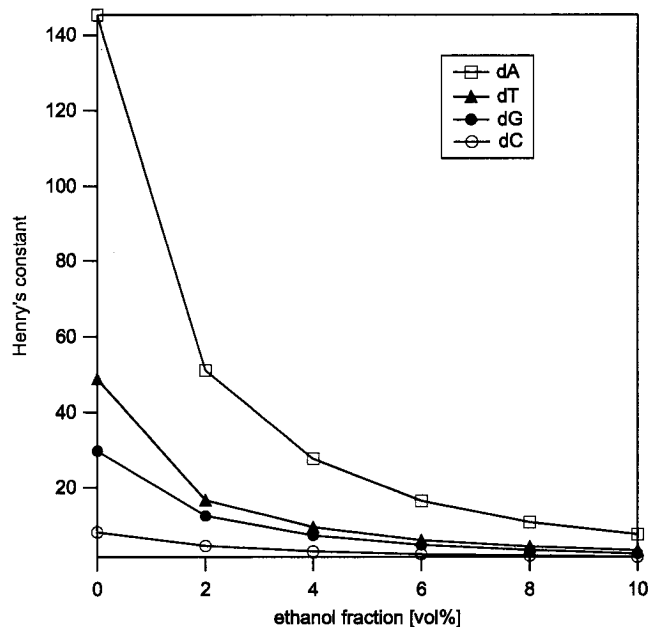


Figure 6.2: Henry's constants of the 4 nucleosides at 30°C as a function of the ethanol volume fraction in an aqueous mobile phase.

6.3 Two fraction SMB separation

To perform a standard binary two fraction SMB separation, the two nucleosides dG and dT have been selected. From Fig. 6.2 it is obvious, that for any ethanol content this pair is the most difficult to separate. In order to choose a reasonable range in Henry's constants for plant operation, the ethanol fraction of 6 vol % has been chosen, corresponding to $H_{dT} = 4.54$ and $H_{dG} = 6.13$. For the experiments described in this chapter column set α (see chapter 6.2) was used.

6.3.1 Experimental setup

A modified ÄKTATMexplorer 100 (Amersham Biosciences AB, Uppsala, Sweden) was used (Fig. 6.3).

The ÄKTAexplorer is a batch chromatography system for fast method and process development, suitable for scale-up of chromatographic separations of biomolecules. To upgrade this system to an SMB, it was necessary to add a number of extra features, which could be achieved by the use of standard components, namely pumps and valves. A custom designed 'SMB strategy', based on standard UNICORNTM control software (Amersham Biosciences AB, Uppsala, Sweden) allows to control all the extra devices. The column

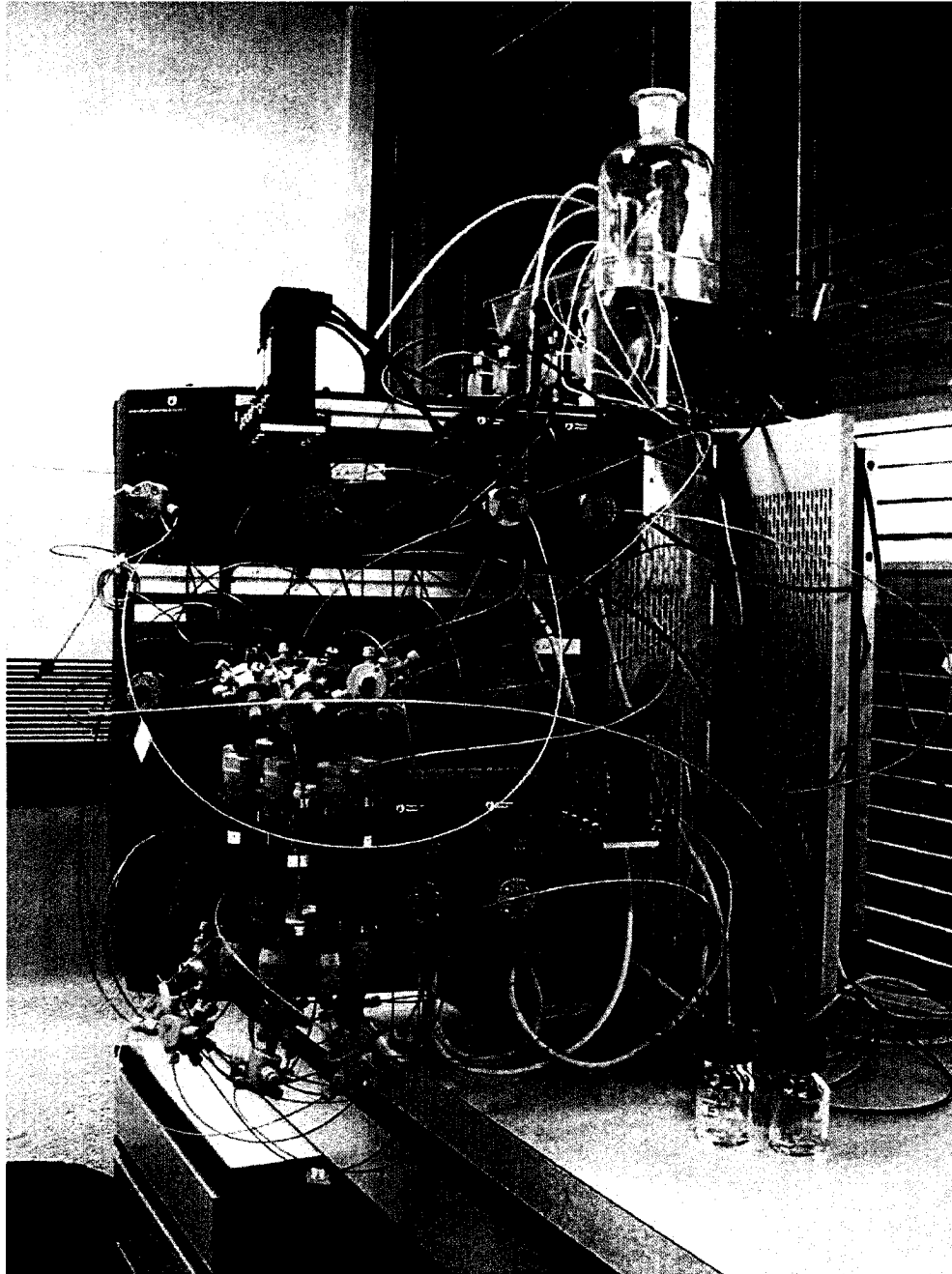


Figure 6.3: Modified batch chromatography system ÄKTAexplorer used as a SMB.

loop of the SMB was built using identical subunits repeating for every column, as shown in Fig. 6.4.

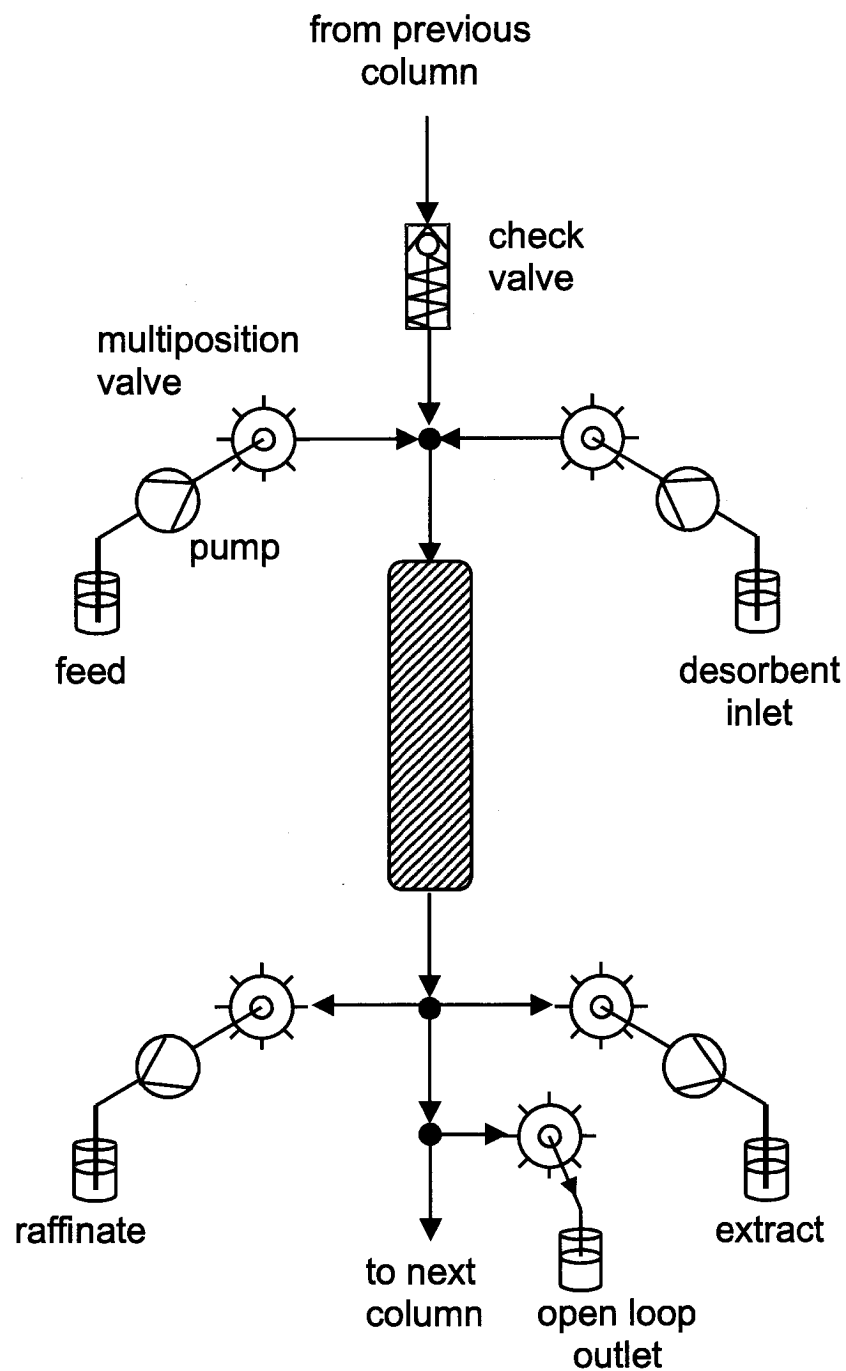


Figure 6.4: Plant setup: single column building block for a conventional SMB as shown in Fig. 6.1.

For the standard SMB setup 4 HPLC pumps are needed, one of each to control the

individual feed and desorbent inlet flows as well as the raffinate and extract outlet flows. In the configuration described here, pump 1 and 2 are provided by the standard P900 gradient pump of the ÄKTAexplorer system. The functionality of two separately operating pumps is achieved by disconnecting the outlets A and B of such a gradient pump from the normally used mixer. In order to control the third and fourth flow of the SMB unit, the system was upgraded by a second P901 module. Each pump has a flow rate range of 0.01 to 100 ml/min. For higher accuracy at low flow rates, pump type P903 (0.001 - 10 ml/min) would be even more ideal. In order to maintain a standardized working pressure in the pumps controlling the raffinate and extract flows, two flow restrictors (4bar) have been installed at the corresponding pump outlets. Each of these four pumps is connected to a multi-position valve of the type PV-908 (one inlet open to one of 8 outlets, or one outlet open to one of 8 inlets), whereas four PV-908 valves are built-in, and an additional PV-908 valve needed for the solvent outlet used in the open loop configuration was added (see Fig. 6.4). Each of the 8 positions of a multi-position valve is assigned to a specific physical column and connected according to the setup shown in Fig. 6.4. The experiments in this chapter have been performed using only six columns, so two positions of the valves remained unused. The column switching is realized by turning the multi-position valves after each switching period to the next position in use. Check valves (CV 3301, Upchurch Scientific, Oak Harbor, USA) between each pair of columns are installed to ensure the correct flow direction. The plant has no temperature control and was operated at $30 \pm 1.5^\circ\text{C}$. Temperature variations of a few degrees, which lead to slight isotherm inaccuracies, had to be accepted.

6.3.2 2-1-2-1 configuration

First, a 2-1-2-1 configuration for an open loop SMB was adopted. The dead volume of the plant was measured to be $V_1^D = 0.598$ ml, $V_2^D = 1.066$ ml, $V_3^D = 0.598$ ml and $V_4^D = 0.754$ ml. It is worth noting that, even in the case of identical assembly for all columns, the dead volume varies from section to section due to the different tubing parts assigned to each individual section: e.g. section 2 goes from the extract outlet to the feed inlet one column further, including the tubing with two check valves and one column, while section 3 goes from the feed inlet to the raffinate outlet two columns downstream including tubing with only one check valve and two columns. The effective liquid flow rate in a SMB is reduced by the extra-column dead volume, which has to be accounted

for when calculating the flow rate ratios m_j [11, 31]:

$$m_j = \frac{Q_j t^* - V\varepsilon - V_j^D}{V(1 - \varepsilon)}, \quad j = 1, \dots, 4 \quad (6.2)$$

For all experiments the external flow rates were kept constant at $Q_D = 2.5$ ml/min, $Q_E = 0.564$ ml/min, $Q_F = 0.08$ ml/min and $Q_R = 0.498$ ml/min. A feed concentration of $c_i^F = 0.5$ g/l for each nucleoside was adopted. Six SMB experiments were carried out with a switch time t^* varying between 7.7 min and 9.5 min, and the outlet concentrations and purities were measured at cyclic steady state. This corresponds to a series of six operating points crossing the region of complete separation in the (m_2, m_3) plane, going from the pure raffinate region, through the complete separation region, to the pure extract region [10]. The results are illustrated in Fig. 6.5 and 6.6, where the extract and raffinate purity, and the dG and dT concentrations in the product outlets, respectively, are plotted as a function of the switch time.

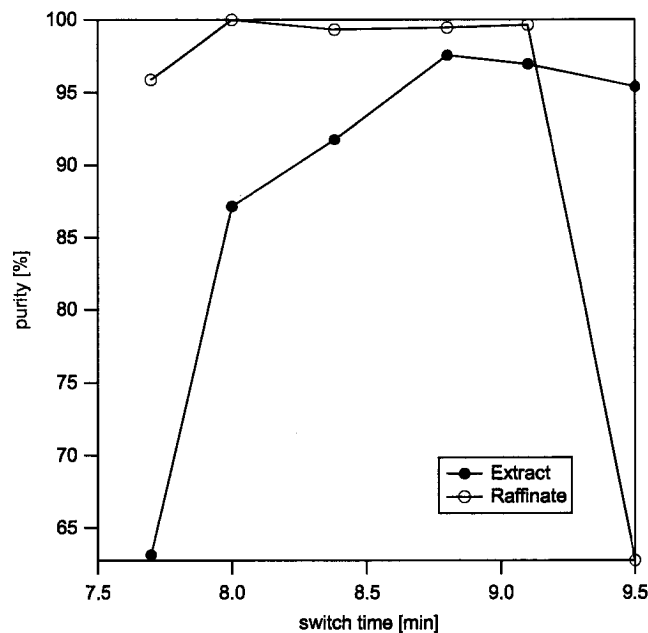


Figure 6.5: Two fraction separation of dG and dT . Purity of extract and raffinate as a function of the switch time, with all flow rates kept constant. SMB configuration: 2-1-2-1.

When looking at Fig. 6.6, it is rather evident that as expected both species essentially increase their concentration in the raffinate and decrease it in the extract as the switch time increases. This leads to an increase in extract purity and decrease in raffinate purity as t^* increases. Such trends are confirmed by the purities plotted in Fig. 6.5, but with exceptions at small and large values of the switch time. In fact, the extract

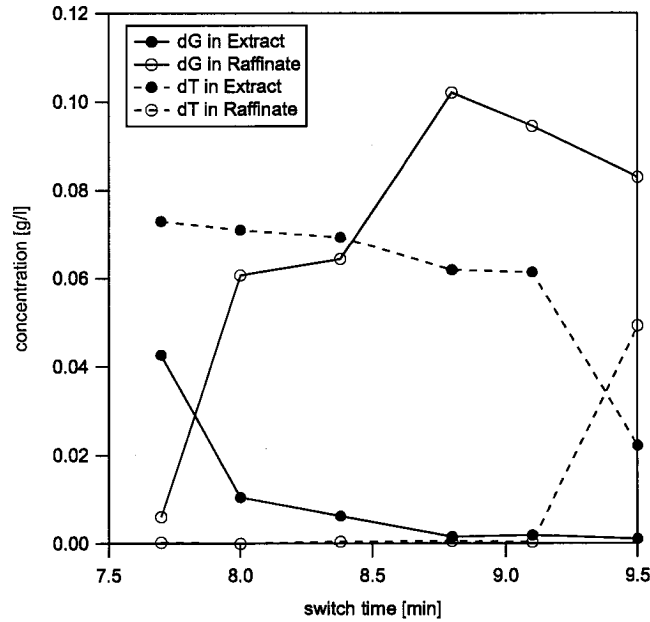


Figure 6.6: Two fraction separation of dG and dT . Outlet concentrations of the nucleosides dG and dT vs. switch time, for the same experiments shown in Fig. 6.5.

purity decreases for $t^* > 9$ min, whereas the raffinate purity decreases (for decreasing t^*) for $t^* < 8$ min. In both cases, the concentration of the main product in the relevant product stream is very low (see Fig. 6.6), and this makes the effect of the presence of the slightest impurity of the other species rather detrimental in terms of purity values. It is also worth noting that very high values of P_R are not accompanied by similarly high values of P_E , which is always below 98 %. We attribute such behavior to the unit configuration, where only one column is used in section 2. This can be viewed as an insufficient way of simulating a countercurrent contact between fluid and solid in section 2. This conjecture has been confirmed by simulation results not reported here, and has led to the series of experiments reported in the next section.

6.3.3 2-2-2-0 configuration

A second series of experiments has been carried out using the same column set α as before, but adopting a 2-2-2-0 configuration. This means that there are two columns in each section from section 1 to 3. There is no section 4 and the raffinate is constituted of the whole stream leaving section 3. In this case, the extra-column dead volume is $V_1^D = 0.598$ ml, $V_2^D = 0.91$ ml, and $V_3^D = 0.598$ ml. Four SMB experiments have been performed using constant external flow rates ($Q_D = 2.5$ ml/min, $Q_E = 0.583$ ml/min,

$Q_F = 0.098$ ml/min), leading to similar operating parameters m_j , as in section 6.3.2. The switch time t^* was varied between 8.4 min and 9.3 min, and the outlet concentrations and purities were measured at cyclic steady state. The results are illustrated in Fig. 6.7, that should be compared with Fig. 6.5. It can be observed that indeed the extract purity has achieved about 99 %, which is a value much closer to the maximum raffinate purity, i.e. 99.5 %. It is worth noting that the raffinate product is significantly more diluted due to the lack of section 4, and this leads also to slightly lower P_R values than in the case of the 2-1-2-1 configuration.

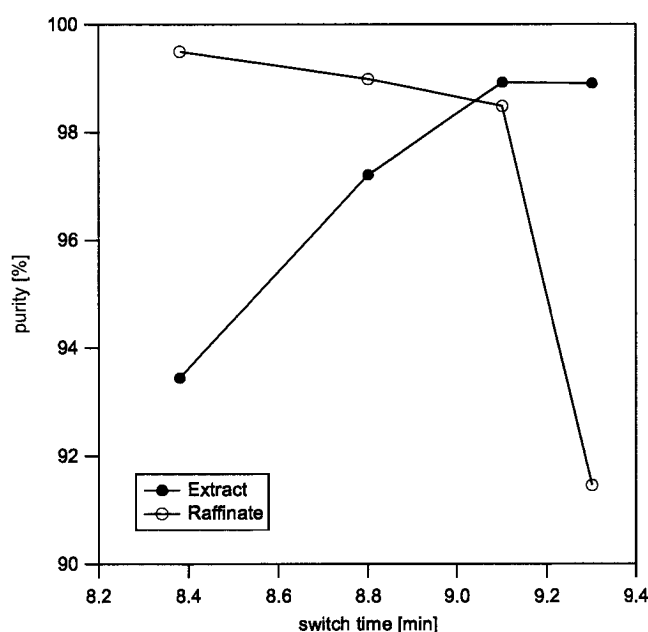


Figure 6.7: Two fraction separation of dG and dT . Purity of extract and raffinate as a function of the switch time, with all flow rates kept constant. SMB configuration: 2-2-2-0.

6.4 Three fraction SMB separation

6.4.1 Experimental setup

In order to implement the 3F-SMB scheme described above, it is necessary to modify the standard column assembly (Fig. 6.4) to that illustrated in Fig. 6.8, which has to accommodate more inlet- and outlet connections to realize the scheme of Fig. 5.1.

An additional pump and the corresponding multi-position valve PV-908 was installed to control Q_{D1} in the 'equilibrate' section. For this purpose the P950 'sample pump' of the ÄKTAexplorer system has been used, which is not a piston pump and not as accurate as

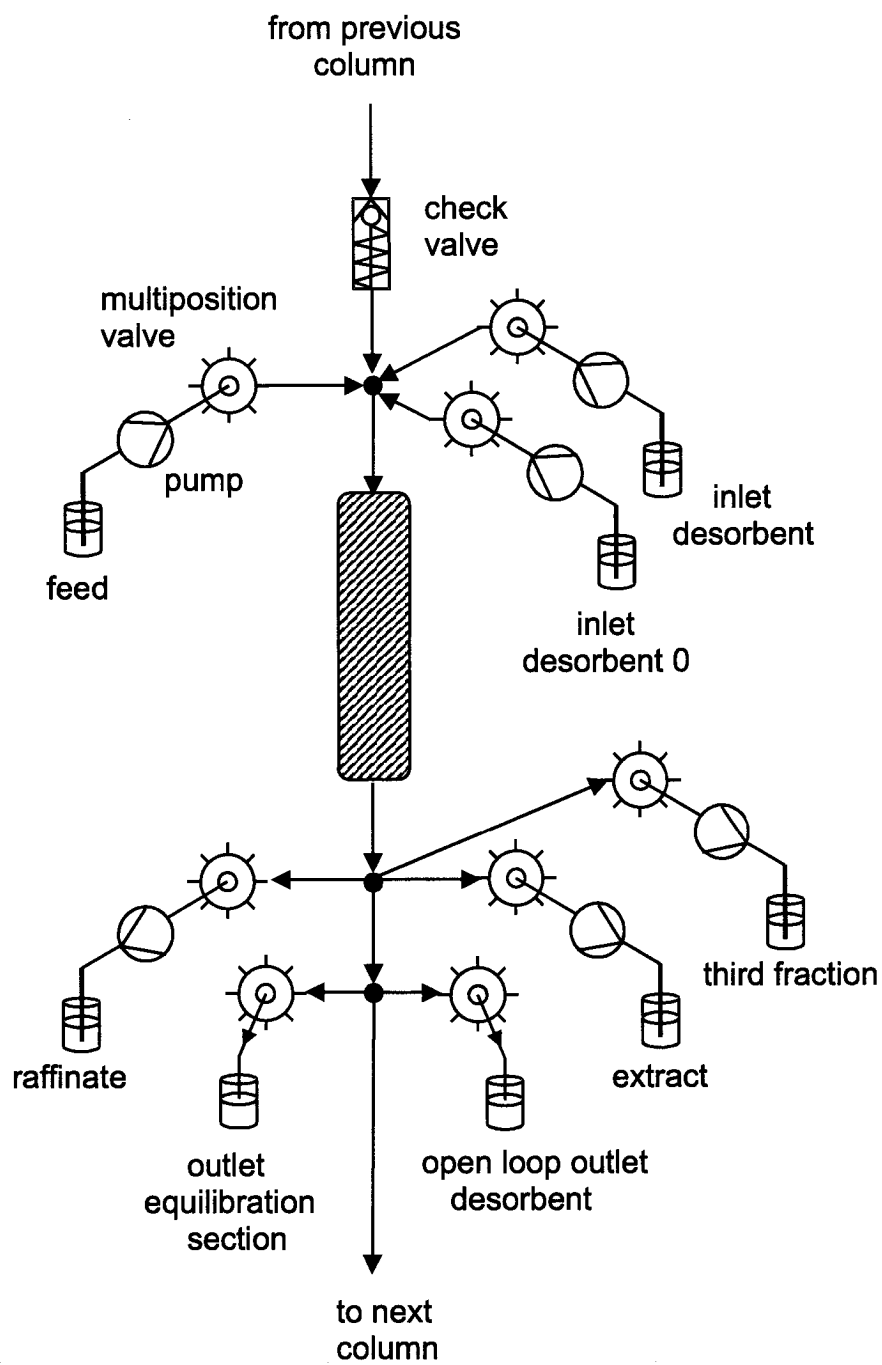


Figure 6.8: Plant setup: single column building block for a 3F-SMB, e.g. as shown in Fig. 5.1.

the P-900 used at the other pump positions of the SMB. For the flow rate the accuracy is less critical. In the following experiments, a 2-1-2-0 configuration in the main SMB part is adopted. This means that since there is no section 4, the raffinate pump is not needed and can be used to pump Q_{D2} to section 0. At the $D2$ inlet another multi-position valve P-908 is used. In order to segregate properly the different parts of the SMB which use different solvents, the functioning of the check valve between the last column of section 0 and section 1 is very important. To allow for a clean partition, the pressure at the inlet of the first column in section 1 has to be higher than the pressure at the third fraction outlet 'T' at any time, which is usually the case when using reasonable flow rates in the main SMB.

6.4.2 Results

The new SMB concept presented above has been investigated experimentally in a series of preliminary tests. Four 3F-SMB runs have been carried out adopting the operation mode described above. The nucleosides dA , dG and dT have been selected for this separation, where dA is to be collected in the third fraction, dT in the extract, and dG in the raffinate. Column set β (see chapter 6.2) was used in an open loop 2-1-2-0 configuration in the main SMB part with one column in section 0 and one column in the equilibration section. The dead volume per column was determined as $V_1^D = 0.245$ ml, $V_2^D = 0.5$ ml and $V_3^D = 0.245$ ml. The operating window of m_1 values according to Eq. (5.11) is a function of the Henry's constants which depend on the ethanol content in the solvent and on the operating point in the (m_2, m_3) plane. It can be readily demonstrated that the ethanol fraction in the solvent is restricted to values below 2.1 vol% for this kind of separation. For the experiments presented in this chapter an ethanol fraction of 1.5 vol%, a bit smaller than the limit, has been adopted in order to work under more robust conditions. In section 0 an ethanol fraction of 12 vol% has been chosen to ensure complete desorption in a reasonable time. All flow rates were kept constant ($Q_{D0} = 1.000$ ml/min, $Q_D = 1.042$ ml/min, $Q_E = 0.258$ ml/min, $Q_F = 0.013$ ml/min and $Q_R = 0.797$ ml/min) and the switch time was varied from $t^* = 14$ min 15 s to $t^* = 16$ min 24 s. A feed concentration of $c_i^F = 0.5$ g/l for each nucleoside was adopted.

In Fig. 6.9 the experimental points are plotted in the (m_2, m_3) plane, together with the triangular region of complete separation for dG and dT , and the critical line below which 3F-SMB operating points should lie (see chapter 5). The grey area in Fig. 6.9 defines the

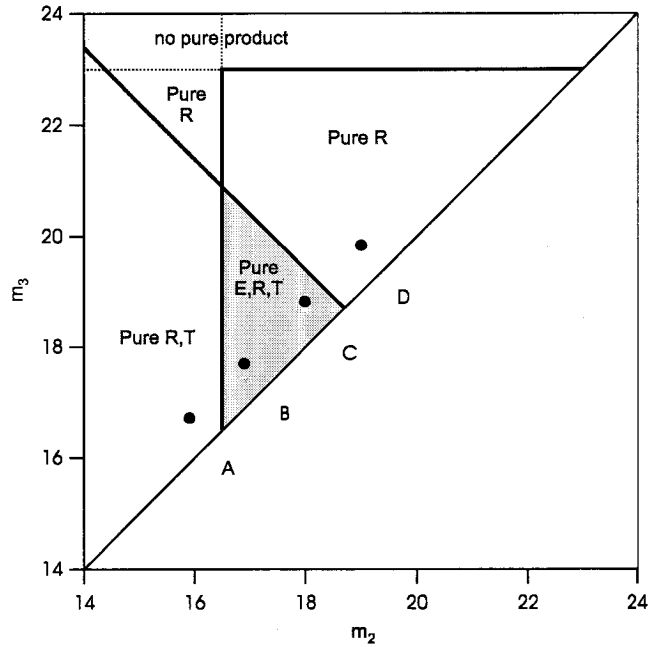


Figure 6.9: Separation regions in the (m_2, m_3) plane for the three fraction separation of dA , dT and dG including experimental operating points. The grey area consists of points achieving complete three fraction separation.

only operating points in the (m_2, m_3) plane leading to a complete three fraction separation, provided m_1 is chosen to fulfill Eq. (5.11). All operating parameters of the experiments together with the corresponding upper and lower bounds on m_1 (m_1^U and m_1^L) according to Eq. (5.11) are reported in Table 6.1.

It can be observed that point C and D do not fulfill Eq. (5.11), whereas for point D no good value for m_1 can be found, since $m_1^L > m_1^U$. The purities of the three product streams are plotted versus the switch time in Fig. 6.10.

It can be observed that the raffinate purity is always 100 %, which is consistent with the theoretical prediction (see Fig. 6.9). The purity of the third fraction increases from A to B , and remains constant in runs C and D at a value slightly below 95 %. It has to be kept in mind that with the adopted experimental strategy of keeping the flow rates constant and just changing the switch time, not only the values of m_2 and m_3 , but also that of m_1 changes according to Eq. (6.2). It can be observed that point A is very close to the lower bound for m_1 , hence the low purity of the third fraction in this case can be explained by its pollution with dT due to a too low m_1 value. The purity of the third fraction increases from point A to B , which is consistent with the increased m_1 value that allows desorbing dT before it reaches section 0. The extract purity increases from A to

	t^* [s]	m_0	m_1	m_2	m_3	m_1^L	m_1^U
A	855	22.15	23.08	15.91	16.72	23.00	27.77
B	896	23.39	24.37	16.89	17.70	23.00	26.79
C	942	24.79	25.84	17.99	18.82	23.00	23.59
D	984	26.07	27.17	18.99	19.84	23.00	21.57

Table 6.1: 3F-SMB separation of dA , dT and dG . Operating conditions of the experimental runs. Flow rates: $Q_0=1.000$ ml/min; $Q_1=1.042$ ml/min; $Q_2=0.784$ ml/min; $Q_3=0.797$ ml/min. Ethanol in section 0: 12 vol% ($H_{dA} = 1.26$); Ethanol in sections 1 to 3: 1.5 vol% ($H_{dA} = 69.0$, $H_{dT} = 23.0$, $H_{dG} = 16.5$); column set β ($\varepsilon=0.78$, $ID = 0.46$ cm, $length=15$ cm); dead volume per column $V_0^D = 0.160$ ml, $V_1^D = 0.245$ ml, $V_2^D = 0.5$ ml and $V_3^D = 0.245$ ml; column configuration in main SMB: 2-1-2-0, 1 column in section 0 and 1 column in the equilibration section; $c_i^F = 0.5$ g/l for each nucleoside.

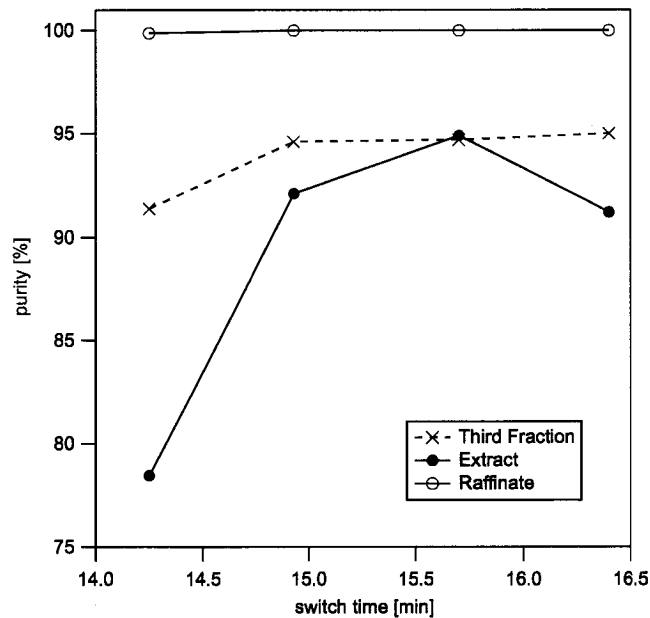


Figure 6.10: Three fraction separation of dA , dT and dG . Product purity vs. switch time, with all flow rates kept constant. SMB configuration as shown in Fig. 5.1.

C , where the maximum purity of about 95 % is reached. It can be concluded that this is the maximum possible value reachable with this configuration where only one column in section 2 is used (see chapters 6.3.2 and 6.3.3). The extract purity decreases again from point C to D . Also this behavior is in accordance with our expectations, since m_1 is larger than its upper bound thus leading to dA leaking out of section 1 and polluting the extract.

As a result it can be stated that it was possible to find an experimental point for a three fraction separation with purities for all three products above 94%. The theoretical approach used to find the region of complete separation could be used to explain the trends observed in the experiments. We believe that by using more columns in section 2 the purity of the extract with respect to the impurity dG could be improved, as this was the case for the binary separation described in chapter 6.3.2. On the other hand using two columns at this point narrows the possible operating window for m_1 , due to its upper bound in Eq. (5.11). This implies that the application of the 3F-SMB operation mode is limited to cases where the selectivity between the two more retained components is large enough.

6.5 Concluding remarks

In this paper, we report three rather significant new results. First, we have realized a desktop SMB unit, by modifying a standard ÄKTAexplorer workstation. This has been made possible by the rather flexible, modular hardware configuration of the standard ÄKTA system that has allowed for changes and extensions, and by the powerful UNICORN software, for which a non-standard extension could be developed to control a much larger number of devices than the commercial configuration.

Secondly, on this machine we have studied experimentally the separation of different mixtures of nucleosides, and we have shown how critical the number of columns used in section 2 of a conventional SMB is for the extract purity.

Finally, we have introduced and experimentally tested a new operation mode, i.e. the 3F-SMB, that allows for the separation with high purity of three fractions in a single unit and in a single process step. Such a unit has a minimum of four sections when a single mobile phase composition is used, and a minimum of five sections if two different mobile phases are used. In the latter case the 3F-SMB process allows for continuous cleaning in place in section 0 to eliminate impurities that have been irreversibly bound to the

stationary phase. Criteria to design such a new SMB operation have been identified, that allow to evaluate a priori whether the new operation can be applied, and which operating conditions should be selected to achieve complete three fraction separation.

7 Optimizing Control of SMBs

7.1 Introduction

Contrary to true countercurrent processes such as the TMB, SMB does not reach a steady state with constant profiles of all the process variables. Its stationary regime is a cyclic steady state where the concentration profiles along the unit move in the direction of the liquid flow. To simulate the solid movement, the inlet and outlet ports are switched periodically by one column position in the direction of the fluid flow. With respect to the inlet and outlet ports, the concentration profiles shift at each switch by one column position in the direction of the simulated solid movement. As a result, SMB units repeat the same time dependent behavior during each time period between two successive switches of the inlet and outlet ports, and, contrary to the TMB unit, modelling an SMB unit even in the stationary regime requires a time dependent model.

SMB separations are designed using models of different complexity. On the one hand, the Triangle Theory approach can be used, which is based on a local equilibrium model that accounts for competitive adsorption thermodynamics, but neglects column efficiency effects [10]. The advantages of this approach are: easy selection of near-optimal operating conditions based on simple algebraic computations, straightforward analysis of feed composition effects, thorough understanding of how flow rate changes affect separation performance, and the possibility of gaining a good understanding of SMB behavior, which is most useful when developing a new separation. On the other hand, detailed SMB models accounting for column efficiencies are best suited to find the best compromise between separation performance, e.g. productivity, eluent consumption, product purities and separation robustness [14].

How good the choice of the optimal operating conditions made by either approach is depends on the accuracy of the model parameters used in the model. Particularly the adsorption isotherms play a key role, due to their importance in determining the separation performance and to the intrinsic difficulty of their measurement. An additional issue in SMB operation is related to the fact that the unit is rather sensitive to a number of disturbances, e.g. feed composition or temperature changes, when it is operated close to its optimal operating conditions in terms of productivity and solvent consumption, and the stationary phase may undergo aging processes of a chemical and mechanical nature. It is a common practice to keep the operating point of the SMB at a reasonable

distance from these optimal operating conditions in order to guarantee a certain level of robustness. In this case, since the SMB chromatography is a slow process, the unit can be controlled manually by the operator to keep the product specifications. On the other hand, the need for feedback control schemes becomes critical when the SMB units are operated at their optimal operating conditions. Therefore, there is a need to develop a closed-loop control system, which is capable on the one hand of controlling the SMB unit at the desired operating conditions, and on the other hand, of adapting the operating conditions to achieve the best possible separation and to fulfill the process specifications regardless of the disturbances that might occur. Such a control strategy would exploit the full economical potential of the SMB technology. Developing an automatic control concept for an SMB unit is a challenge not only due to its non-steady-state, non-linear, mixed continuous and discrete (the inlet-outlet switches) nature, but also due to the strong lag times that characterize the response to most disturbances. There are a few control approaches in the literature that have been proposed recently. One of them is based on the principle of asymptotically exact input/output-linearization [17, 35]; the controller is based on a nonlinear state estimator using the TMB model. In another one, a model based SMB control is suggested where an optimal trajectory calculated off-line should be followed [36]; the optimal operating trajectories are recalculated and the local controllers are re-synthesized to account for the changes in the system characteristics. Another recently proposed approach makes use of nonlinear wave propagation phenomena and aims to control the two central sections of the SMB unit provided that the regeneration of the solid and liquid phases is guaranteed [37]. The bottle neck of these approaches is the requirement of precise physical data of the system and this would be a significant limitation especially in the case of SMBs applied to systems characterized by nonlinear isotherms. We believe that the SMB control strategy should be based on a small amount of information from basic system characterization measurements. It can be extended and applied easily for SMBs operating under overloaded conditions, i.e. characterized by non-linear adsorption isotherms, without any need of precise system characterization, which already poses itself as a difficult issue. In addition, the control concept should be able to handle multi-variable dynamics with time delays and hard constraints both on the process inputs and the states in a general manner. Model Predictive Control (MPC) has been proven to be the most effective control strategy for this type of problems [38, 39] and will be applied in this work along the lines of what was proposed recently in the literature [40, 41], i.e. the so-called Repetitive Model Predictive Control (RMPC) combining the

concepts of MPC and Repetitive Control (RC). The presented work is the outcome of a collaboration with another Ph.D. student, Gültekin Erdem (Prof. M. Morari) within a joined project of three institutes at ETH, i.e. Prof. M. Mazzotti (Institute of Process Engineering), Prof. M. Morbidelli (Institute for Chemical and Bio-Engineering) and Prof. M. Morari (Automatic Control Laboratory).

7.2 SMB model

Let us consider a four-section, closed-loop SMB comprising various chromatographic columns of volume $V = LA$, where L and A are the column length and the cross-section, respectively. Each section j , ($j = 1, 2, 3, 4$), has a volume V_j , which is V multiplied by the number of columns in section j . For the sake of simplicity, but without loss of generality, all examples in this work will refer to an eight column SMB with two columns per section, i.e. a 2-2-2-2 configuration where $V_j = 2V$. We will also limit the analysis to linear adsorption equilibria, but allow for column-to-column variability by considering different values of the total packing porosity ε_h in the h -th column, $h = 1, \dots, 8$, that can differ from the nominal value ε . Each chromatographic column is modelled using the equilibrium dispersive model (see the Notation section for the meaning of the symbols):

$$\varepsilon_h \frac{\partial c_{i,h}}{\partial t} + (1 - \varepsilon_h) \frac{\partial q_{i,h}^*}{\partial t} + v_h \frac{\partial c_{i,h}}{\partial z} = \varepsilon_h D_i \frac{\partial^2 c_{i,h}}{\partial z^2} \quad (7.1)$$

$$q_{i,h}^* = H_i c_{i,h} \quad (i = A, B; h = 1, \dots, 8), \quad (7.2)$$

In the equations above v_h is the superficial velocity, which is the same for the columns belonging to the same section, i.e. $v_1 = v_2 = Q_1/A$, $v_3 = v_4 = Q_2/A$, $v_5 = v_6 = Q_3/A$ and $v_7 = v_8 = Q_4/A$ for the 2-2-2-2 configuration. Proper boundary conditions (enforcing the inlet/outlet switching mechanism), proper initial conditions, and the following node balances complete the mathematical model (where $Q_h^{I/O}$ identifies the inlet or outlet stream entering or leaving the SMB loop just before column h):

$$v_1 = v_8 + \frac{Q_1^{I/O}}{A} \quad (7.3)$$

$$v_1 c_{i,1}^{in} = v_8 c_{i,8}^{out} + \frac{Q_1^{I/O}}{A} c_{i,1}^{I/O} \quad (7.4)$$

$$v_{h+1} = v_h + \frac{Q_{h+1}^{I/O}}{A}, \quad (h = 1, \dots, 7) \quad (7.5)$$

$$v_{h+1} c_{i,h+1}^{in} = v_h c_{i,h}^{out} + \frac{Q_{h+1}^{I/O}}{A} c_{i,h+1}^{I/O}, \quad (h = 1, \dots, 7) \quad (7.6)$$

	L [cm]	A [cm ²]	ε^*	t^* [s]	N_p	H_A	H_B
base case	10	1	0.7	480	100	4	2

Table 7.1: Summary of system parameters for the base case.

The SMB configuration in Fig.1.2 corresponds to the following specifications: $Q_h^{I/O} = 0$, for $h = 2, 4, 6, 8$; $Q_1^{I/O} = Q_D$; $Q_3^{I/O} = -Q_E$; $Q_5^{I/O} = Q_F$; $Q_7^{I/O} = -Q_R$. Moreover, we have $c_{i,1}^{I/O} = c_i^D$; $c_{i,3}^{I/O} = c_{i,2}^{out}$; $c_{i,5}^{I/O} = c_i^F$; $c_{i,7}^{I/O} = c_{i,6}^{out}$, where $c_{i,h}^{out}$ is the concentration of component i at the outlet of column h . All the column dead volumes are assumed to be negligible.

All the computations in this work refer to a base case where the model parameters summarized in table 7.1 are used. Axial dispersion is such that each column with respect to each solute corresponds to 100 theoretical stages, whereas differences among columns due to packing heterogeneity and velocity variations are neglected. The retention behavior of the two components to be separated is characterized by their Henry's constants in Eq. 7.2.

In implementing the model, axial dispersion, i.e. the right hand side of Eq. 7.1, will be accounted for through numerical dispersion, as discussed elsewhere [14, 42]. It is worth noting that the equilibrium dispersive model is regarded as a good compromise between model accuracy and computational efficiency. The SMB mathematical model presented in this section has been used as a virtual plant in this work, and will be referred to simply as SMB plant in the following. Though the adsorption isotherm is linear, the SMB model is nonlinear due to the presence of the convective terms in Eqs. (7.1), (7.4) and (7.6).

7.3 SMB Control

The wish of SMB users is to run an SMB separation where, regardless of the external disturbances, extract and raffinate have constantly the desired properties, e.g. product purity and concentration, while throughput, i.e. the amount of feed processed, is maximized, eluent consumption is minimized, and at the same time process constraints, e.g. maximum pressure drop due to pump limitations or to avoid leakage or damage of the column packing, are fulfilled. Ideally, this should be achieved having only limited information about the system's internal parameters, e.g. the adsorption isotherm that may be difficult to measure or may change during operation due to aging of the packing, and about the state of the system, that can be monitored through appropriate on-line detec-

tors. RMPC is based on the idea that possible model prediction errors and the effect of period-invariant disturbances can be compensated using the measurements of the plant outputs. In essence, as sketched in Fig.7.1, RMPC makes use of an approximate process model to predict the future evolution from the present state of the process. Using these results and the knowledge of the state of the system, the optimizer selects the set of inputs, i.e. the manipulated variables, that allows for the achievement of process specifications and optimal performance.

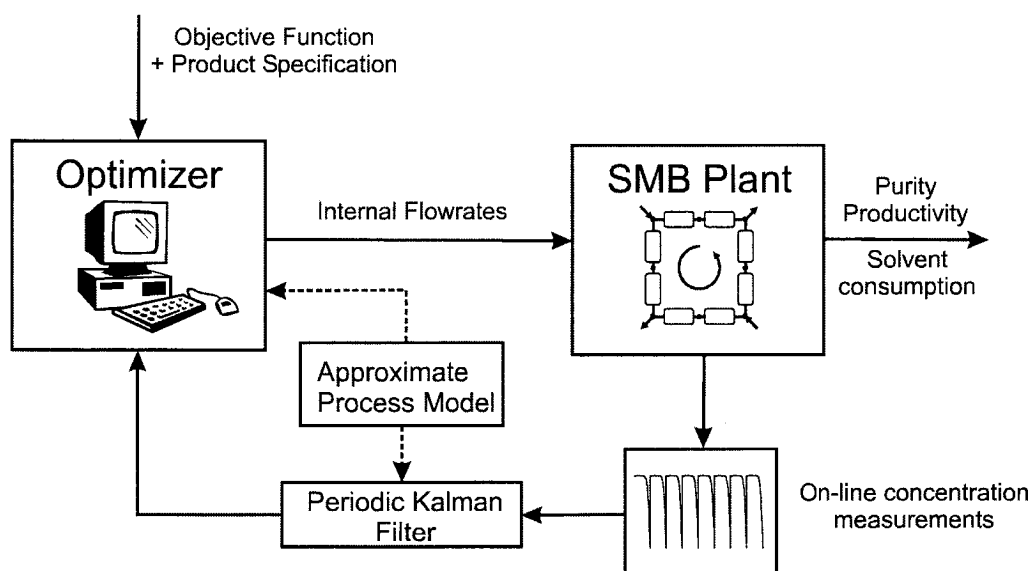


Figure 7.1: Scheme of the Optimizing Control concept.

In the practical implementation a number of problems must be overcome. First, the detailed SMB model presented in section 7.2 is nonlinear, and its solution requires significant computational time. Such a model leads to a nonlinear on-line optimization, which is computationally demanding. This implies that a simplified model of the plant must be used. Next, the state of the system is not easily accessible experimentally. Therefore, it has to be estimated by combining the information coming from the model and the available on-line measurements, e.g. the extract and raffinate compositions in our case. Filtering is needed to account for both the noise in the experimental measurements and for model inaccuracy, and a periodical Kalman filter is best suited for this purpose.

A summary of the features of the proposed control system is reported in the following. A more detailed description will be provided elsewhere [43]. In our approach, the manipulated variables are the four internal SMB flow rates, i.e. Q_1 , Q_2 , Q_3 and Q_4 , which are

adjusted by acting on Q_1 itself and on the external flow rates Q_E , Q_F and Q_R . RMPC requires a predefined process period, therefore the switch time is not used as a manipulated variable, and is kept unchanged during SMB operation. It is worth noting that changing Q_j ($j = I, 2, 3, 4$) affects in a linear manner the value of the corresponding flow rate ratio m_j :

$$m_j = \frac{Q_j t^* - V\varepsilon}{V(1 - \varepsilon)}, \quad (j = I, 2, 3, 4) \quad (7.7)$$

and these are the key variables in determining SMB performance as can be seen easily in the frame of triangle theory.

7.3.1 Simplified SMB model

A simplified SMB model which captures the most important dynamics of the process is derived in the following, starting from the detailed model introduced in section 7.2.

First, the detailed SMB model is used to simulate the cyclic steady state behavior of the plant operated at a reference operating point. In this work, the flow rate ratios $m_I^{ref} = 4.0$, $m_2^{ref} = 2.1$, $m_3^{ref} = 3.9$ and $m_4^{ref} = 2.1$ have been selected as the reference values, with t^* , V as indicated above. The column-to-column variations are unavoidable and not easy to measure precisely, hence it is preferable to have a controller based on only an average porosity value for the columns constituting the SMB unit. Therefore, the nominal porosity value is assigned for each column, i.e. $\varepsilon = 0.7$. The column-to-column variations are considered as a part of the uncertainties that should challenge the controller. The reference operating point is within the complete separation region in the (m_2, m_3) plane very close to its vertex; on the contrary, m_I and m_4 are such that neither the solid nor the fluid phase are fully regenerated. As a result, it leads to a purity of 96.8% for both raffinate and extract. The concentration profiles along the unit change with time, and we define a number of discrete time intervals to capture the dynamics during a switching period at steady state. In this work time steps of a length of $t^*/8$ have been selected, so that between two switches eight different internal concentration profiles are obtained. The numbering of the columns 1 to 8 in Fig.1.2 refers to their logical position in the SMB, i.e. to their position with respect to the inlet and outlet ports. During a cycle, which consists of eight switches, the logical position of the physical columns labeled A,B,...,H, changes from right to left, until every physical column has occupied each logical position once. In the first interval of a cycle, between $t = 0$ and $t = t^*$, the logical positions 1, ..., 8 correspond to the physical columns A, ..., H; between $t = t^*$ and $t = 2t^*$ these

correspond to B, . . . , H, A, and so on until the interval between $t = 7t^*$ and $t = 8t^*$, where they correspond to H, A, . . . , G. At time $t = 8t^*$ one cycle has been completed and the sequence starts again.

The defined number of time steps per switch N_t , e.g. in our case $N_t = 8$, divides a switching period into N_t time intervals of the length t^*/N_t . This subdivides a cycle consisting of N_c switches (here $N_c = 8$) into $N = N_t N_c$ time steps, i.e. $N = 8 \times 8 = 64$ time steps in our case. A discretization in space is also performed using finite differences: ten grid points per column with $N_c = 8$ corresponds to $N_g = 80$ grid points in all. With this space discretization, from Eq. (7.1) we generate one ordinary differential equation (ODE) for every species at each grid point, which in our case with 2 species and $N_g = 80$ leads to a set of 160 ODEs. The $N_t = 8$ internal concentration profiles per switch calculated by the detailed SMB model are used to generate N concentration profiles along the physical columns, each corresponding to one of the 64 discrete time values in the whole cycle. Each of these profiles at the n -th time step is constituted of the concentration values $c_{i,g}^{ref}(n)$, where $i = A, B$ is the component index, and $g = 1, \dots, 80$ is the space index. Now, we should consider that the SMB process is described by eight different models in the eight switching time periods within one cycle, since the outlet and inlet streams have different locations. These are constituted of the same equations (7.1) and (7.2), but different node balances (7.3) to (7.6). For instance Eq. (7.3) reads $u_A = u_H + Q_D/A$ in the first switching period of a cycle, whereas it reads $u_B = u_A + Q_D/A$ in the second, and similarly for the other switching periods and the other columns. By linearizing the SMB model with respect to the state and the manipulated variables around each of the 64 reference internal concentration profiles determined above, we obtain 64 different linearized models, each valid for one of the 64 time steps into which a cycle is divided. As an illustration, nine successive reference composition profiles are shown in Fig.7.2.

The linearization procedure is done as follows: using the detailed model (see Eq. 7.1), 64 reference concentration profiles were determined as described above. For these calculations 100 grid points per column were chosen to obtain a realistic profile. When choosing less grid points, the effect of numerical dispersion will increase [14]. To linearize the model, first of all the system of PDEs of Eq. (7.1) was transformed into ODEs by the method of finite differences. The columns were assumed equal, the axial dispersion term was neglected and a linear adsorption isotherm was assumed. This leaves us with the following

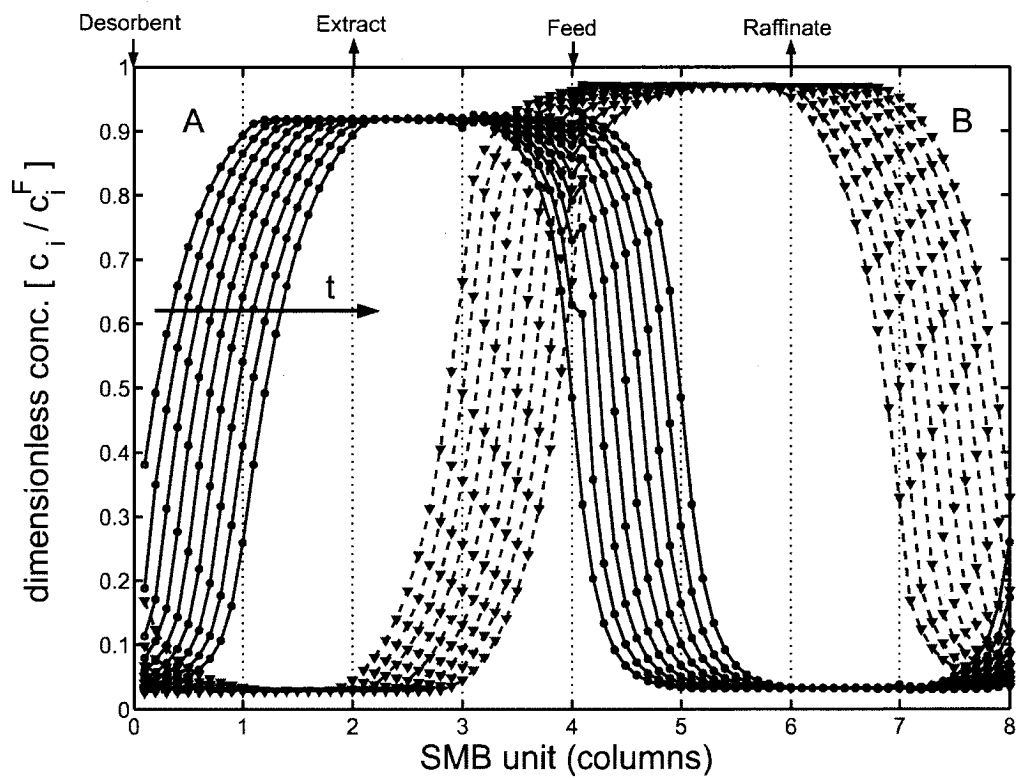


Figure 7.2: Propagation of the concentration profile of substance *A* and *B* inside the SMB unit showing the time and space discretization of the model.

equation for substance i at grid point g :

$$\frac{\partial c_{i,g}}{\partial t} = \frac{v_h}{(\varepsilon + (1 - \varepsilon) H_i) \Delta z} (c_{i,g-1} - c_{i,g}) \quad (7.8)$$

To linearize this equation, a Taylor expansion around each reference concentration profile was performed and the terms from the second derivative on were neglected:

$$\frac{\partial c_{i,g}}{\partial t} = \frac{\partial c_{i,g}^{ref}}{\partial t} + \frac{\partial \frac{\partial c_{i,g}}{\partial t}}{\partial c_{i,g}} (c_{i,g} - c_{i,g}^{ref}) + \frac{\partial \frac{\partial c_{i,g}}{\partial t}}{\partial v_h} (v_h - v_h^{ref}) \quad (7.9)$$

Defining the deviation variables $x = c - c^{ref}$ and $u = v - v^{ref}$, Equ. (7.9) can be rewritten as:

$$\frac{\partial x_{i,g}}{\partial t} = \left(\frac{\partial \frac{\partial c_{i,g}}{\partial t}}{\partial c_{i,g}} \right) x_{i,g} + \left(\frac{\partial \frac{\partial c_{i,g}}{\partial t}}{\partial v_h} \right) u_h \quad (7.10)$$

which is in principle the standard state space formulation of a system of linearized ODEs and can be recast in matrix form:

$$\dot{x} = A_t x + B_t u \quad (t = 1, \dots, N_t) \quad (7.11)$$

where the state vector x (of size 160 in this case) is constituted of the deviations from the reference concentration profiles for both components at each grid point and the input vector u (of a size equal to the number of manipulated variables, i.e. 4 in our case) consists of the deviations of the internal flow rates with respect to the reference values, i.e. $Q_j(n) - Q_j^{ref}(n)$ ($j = 1, 2, 3, 4$), where $Q_j^{ref} = V(m_j^{ref}(1 - \varepsilon) + \varepsilon)/t^*$ from Eq. (7.7). To obtain the output concentrations in extract and raffinate, the following equation is defined:

$$y = C_t x \quad (t = 1, \dots, N_t) \quad (7.12)$$

where vector y holds the concentrations of both components in extract and raffinate.

The set of matrices A_t , B_t and C_t were calculated numerically from Equ. (7.8) for every time step in the cycle. The reference profiles used for linearization are obtained from detailed simulations using 100 grid points per column by sampling every 10th grid point. Being aware that strictly speaking a larger numerical dispersion applies at this decreased number of grid points, the linearization was performed using only 10 grid points in order to keep the size of the resulting simplified model small.

Carrying out analytical integration of the ODEs on a time step of length $t^*/8$, yields a set of equations describing the system dynamics:

$$x_k(n+1) = \mathbf{A}(n)x_k(n) + \mathbf{B}(n)u_k(n), \quad (n = 0, \dots, N-1) \quad (7.13)$$

where k is the cycle index. The matrices A and B are the operators defining the linearized model, which are calculated at the reference state, which is different at every time step n . The transition from one cycle to the next must satisfy:

$$x_{k+1}(0) = x_k(N) \quad (7.14)$$

The output vector y is computed from the state vector x as:

$$y_k(n) = C(n)x_k(n) \quad (7.15)$$

where C is a matrix. In this case the output vector has dimension four since it consists of the concentration levels in the extract and raffinate, which are extracted from the state vector by the operator C . For the sake of clarity, in our case the output is constituted of the values $c_{i,20}$ for the extract and $c_{i,60}$ for the raffinate when t is between 0 and t^* , whereas it consists of $c_{i,30}$ and $c_{i,70}$ for t between t^* and $2t^*$, and so on and so forth. The resultant linear time varying (LTV) state space model given by Eqs. (7.13), (7.14) and (7.15) captures not only the time dependent cyclic steady state dynamics but also the hybrid nature of the SMB process.

As the last step, the LTV model is lifted by grouping the input and output values for one cycle, i.e. for time interval $n = 0$ to N , to obtain a time invariant cycle-to-cycle model [43]. The order of this model is reduced from 160 to 32 by using balanced model reduction [44]. The lifted model is then converted back to an equivalent time-to-time transition model, as proposed by Lee [41]:

$$\tilde{x}_k(n+1) = \tilde{A}(n)\tilde{x}_k(n) + \tilde{B}(n)\tilde{u}_k(n), \quad (n = 0, \dots, N-1) \quad (7.16)$$

$$\tilde{x}_{k+1}(0) = \tilde{P}\tilde{x}_k(N) \quad (7.17)$$

$$y_k(n) = \tilde{C}(n)\tilde{x}_k(n) \quad (7.18)$$

The model formulation is similar to Eqs. (7.13)-(7.15), but it has to be noted that in the reduced order model the state vector \tilde{x} can no longer be directly related to the individual concentration values at certain grid points in the unit. The reduced order model in this form is then used to predict and optimize the future behavior of the SMB. As a final remark, it is worth mentioning that ideally one can define the period of the process as the time between two switches and obtain a similar model. This will lead to a smaller model and optimization problem. On the other hand, using the global period, i.e. a complete cycle, is preferable because it allows to correct for column-to-column variations and extra-column effects which will repeat itself over the cycles.

7.3.2 State estimation

As feedback information from the plant the measured concentrations of all components in both extract and raffinate are used. At time n the computation of the new input variables $\tilde{u}_k(n+1)$ to be implemented at time $n+1$ is started. This requires $\tilde{x}_k(n+1|n)$, i.e. the estimate of the states at time $(n+1)$, $\tilde{x}_k(n+1)$, based on data available at time n . This is determined by a measurement correction step

$$\tilde{x}_k(n|n) = \tilde{x}_k(n|n-1) + \tilde{K}(n)[y_{k,measured}(n) - y_{k,predicted}(n)], \quad (7.19)$$

with

$$y_{k,predicted}(n) = \tilde{C}(n)\tilde{x}_k(n|n-1), \quad (7.20)$$

followed by a model forwarding step:

$$\tilde{x}_k(n+1|n) = \tilde{A}(n)\tilde{x}_k(n|n) + \tilde{B}(n)\tilde{u}_k(n), \quad (7.21)$$

where $\tilde{K}(n)$ is called the filter gain matrix and should be chosen such that the variance of the estimation error is minimized. The resulting estimator is called the Kalman filter and based on the steady-state solution of Riccati Difference Equation [45]. Detailed description of periodic time varying Kalman Filter design and implementation can be found elsewhere [43, 46]. It is worth noting that Eq. (7.21) provides the prediction of the future behavior of the process based on the simplified model and the feedback correction based on the on-line measurements. This is used by the optimizer as described in the following section.

7.3.3 Optimization

For the optimization we use a moving horizon strategy. We determine how to change the manipulated variables over the *control horizon* such that some objective function evaluated over the *prediction horizon* (\geq control horizon) is optimized. We implement the first one of the computed changes and after one time interval we repeat this procedure. Here the control and prediction horizons have been chosen as 1 cycle and 2 cycles, respectively. We seek the minimization of the following objective function, which implies the maximization of production and the minimization of solvent consumption and directly related to the production cost:

$$F = \lambda_1 Q_D^{contr} - \lambda_2 Q_F^{contr}, \quad (7.22)$$

where Q_D^{contr} and Q_F^{contr} are the cumulative solvent consumption and throughput over the control horizon, respectively. λ_1 and λ_2 are the relative weights of the corresponding terms. For our examples we have used $\lambda_1 = 0.25$ and $\lambda_2 = 1.5$. The function F will be referred to as the production cost in the following.

Of course, this problem is subjected to constraints both on the states and the inputs. First of all the purity requirements in the extract and raffinate stream have to be fulfilled; both purity constraints are formulated in terms of the average purity P_E^{pred} and P_R^{pred} over the whole prediction horizon. These nonlinear constraints are linearized around the steady-state values at each time step.

$$P_E^{pred} \geq P_E^{min} \quad (7.23)$$

$$P_R^{pred} \geq P_R^{min} \quad (7.24)$$

Beside the constraints on product specifications, constraints on inputs arising from the physics of the process have to be introduced and must be fulfilled during the whole control horizon. The external flow rates must be nonnegative:

$$Q_R = Q_3 - Q_4 \geq 0 \quad (7.25)$$

$$Q_E = Q_1 - Q_2 \geq 0 \quad (7.26)$$

$$Q_F = Q_3 - Q_2 \geq 0 \quad (7.27)$$

Also the flow rates are limited by the maximum allowable pressure drop resulting in an upper bound for the internal flow rates in section 1 or 3:

$$Q_1 \leq Q_{max} \quad (7.28)$$

$$Q_3 \leq Q_{max} \quad (7.29)$$

In addition the internal flow rates have a physical lower limit of zero.

$$Q_2 \geq 0 \quad (7.30)$$

$$Q_4 \geq 0 \quad (7.31)$$

Finally, it might be necessary for operational reasons to limit the maximum allowable change in internal flow rates:

$$|\Delta Q_j| \leq \Delta Q_j^{max} \quad (j = 1, 2, 3, 4) \quad (7.32)$$

This guarantees that no excessive pressure changes occur that may damage the column packing.

Note that purities less than the desired, P_E^{min} and P_R^{min} , may occur during a transient phase, e.g. during plant start-up or during a response to disturbances. Indeed, there may not exist any flow rate sequence over the given control horizon to meet the purity constraints (Eqs.7.23-7.24) that would render the optimization problem infeasible and would cause problems for online applications. Therefore, the purity constraints are relaxed by introducing nonnegative slack variables s_E and s_R .

$$P_E^{pred} \geq P_E^{min} - s_E \quad (7.33)$$

$$P_R^{pred} \geq P_R^{min} - s_R \quad (7.34)$$

The following cost function together with the constraints (7.23) to (7.32) constitute the optimization problem that is formulated to minimize the cumulative solvent consumption and maximize the total productivity over the control horizon,

$$\min_{Q_j(n'), s_E, s_R} [F + \lambda_3 s_E + \lambda_4 s_R] \quad (7.35)$$

For sufficiently large s_E , s_R values the feasibility of the purity constraints is guaranteed. The slack variables are included in the cost function of the optimization problem (Eq.7.35) with large weights, λ_3 and λ_4 , so that they will be kept as small as possible ($\lambda_3=\lambda_4=10^3$ in our examples). Generally speaking, the higher the weight of a term, the higher its contribution to the cost and the more it is pronounced in the control behavior. On the other hand, it is worth noticing that one should consider the relative order of magnitude of each term constituting the cost function (Eq.7.35) in order to decide on the weights λ_1 to λ_4 . The manipulated variables are the internal flow rates over the control horizon, $Q_j(n')$ with $j = 1, \dots, 4$ and $n' = n + 1, \dots, n + N_{contr}$. N_{contr} corresponds to the number of time steps within the control horizon (64 in our case). The total number of variables for the optimization problem becomes $4N_{contr} + 2$ slack variables. The structure of the optimization problem allows other constraints or different performance indices which may be more appropriate for specific applications. The cost function together with the defined constraints constitutes a Linear Program (LP) to be solved at each time step based on the available new measurements. The flow rate sequence obtained as a result of the optimization problem is applied according to a *receding horizon* strategy, i.e. only the first element of the calculated optimal flow rate sequence corresponding to the current

time is implemented. A new optimization problem is solved at the next time instance based on the new measurements obtained from the plant output.

With reference to a practical implementation of the control algorithm, it should be noted that the computations needed to solve the optimization problem must be carried out in a time smaller than or equal to the duration of a time step, i.e. $t^*/8=60$ s in our work here. It is worth noting that we have used ILOG CPLEX 7.0 as the LP solver and the maximum calculation time to solve the LP was 1.2 seconds (on a PC with a 3 GHz processor) which is far below the sampling time.

7.4 Simulation results for a linear adsorption isotherm

In this section, we present and discuss a number of cases corresponding to different control scenarios, which are meant to assess the performance of the controller. In all simulations the same initial operating point has been selected, i.e. $m_1^{ref} = 4.0$, $m_2^{ref} = 2.1$, $m_3^{ref} = 3.9$ and $m_4^{ref} = 2.1$, which is also the one used as a reference for the model linearization. The same lower bound for product purities has been selected for extract and raffinate, i.e. $P_E^{min} = P_R^{min} = 99\%$. These initial conditions lead to off-spec production in all examined scenarios. The reason is not the bad choice of the operating point in the (m_2, m_3) plane, but rather the wrong values of m_1 and m_4 , which lead to poor regeneration of the adsorbent and the mobile phase, respectively. Poor initial conditions and reference values have been chosen on purpose to better appreciate the performance of the controller. In the following examples, first the cyclic steady state that the SMB reaches in an open loop operation, i.e. without controller action, will be shown; then, the controller is switched on and the attainment of conditions fulfilling product specifications is monitored; later a disturbance is introduced and the SMB operation with on-line control is compared with what happens without the controller.

7.4.1 Base Case

In the first example, the model parameters used by the controller and those of the plant are the same, as far as both the adsorption isotherm and the packing characteristics are concerned. This means that the only source of inaccuracy for the controller model are the numerical approximations introduced, e.g. linearization and model reduction. With reference to Fig.7.3, after letting the SMB operate uncontrolled for 10 cycles, the controller is switched on.

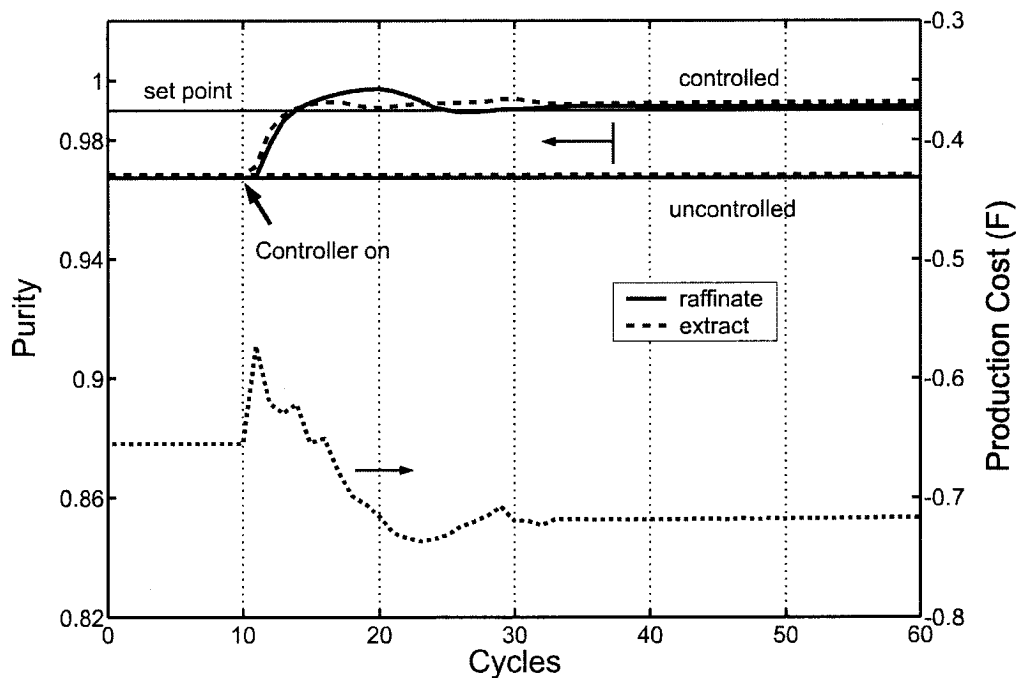


Figure 7.3: Outlet purities for the controlled and the uncontrolled SMB and values of the production cost function, F . The plant and controller models have identical parameters.

It is seen that the controller is able to achieve product specifications from the initial value below 97% in less than five cycles, and stable conditions are achieved about 25 cycles after its activation. Obviously, the uncontrolled plant keeps on operating at the initial off-spec conditions. In Fig.7.3 also the production cost F defined by Eq. (7.22) is shown. It is seen that the controller changes the desorbent and feed flowrate in order to achieve the lowest possible value of F while fulfilling all constraints. When the controller is switched on after cycle 10, it first makes the separation meet process specifications rather quickly, even though this requires a significant increase of F . After the purity specifications are satisfied, the controller adapts the operating conditions to improve the production cost. This continues until about cycle 24 where the purity values approach the lower bound. Therefore, the controller reacts to correct the purities, and this again implies an increase of the production cost. Finally, at about cycle 35, the system settles and the unit operates at a constant value of F , representing the minimum value that the controller was able to achieve while satisfying all the constraints.

In a practical application this behavior would be rather convenient. In fact, the controller first makes sure that the purity specifications are satisfied, which means that the unit produces soon with the desired specifications, and then, on a larger time scale, improves

the production cost by minimizing the function, F . If needed one could, of course, change the relative dynamics of these two processes by acting on the values of the coefficients λ_1 and λ_2 in Eq. (7.22) relative to λ_3 and λ_4 in Eq. (7.35).

A final remark concerns the accuracy of the developed controller in determining the optimal operating conditions. The on-line optimization is based on an approximate model of the plant, which is obtained linearizing the detailed model, and an estimate of the state of the plant given by a Kalman filter. This implies that the optimization achieved can only approximate the optimal performance that can be identified by carrying out nonlinear off-line optimization using the detailed SMB model, i.e. the plant model. A further consequence relates to the specifications or set points. The output purities calculated by the controller are based on a limited number of data points within a cycle, i.e. output concentration values at N different time instances within a cycle. As a consequence, the purity values calculated and fulfilled by the controller and the purity of the actual plant outputs may show slight differences. This explains the minor differences between the attained purity values and the set values, i.e. P_E^{min} , P_R^{min} . Finally, it is also worth noting that no special effort has been made to optimize the controller performance; this is left for a further investigation.

7.4.2 Model/plant mismatch: adsorption isotherms

A typical situation in SMB chromatography is that there is some uncertainty about the parameters of the adsorption isotherm describing the system under consideration. This may be due to several reasons, from measurement errors and uncertainties during isotherm characterization, to packing material degradation, or due to improper temperature control of the chromatographic columns during operation. Although this problem is certainly more significant in the case of nonlinear isotherms for multi-component systems, it is worth considering it also in the case of linear binary isotherms. Therefore, in the second example illustrated in Fig.7.4 we consider a model plant mismatch regarding Henry's constants, H_A and H_B , where the "real" plant values are 4.4 and 2.3, i.e. 10% and 15% larger than the values used by the controller, respectively.

This implies that the plant operates with a selectivity $S = 1.9$, i.e. 4% less than the nominal one. Such discrepancy leads to very poor purity performance when the plant is operated without controller for the given initial conditions. As in the case illustrated in Fig.7.3, the controller is switched on after 10 cycles; the SMB meets the product

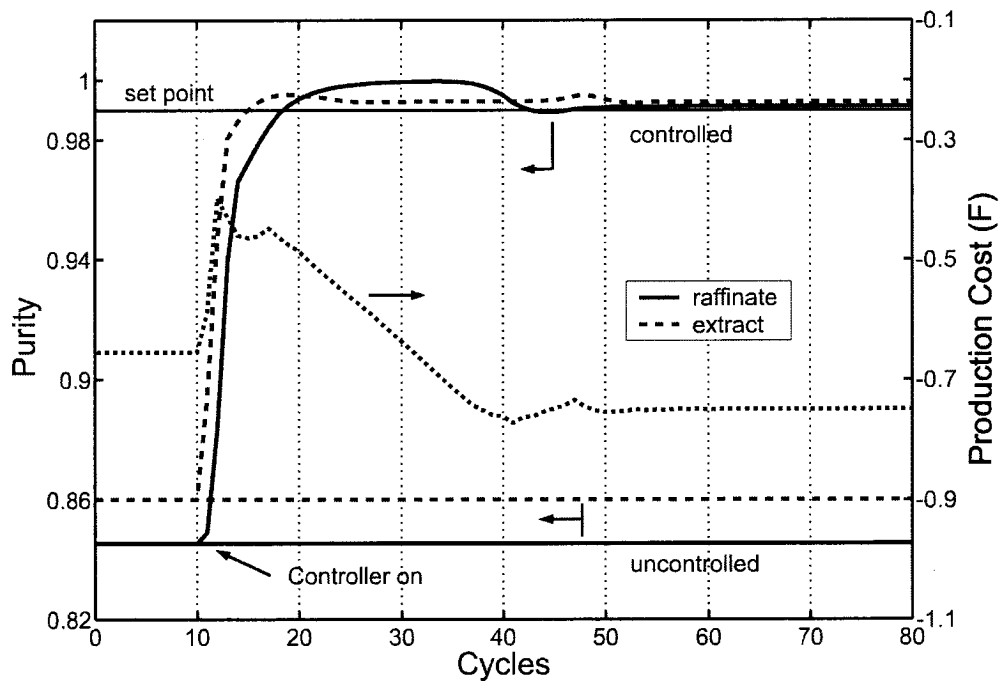


Figure 7.4: Outlet purities for the controlled and the uncontrolled SMB and values of the production cost function, F . The Henry's constants of the model plant are larger than in the controller model ($\Delta H_A = +10\%$, $\Delta H_B = +15\%$).

specifications within eight cycles, and reaches a cyclic steady state about forty cycles later. Also the production cost function F behaves similarly as in the base case. First, the purity specifications are fulfilled at the expense of an increase of F , then the performance is optimized and F decreases, until the purity hits the lower bound. This causes a small increase in F , but then the optimal separation performance is attained and the operation continues with a constant value of F .

In Fig.7.5, the control action is analyzed in terms of operating parameters, i.e. of the flow rate ratios m_j . Fig.7.5a refers to m_2 and m_3 , whereas Fig.7.5b refers to m_4 and m_1 . In the former the complete separation regions defined as $H_B \leq m_2 \leq m_3 \leq H_A$ are shown [10]; the one with solid boundaries applies to the "real" plant, whereas that with dashed boundaries applies to model available to the controller. In Fig.7.5b, the regions of complete regeneration defined by $m_1 \geq H_A$ and $m_4 \leq H_B$ are shown, using the same convention as in Fig.7.5a. In the frame of equilibrium theory, i.e. assuming negligible axial dispersion and mass transfer resistance, high purity separations can be achieved only for operating points located inside the complete separation and regeneration regions shown in Figs. 7.5a and 7.5b, respectively. It can be readily observed that the initial operating point is inside

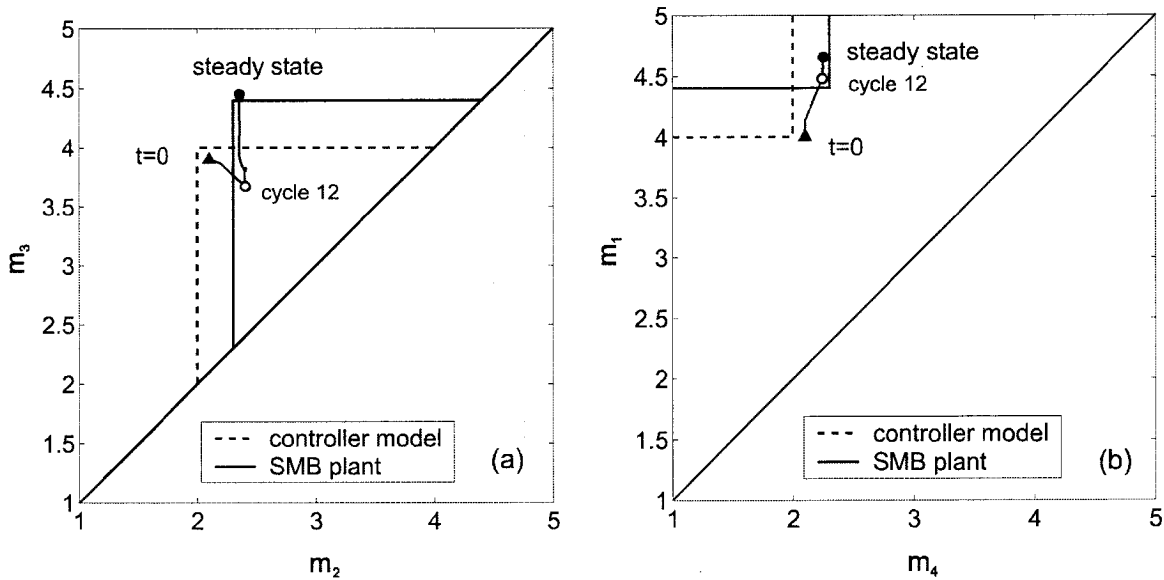


Figure 7.5: Trajectory of the operating point (a) in the (m_2, m_3) plane and (b) in the (m_1, m_4) plane compared to the complete separation and regeneration regions, respectively for the controlled separation shown in Fig.7.4. m values are averaged for each cycle.

the complete separation region of the controller model in the (m_2, m_3) plane and slightly outside its complete regeneration region in the (m_4, m_1) plane. However, it is outside both regions for the SMB plant, which explains the poor initial purity values in Fig.7.4. As soon as the controller is switched on, the operating point moves rapidly towards the correct regions for the plant and enters them after only 2 cycles, i.e. at cycle 12. The operating conditions are adjusted in order to meet first the purity requirements, which occurs after only 8 cycles, and then to improve performance, which requires more time. The operating point moves towards the vertex of the triangle region in Fig.7.5a and to that of the rectangular region in Fig.7.5b (both with solid boundaries, i.e. those applying to the plant). The final operating point is reached about 40 cycles after activation of the controller and is close to the equilibrium theory optimum, which is located at the vertex of both the triangular (complete separation) and rectangular (complete regeneration) regions [10]. This is because high efficiency columns are used in this example, i.e. columns with $N_p = 100$. If lower efficiency columns had been considered, the final operating point would have been further away from the theoretical vertex [14].

7.4.3 Model/plant mismatch: column packing

Another critical issue, particularly in SMB operation, has to do with column packing, which should in principle be exactly the same in all SMB columns, but may exhibit more or less significant differences. Moreover, column efficiency may be difficult to assess, particularly under overload conditions, or may change during operation due to aging of the packing. The example illustrated in Fig.7.6 addresses these issues, by considering a situation where the packing parameters of the plant differ from the nominal ones used by the controller model.

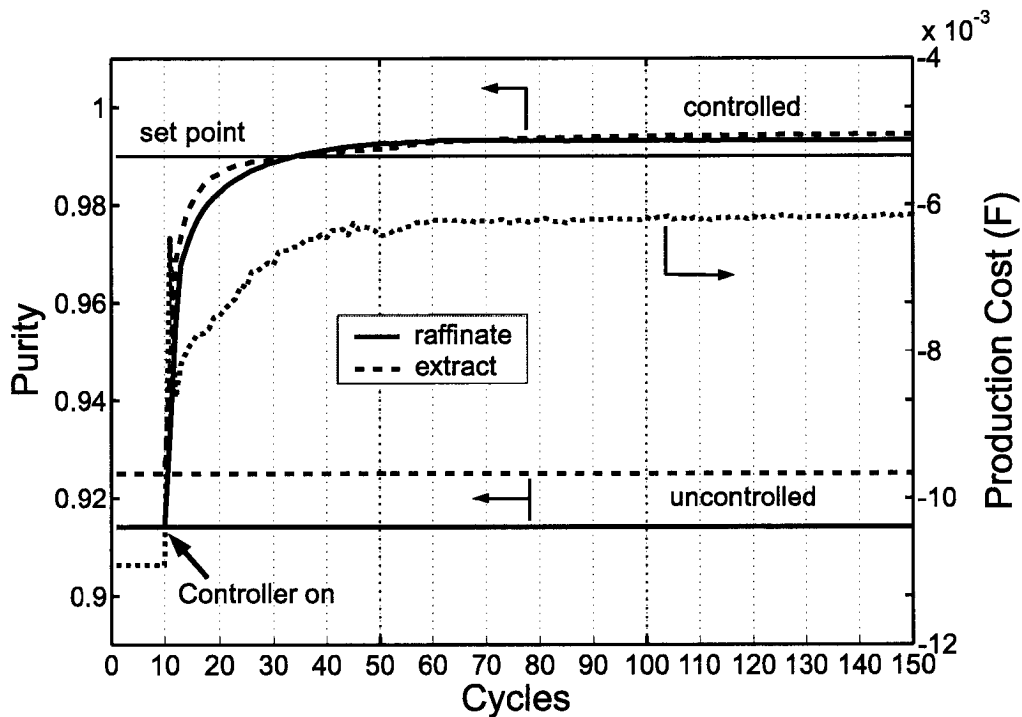


Figure 7.6: Comparison of the SMB outlet purities in the controlled and uncontrolled case. The model plant has the following packing porosity values: $\varepsilon_A = 0.6300$, $\varepsilon_B = 0.8505$, $\varepsilon_C = 0.8505$, $\varepsilon_D = 0.7380$, $\varepsilon_E = 0.4500$, $\varepsilon_F = 0.5220$, $\varepsilon_G = 0.5895$, $\varepsilon_H = 0.4095$, which give a mean porosity that is 10% smaller than that of the controller model. Number of theoretical plates: $N_p = 100$ in the controller model, $N_p = 20$ in the plant model.

In particular, we assume that the average column void fraction in the plant is $\varepsilon = 0.63$, i.e. 10% less than in the model, and that the values for the individual columns differ in a range of $\pm 35\%$ ($\varepsilon_A = 0.6300$, $\varepsilon_B = 0.8505$, $\varepsilon_C = 0.8505$, $\varepsilon_D = 0.7380$, $\varepsilon_E = 0.4500$, $\varepsilon_F = 0.5220$, $\varepsilon_G = 0.5895$, $\varepsilon_H = 0.4095$). In addition, the efficiency of the plant is significantly lower than that of the model; the number of theoretical plates is 20 instead of 100. These deviations might be extreme, but they provide a significant challenge to the robustness

and capabilities of the controller. As in the case considered in the previous section, Fig.7.6 shows that the controller is able to meet the product specifications, even though its action is more sluggish and about 25 and 80 cycles are needed to reach the purity set point and performance stabilization, respectively.

7.4.4 Step disturbance

The next two examples analyze how the controller copes with disturbances that perturb the stationary operation of the SMB unit achieved as described in section 7.4.1 and illustrated in Fig.7.3. In the first case we consider a sudden temperature change, which leads to a step change of the model parameters characterizing the plant operation, e.g. the adsorption isotherm parameters. Such a situation is addressed in Fig.7.7, where it is assumed that after 60 cycles of 'base case' operation (see Fig.7.3) Henry's constants of the plant change by $\pm 15\%$, i.e. they attain the new values $H_A = 3.4$ and $H_B = 2.3$, corresponding to a much reduced selectivity $S = 1.5$, i.e. 25% less than the model value. Such a disturbance leads to a dramatic, unacceptable drop of product purity in the case of the uncontrolled operation, as shown in Fig.7.7*b*. On the other hand, in the case of the controlled SMB operation, the purity drops immediately after the disturbance, but then the controller is able to bring the operation back to fulfill the product specifications in a rather short time, i.e. in about six cycles as seen in Fig.7.7*a*. In the same figure we also see that the production cost, after the product specifications are satisfied, decreases continuously and reaches its minimum value after about forty five cycles. This result shows that even in the presence of a rather dramatic, sudden disturbance, the controller is able to limit the amount of off-spec product that has to be discarded or recycled, and to optimize the separation.

7.4.5 Ramp disturbance

In this example, we consider a similar disturbance as the one analyzed in the previous section, which manifests itself gradually over a finite time interval. We assume that a change of Henry's constants takes place linearly with time. In this case H_A increases from 4 to 4.4, and H_B from 2 to 2.3 in a period of time corresponding to fifty cycles starting from fifty cycles after the controller is switched on. We expect that the final SMB regimes in the controlled and in the uncontrolled case will be similar to those illustrated in Fig.7.7, but that the system transient will be different. The situation considered here is representative

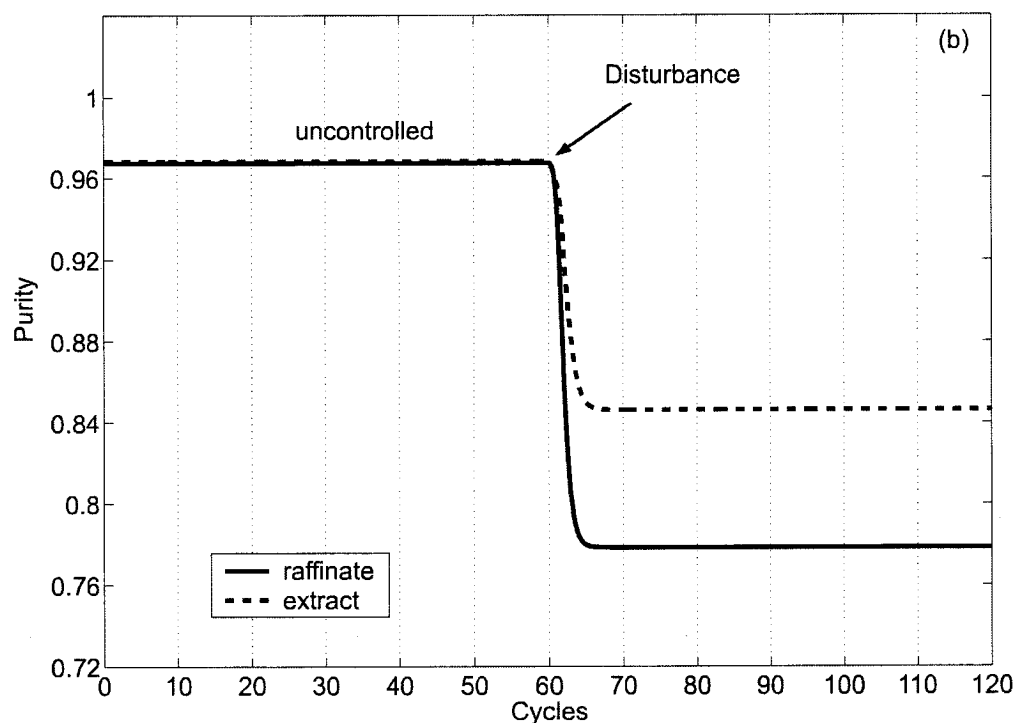
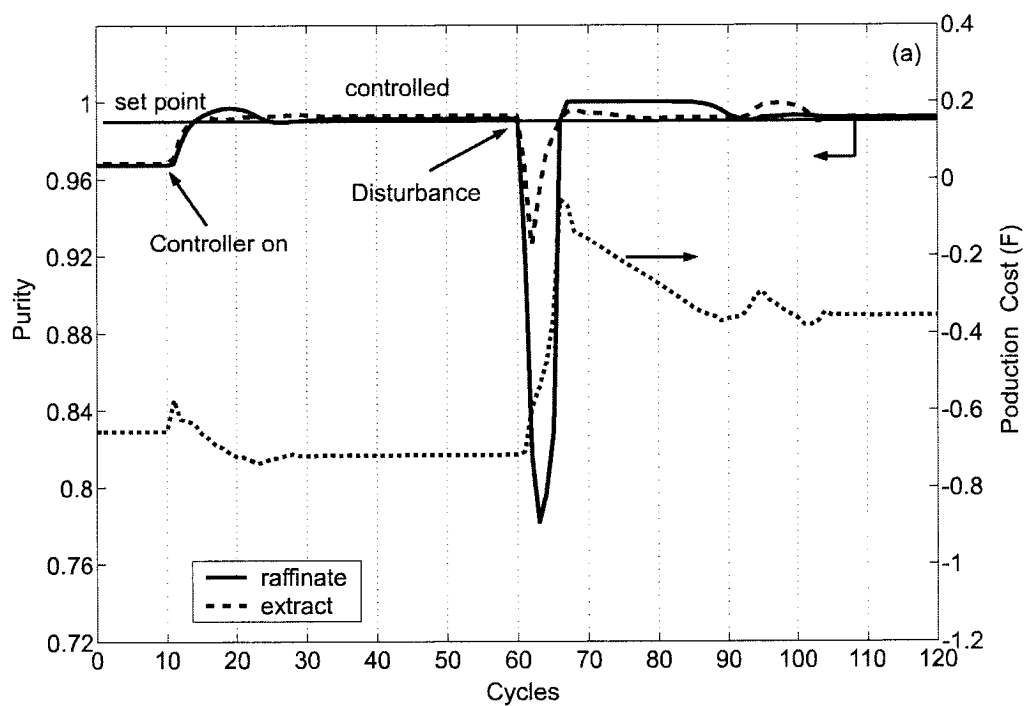


Figure 7.7: Outlet purities for the controlled and the uncontrolled SMB and values of the production cost function, F . The controller is switched on after reaching the steady-state and a step disturbance in Henry's constants takes place at cycle 60. ($\Delta H_A = -15\%$, $\Delta H_B = +15\%$).

of cases where there is a slow aging of the stationary phase, thus modifying gradually the retention behavior of the species to be separated, or where the SMB unit undergoes periodic, e.g. daily, temperature variations.

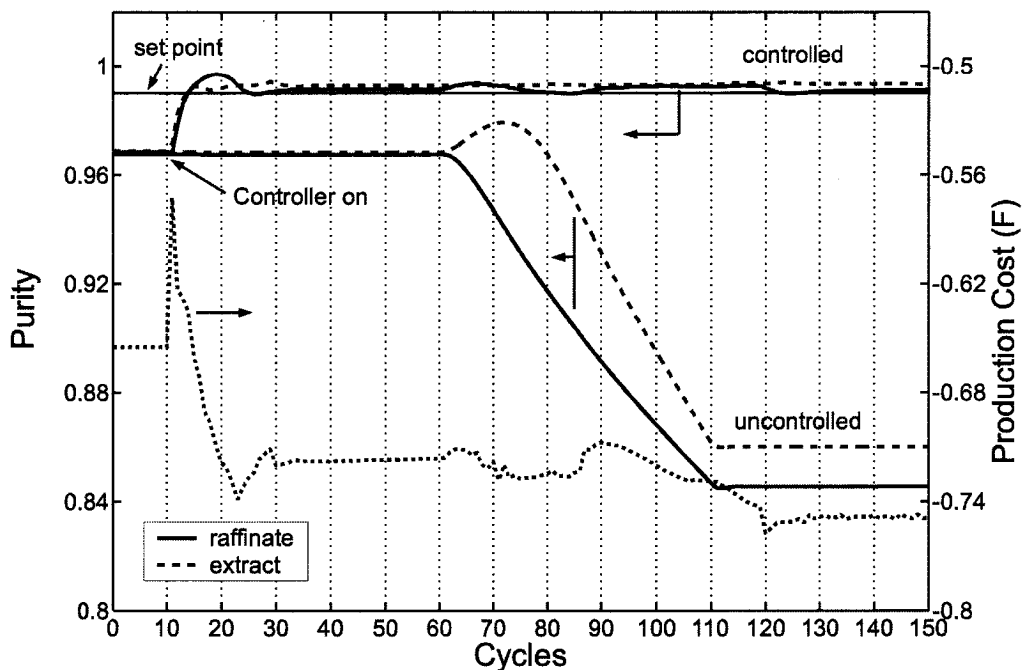


Figure 7.8: Outlet purities for the controlled and the uncontrolled SMB and values of the production cost function, F . The controller is switched on after reaching the steady-state and a ramp disturbance in Henry's constants is applied between cycle 60 and cycle 110. ($\Delta H_A = +10\%$, $\Delta H_B = +15\%$).

The results obtained are illustrated in Fig.7.8. It is seen that starting at cycle 60 the uncontrolled plant exhibits a slow drift towards very low purity values. On the contrary, the controller is able to keep the purity of both extract and raffinate within specifications at all times during and after the change of adsorption parameters.

Fig.7.9 shows how the operating point moves with respect to the actual separation region in the (m_2, m_3) plane, until optimal operating conditions are reached. The three triangles show the complete separation regions corresponding to values of Henry's constant values prevailing at the point in time (cycle number) indicated in the same figure, while the symbols indicate the operating conditions of the controlled plant at the same time. It is seen that these points follow rather closely the vertex of the triangle as expected based on triangle theory. In addition, one can observe that during the ramp disturbance, the distance of the vertex of the complete separation region from the diagonal, which according to triangle theory is proportional to the feed flow rate, increases. This indicates that the

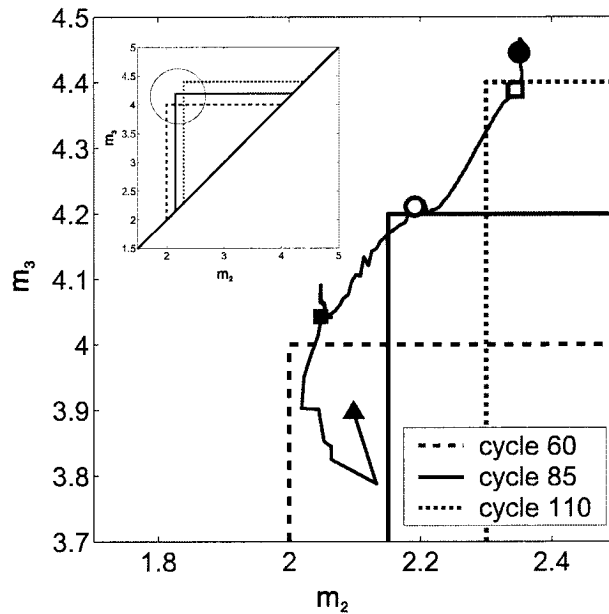


Figure 7.9: Trajectory of the operating point and of the corresponding complete separation region in the (m_2, m_3) plane during the controlled separation shown in Fig.7.8. The symbols correspond to the time $t = 0$ (\blacktriangle), cycle 60 (\blacksquare), cycle 85 (\circ), cycle 120 (\square) and the steady state (\bullet). m values are averaged for each cycle.

function F can achieve better values, since in our case the relative weight given to the feed flow rate, λ_2 in Eq. (7.22), is much larger than that of the desorbent flow rate, λ_1 . As shown in Fig.7.8, better values of F , where the value decreases from -0.71 before the disturbance to -0.75 after it, are in fact found by the controller. This is confirmed by the results shown in Fig.7.7 for the step disturbance. In that case the vertex of the complete separation region after the disturbance is closer to the diagonal, and in fact the controller reaches an optimal value for the production cost at the end of the disturbance which is worse than before, i.e. -0.35 instead of -0.70 . These observations support the fact that the controller is actually able to identify the optimal operating conditions or at least to move in the right direction.

7.5 Conclusions

An optimization based adaptive control strategy for SMBs using Repetitive Model Predictive Control has been developed. The controller uses a simplified, approximate model of the real plant. The strength of this controller is its effectiveness also when the simplified model is not accurate, e.g. where only approximate thermodynamic data, i.e. Henry's

constants, are available. The performance of the controller has been tested thoroughly under extreme model/plant mismatch conditions or large disturbances of various origin; we consider all the results shown here rather encouraging. They indicate that the developed approach provides a promising tool to develop a fully automatized SMB unit. The behavior of the same controller, which is based on a linear isotherm model, has also been successfully tested for separations with nonlinear isotherms. These very promising results are reported in [47].

8 Experimental implementation of SMB control

8.1 System characterisation: SMB separation of nucleosides

The separation of the nucleosides uridine and guanosine (in the following also referred to as *U* and *G*, respectively), purchased from Sigma-Aldrich Chemie GmbH (Steinheim, Germany), on the reversed phase SOURCETM 30RPC (Amersham Biosciences AB, Uppsala, Sweden), was considered. This stationary phase is designed for fast, high performance preparative separations of bio-molecules such as proteins, peptides and oligonucleotides and has a matrix based on rigid, polystyrene/divinyl benzene 30 μm mono-sized beads. This material was slurry packed into 9 standard stainless steel columns (10 cm \times ID 1 cm) using a solvent mixture of 95% water and 5% ethanol with a flow rate of $Q = 20$ ml/min and 30 min packing time. This mixture was assumed to have a similar composition as that to be chosen as mobile phase for the SMB experiments. This was done to avoid shrinking or swelling of the packing material at a later point in time, that might change the packing structure of the columns. The columns were all checked using a test pulse of uridine (see table 8.1).

As a result of the tests, columns 2 to 9 were utilized in the SMB, whereas column 1, where the shape of the test pulse deviated slightly, was kept as a spare column. The overall void fraction, ε^* , of each column has been determined by measuring the retention time of a pulse of pure water, which has been assumed to be a non-retained species and using the following equation:

$$t_0 = \frac{V\varepsilon^*}{Q} \quad (8.1)$$

where t_0 is the retention time of the non-retained species, V is the column volume and Q is the volumetric flow rate. In the following the average void fraction $\varepsilon^* = 0.478$ (see table 8.1) has been used to design the separation. In order to choose the solvent composition for the SMB experiments, the adsorption behavior of uridine and guanosine has been investigated. The Henry's constants H_i were measured for ethanol contents from 0 to 10% by calculating them from the retention times $t_{R,i}$ of dilute peaks, from which the dead time due to the HPLC dead volume had to be subtracted previously:

$$H_i = \frac{\varepsilon^*}{1 - \varepsilon^*} \left(\frac{t_{R,i} - t_0}{t_0} \right) \quad (8.2)$$

The adsorption isotherms were found to be linear according to Equ. 1.4 in all cases.

column nr.	H_U	ε^*
1/spare column	1.667	0.472
2	1.672	0.478
3	1.692	0.483
4	1.687	0.476
5	1.659	0.480
6	1.665	0.475
7	1.677	0.484
8	1.675	0.476
9	1.704	0.476
average	1.677	0.478
σ	0.0144	0.0037

Table 8.1: Column test at 3.5% ethanol in ethanol/water. $c_U=0.3$ g/l; $V_{inj} = 0.5$ μ l.

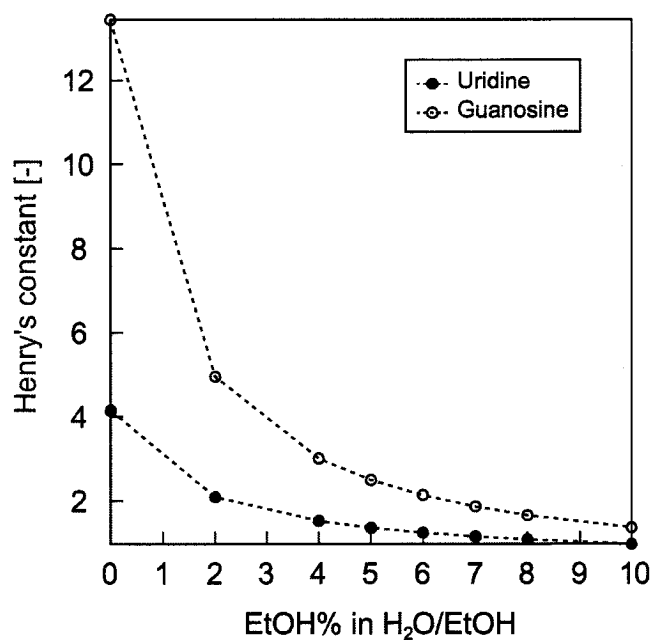


Figure 8.1: Henry's constants of the nucleosides Uridine and Guanosine in mixtures of different ratios of ethanol and water at 22°C.

The temperature sensitivity of the separation has been measured and the Henry's constants for both uridine and guanosine are plotted in Fig. 8.2a for different temperatures. The effect on the region of complete separation in the (m_2, m_3) plane is shown in Fig. 8.2b.

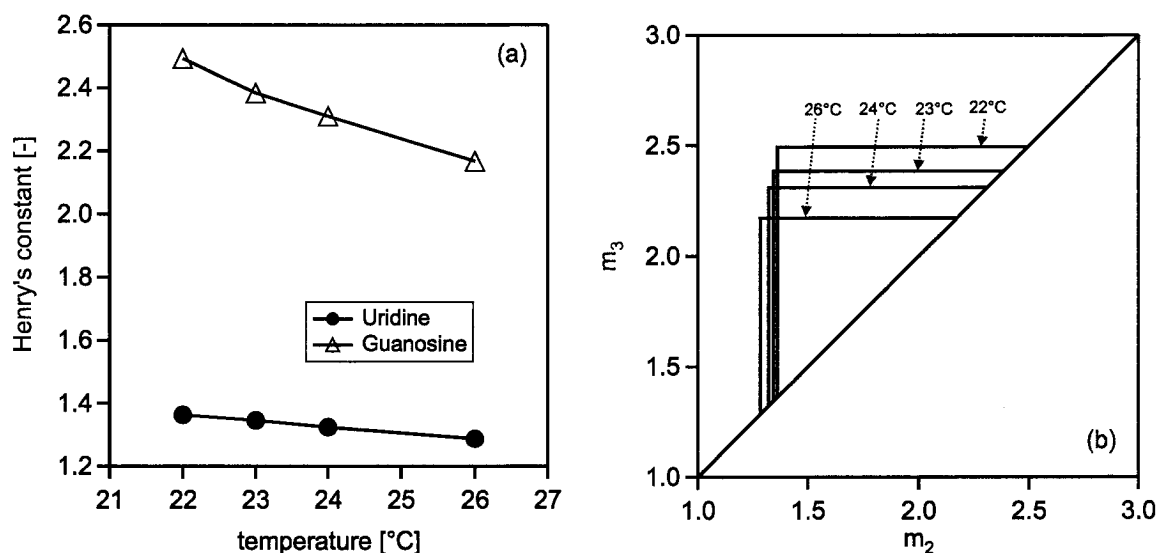


Figure 8.2: (a) Temperature dependence of the Henry's constants of uridine and guanosine at 5% ethanol and (b) the resulting regions of complete separation in the (m_2, m_3) plane at different temperatures.

The effect of the fluid velocity on column efficiency (see Van Deemter plot in Fig. 8.3) and pressure drop (see Equ. (8.5)) has been determined. Column efficiency is expressed in terms of height equivalent to a theoretical plate ($HETP$), where the first term on the right hand side of Equ. (8.3) accounts for eddy diffusion and the second term accounts for mass transfer resistance:

$$HETP_i = a_i + b_i u \quad (8.3)$$

The number of theoretical plates, $N_{p,i}$, and the $HETP_i$ can be determined experimentally according to Equ. (8.4) by measuring the peak width at half height for different fluid velocities under dilute conditions, i.e. for symmetric peaks:

$$N_{p,i} = \frac{L}{HETP_i} = 5.54 \left(\frac{t_{R,i}}{w_{1/2}} \right)^2 \quad (8.4)$$

The pressure drop of the columns is proportional to the velocity and the column length and was measured for an ethanol content of 5%:

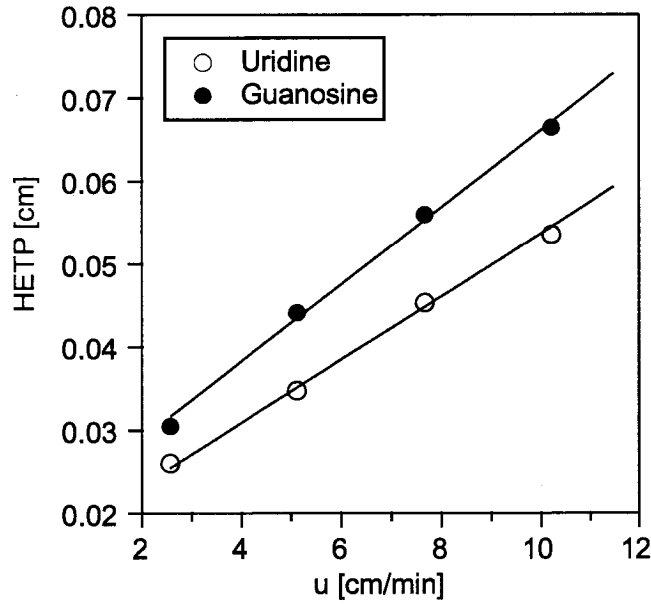


Figure 8.3: HETP measurements and fitted curve according to Equ. (8.14), where molecular diffusion could be neglected; ($D_{L,U} = 0.01645 \text{ cm}^2/\text{s}$ and $D_{L,G} = 0.02069 \text{ cm}^2/\text{s}$ at $u = 1 \text{ cm/s}$, $a_p k_U = 264.68 \text{ 1/s}$, $a_p k_G = 177.54 \text{ 1/s}$).

$$\frac{\Delta p}{uL} = 0.0284 \left[\frac{\text{bar min}}{\text{cm}^2} \right] \quad (8.5)$$

The dead volume in the experimental setup consists of the volume of piping, crossings and check valves. It can be neglected if the ratio between column volume and dead volume is large, which is not the case here but should be the case for most industrial SMB plants. As shown in Fig. 8.4, four different dead volume elements can be identified for each individual SMB column.

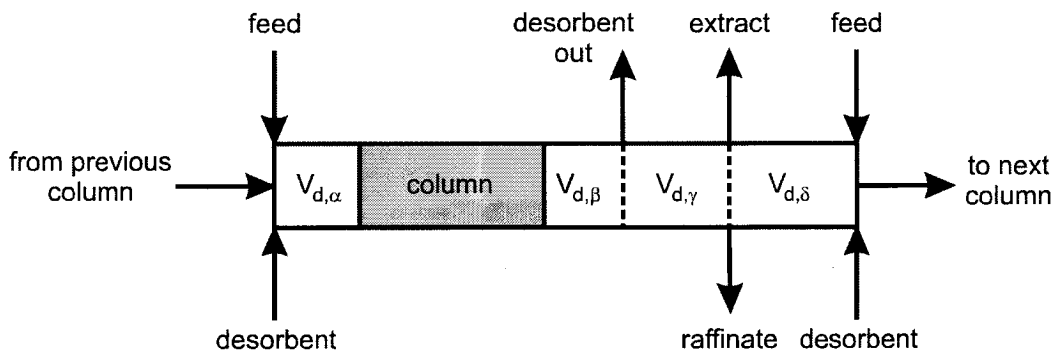


Figure 8.4: Dead volume distribution for one column in the experimental SMB setup.

These dead volume elements have been measured as $V_{d,\alpha} = 0.147 \text{ ml}$, $V_{d,\beta} = 0.407 \text{ ml}$,

$V_{d,\gamma} = 0.035$ ml and $V_{d,\delta} = 1.091$ ml. The dead volume per column in section 1 to 4 can be calculated from the number of columns in the section and the dead volume elements involved:

$$V_1^D = \frac{n_1^{col}(V_{d,\alpha} + V_{d,\beta} + V_{d,\gamma}) + (n_1^{col} - 1)V_{d,\delta}}{n_1^{col}} \quad (8.6)$$

$$V_2^D = \frac{V_{d,\delta} + n_2^{col}(V_{d,\alpha} + V_{d,\beta} + V_{d,\gamma} + V_{d,\delta})}{n_2^{col}} \quad (8.7)$$

$$V_3^D = \frac{n_3^{col}(V_{d,\alpha} + V_{d,\beta} + V_{d,\gamma}) + (n_3^{col} - 1)V_{d,\delta}}{n_3^{col}} \quad (8.8)$$

$$V_4^D = \frac{n_4^{col}(V_{d,\delta} + V_{d,\alpha} + V_{d,\beta}) + (n_4^{col} - 1)V_{d,\gamma}}{n_4^{col}} \quad (8.9)$$

For a 2-2-2-2 column configuration, as it was used in this work, the dead volume was calculated as: $V_1^D = V_3^D = 1.135$ ml, $V_2^D = 2.226$ ml and $V_4^D = 1.663$ ml.

Equ. (8.10) [11] allows to calculate a dead volume correction for the flow rates Q_j to be able to use the same constraints on m_j for process design as in the case of no dead volume in the plant:

$$m_j = \frac{Q_j t^* - V\varepsilon - V_j^D}{V(1 - \varepsilon)} \quad (8.10)$$

As a next step the open loop SMB described in chapter 4.1 has been closed according to the arrangement illustrated in Fig. 8.5.

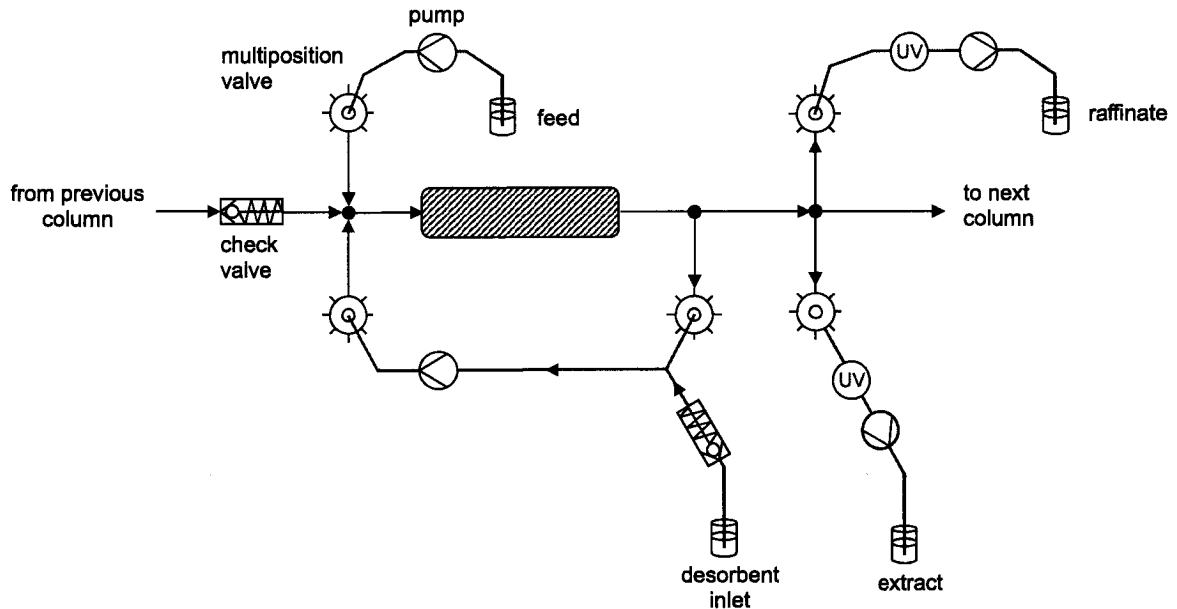


Figure 8.5: Realization of the closed loop SMB setup with online monitoring of the concentrations in extract and raffinate.

Q_E [ml/min]	Q_R [ml/min]	m_1	m_2	m_3	m_4	t^* [min]	P_E	P_R
3.56	1.99	3.35	1.35	2.10	1.00	2	96.65	99.38
3.45	2.12	3.35	1.40	2.15	0.95	2	97.67	99.32
3.04	2.48	3.35	1.60	2.35	1.02	2	98.82	99.08
2.73	2.78	3.35	1.75	2.50	1.02	2	99.07	95.51
2.66	2.86	3.35	1.79	2.54	1.02	2	99.18	93.65

Table 8.2: Operating conditions of the experimental operating points shown in Fig. 8.6. $Q_1 = 9.31$ ml/min and $Q_F = 1.00$ ml/min for all operating points.

There are different ways to close the loop in a SMB setup, where one straight forward method is, as it was adopted in this work, to connect the multi-position valve at the open loop desorbent outlet directly to the desorbent inlet pump via a tee-connection to a bottle with fresh solvent. In this way the solvent from section 4 is directly recycled to section 1 and fresh solvent makes up for the difference in solvent balance. The desorbent inlet pump now directly controls the internal flow rate Q_1 in section 1. By implementing the closed loop in this way, a dead volume between the desorbent outlet multi-position valve across the pump to the desorbent inlet multi-position valve is created. It is not part of the column loop and it doesn't influence V_4^D , but it introduces a short delay time for the profile to propagate from section 4 to section 1, in case of incomplete regeneration in section 4.

Good operating conditions should be chosen in a way that the selectivity is high, which means that the region of complete separation is big, and the Henry's constants are low, in order to be able to use a low switch time t^* . From Fig. 8.1 it can be observed that the selectivity $S = H_G/H_U$ is increasing with decreasing ethanol content, but also the absolute value for the Henry's constants are increasing. As a compromise an ethanol content of 5% has been chosen for the experiments. The switch time was fixed as $t^* = 2$ min.

The region of complete separation in the (m_2, m_3) parameter space was determined and validated experimentally, as shown in Fig. 8.6, where the dead volume of the plant had to be accounted for [11]. The experimental conditions and the purity performance are summarized in table 8.2. The expected trends could be confirmed and the best purities were found within the triangular region of complete separation.

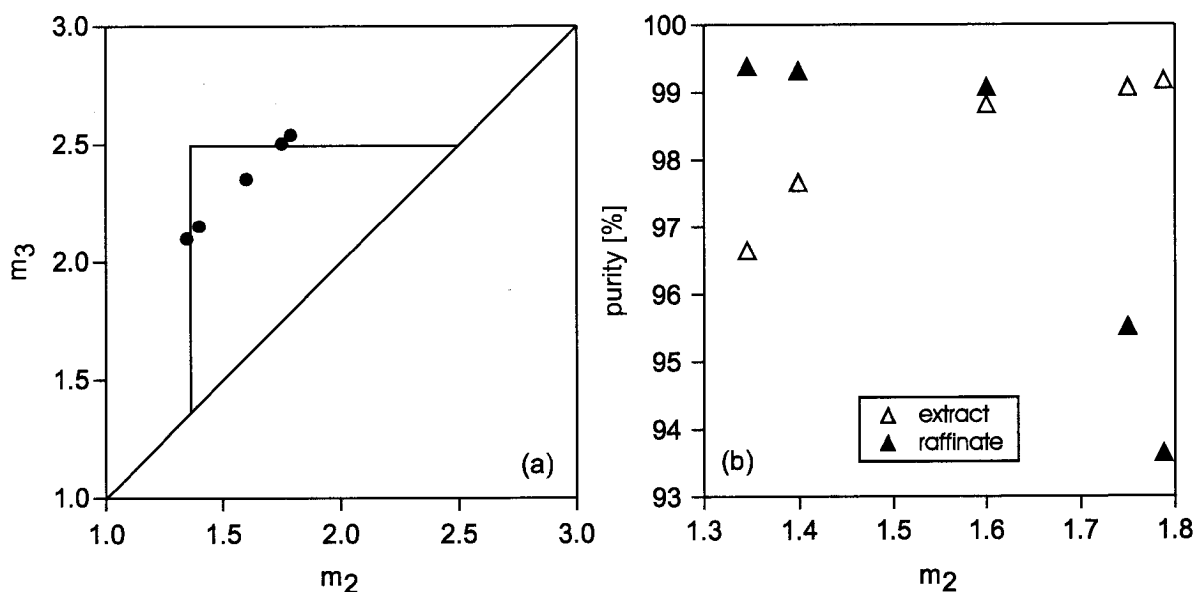


Figure 8.6: (a) Region of complete separation at 22°C for 5% ethanol and operating points in the (m_2, m_3) plane and (b) the obtained purities for extract and raffinate.

8.2 Online monitoring

8.2.1 Sensor setup

To implement a monitoring system suitable for online control as described in chapter 7, two sensors, one at each of the extract and raffinate outlets, are needed. Each sensor should be able to monitor online the concentrations in the binary mixture of nucleosides coming from the plant. To be able to calculate these concentrations, two different signals are needed from each sensor. This results into a system of two equations (one for each signal) with two unknowns (concentration of the nucleosides), which can be solved for the concentrations c_U and c_G .

Two multi-wavelength UV 2077 detectors (Jasco) have been chosen as sensors. The two different signals could be obtained by a simultaneous measurement at two different wavelengths, which exploits the difference in the UV spectra of uridine and guanosine (see Fig. 8.7). For the best measurement accuracy the two wavelengths $\lambda_1 = 212$ nm and $\lambda_2 = 234$ nm have been chosen. The feed concentrations of the SMB experiments were chosen low enough to allow for a linear detector calibration (see Fig. 8.8). The combined signal of both components, i.e. S_{λ_1} and S_{λ_2} , is measured, and the linear system

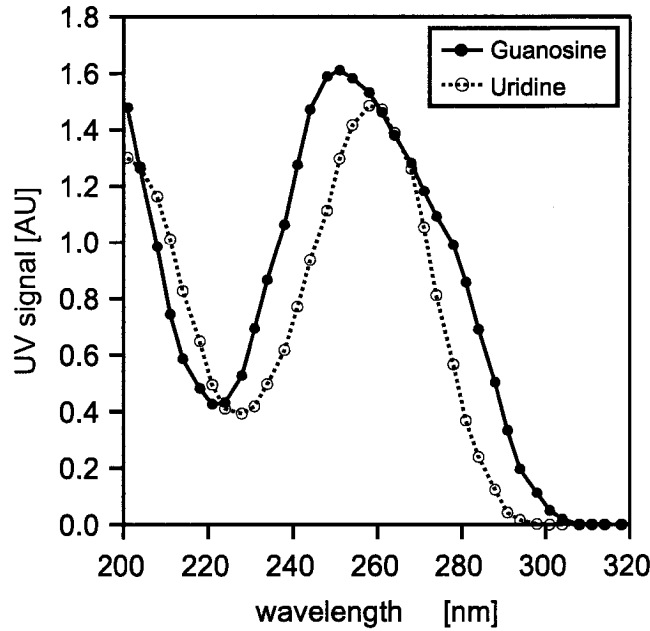


Figure 8.7: Spectra of guanosine and uridine measured with a multi-wavelength UV 2077 (Jasco). $c_U = c_G = 0.08$ g/l.

	$k_{\lambda_1}^U$	$k_{\lambda_2}^U$	$k_{\lambda_1}^G$	$k_{\lambda_2}^G$
UV_R	12.047	6.451	8.245	11.557
UV_E	12.817	6.273	8.920	11.345

Table 8.3: UV detector calibration parameters of Equ. (8.11-8.12).

of equations below can be solved for the concentrations c_U and c_G :

$$S_{\lambda_1} = k_{\lambda_1}^U c_U + k_{\lambda_1}^G c_G \quad (8.11)$$

$$S_{\lambda_2} = k_{\lambda_2}^U c_U + k_{\lambda_2}^G c_G \quad (8.12)$$

The detector calibration is shown in Fig. 8.8 and the resulting parameters $k_{\lambda,i}$ are summarized in table 8.3. It can be readily observed from Fig. 8.8 that the calibration of the two detectors is not identical. As a result the accuracy of the calculated concentrations is different for the two detectors, i.e. the condition numbers of the matrices used to solve the equation system Equ. (8.11-8.12) varies. In this case the detector used for the extract has a better accuracy for the reason mentioned above. The position of the detectors in the plant is shown in Fig.8.9. The UVs were equipped with high pressure flow cells and could be put before the outlet pumps, which exposes them to the pressure of the plant. The plant pressure was always below 20 bar, depending on the flow rates. Another option would have been to put the sensors after the outlet pumps where the pressure is atmo-

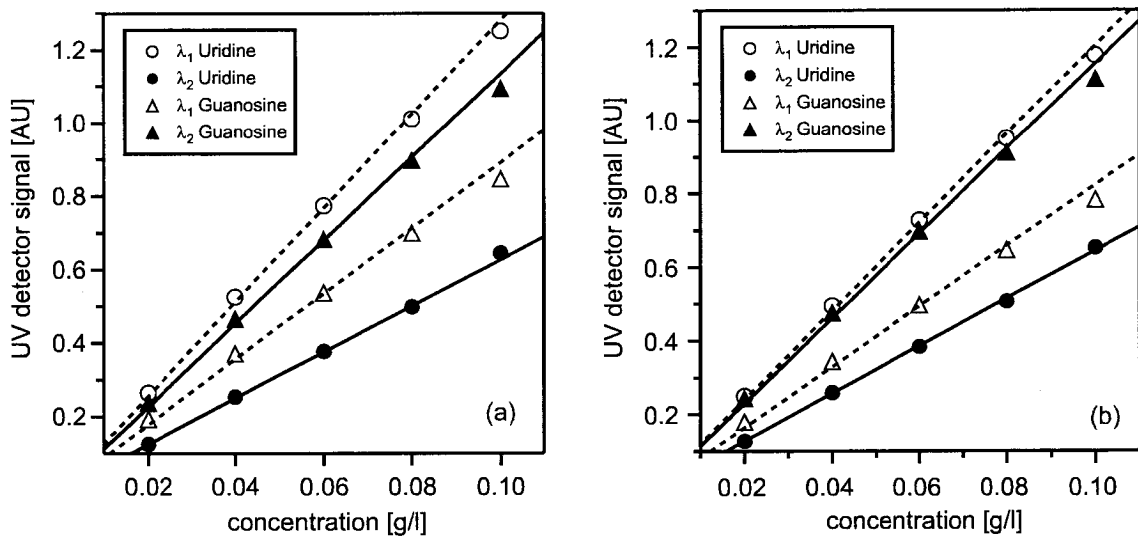


Figure 8.8: UV detector calibration at $\lambda_1 = 212$ nm and $\lambda_2 = 334$ nm for (a) extract and (b) raffinate.

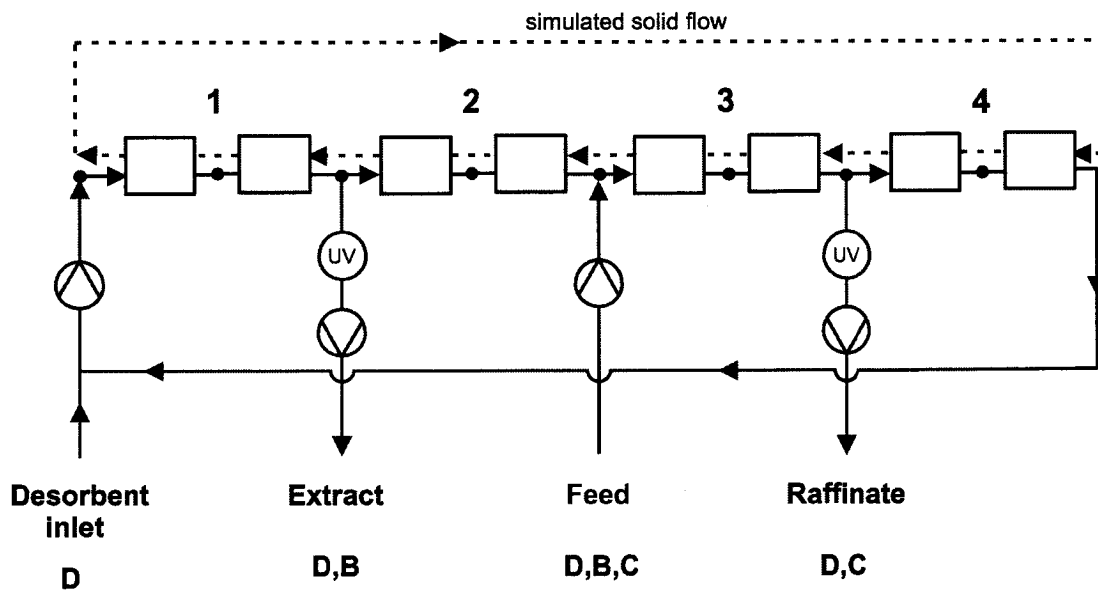


Figure 8.9: Scheme of the SMB with online monitoring of the concentrations.

spheric. In this case the backmixing in the dead volume of the pump and long tubing would influence the signal.

8.2.2 Measurement results

Figures 8.10 and 8.11 show the online monitoring signals, i.e. concentrations of uridine and guanosine, of a SMB run with operating conditions close to the vertex of the triangular region of complete separation in the (m_2, m_3) plane and rather large safety margins for regeneration in section 1 and 4. The start-up of the plant is shown and the cyclic steady state is reached after approximately 5 complete cycles.

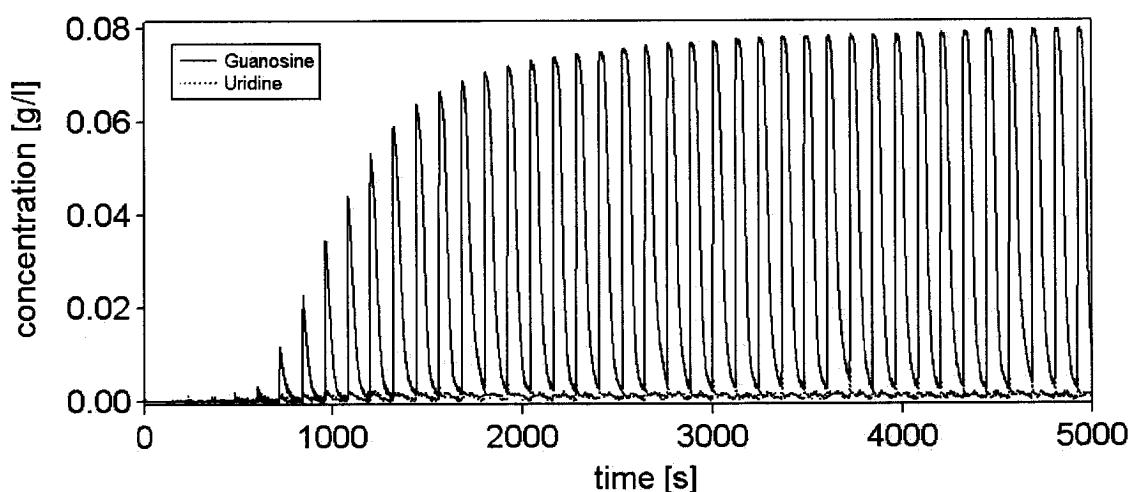


Figure 8.10: Online calculated outlet concentrations from start-up for extract. Duration of a switching period is $t^* = 120$ s. Operating conditions: $m_1 = 3.35$, $m_2 = 1.36$, $m_3 = 2.4$ and $m_4 = 0.97$; $T = 25^\circ\text{C}$.

The dead volume between the multi-position valve at the plant outlet and the detector inlet is almost negligible and a time delay of the measured signal of only 3 seconds at a flow rate of $Q = 2$ ml/min was observed. This implies that there is almost no backmixing in the line between the plant and the detectors and, as it can be observed from Figs. 8.10 - 8.12, the sensor system monitors the process dynamics very accurately. Fig. 8.12 shows a close-up of the extract and raffinate peaks at steady state. Small variations from column to column can not be completely avoided, which is evident from the slight differences from peak to peak. The accuracy from the online monitoring system has been checked by offline HPLC measurements for a limited number of SMB experiments and a statistical error of $\pm 1\%$ on the resulting purity has been estimated. As an example

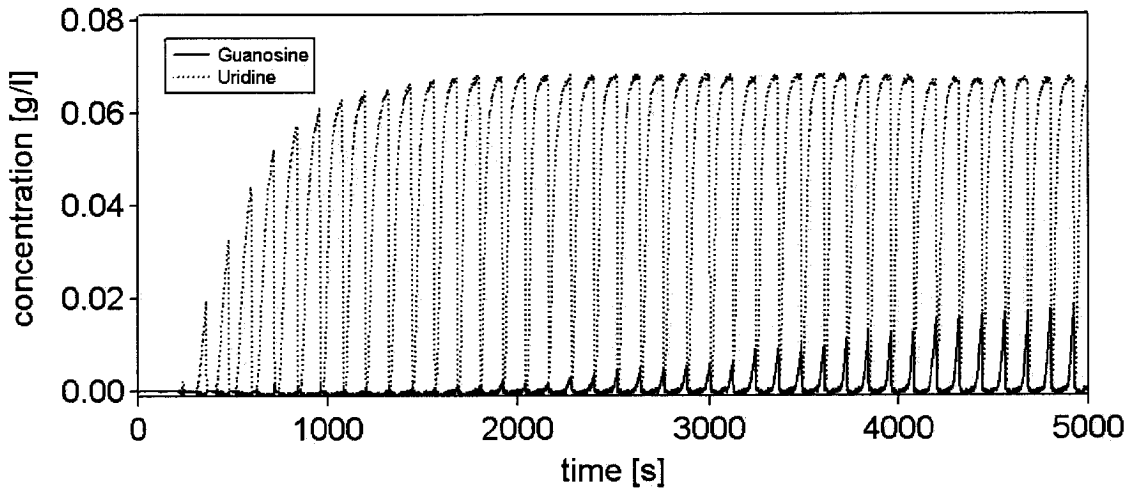


Figure 8.11: Online calculated outlet concentrations from start-up for raffinate. Duration of a switching period is $t^* = 120$ s. Operating conditions: $m_1 = 3.35$, $m_2 = 1.36$, $m_3 = 2.4$ and $m_4 = 0.97$; $T = 25^\circ\text{C}$.

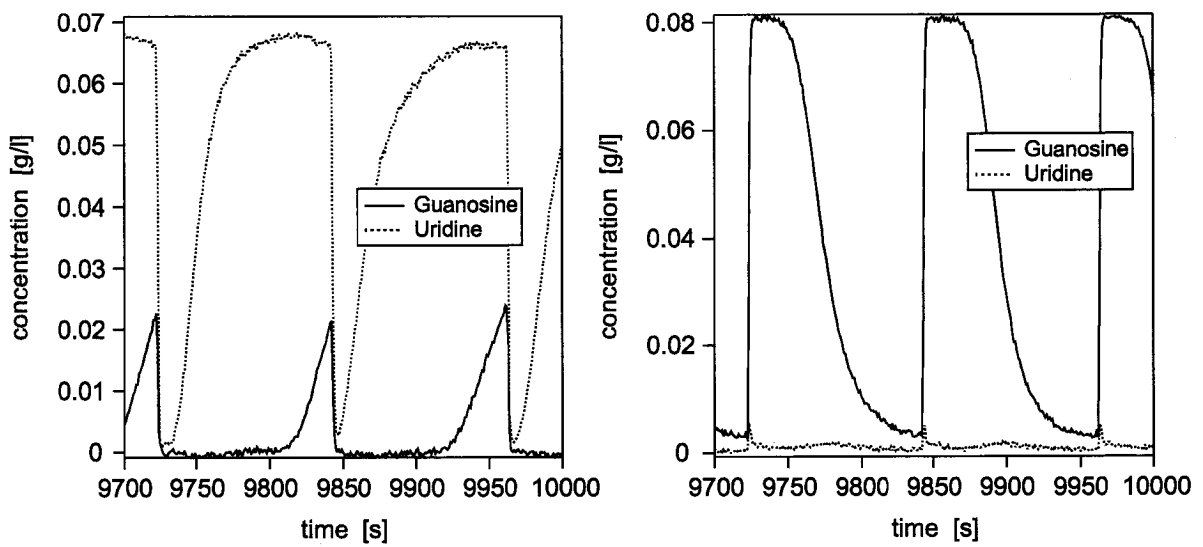


Figure 8.12: Section of online calculated outlet concentrations at steady state for (a) raffinate and (b) extract. Operating conditions: $m_1 = 3.35$, $m_2 = 1.36$, $m_3 = 2.4$ and $m_4 = 0.97$.

the offline purities at cyclic steady state of the SMB run illustrated in Figs. 8.10 - 8.12 are $P_R^{offline} = 93.70\%$ and $P_E^{offline} = 97.53\%$, whereas the purities determined by the online monitoring system are $P_R^{online} = 94.10\%$ and $P_E^{online} = 96.68\%$. It has to be kept in mind that the accuracy largely depends on the UV spectra of the two components to be separated and the possibility to choose two wavelengths with a significant difference in measurement response. This implies that for a system with a larger difference in spectra a better accuracy can be achieved. For the system of uridine and guanosine the spectra are rather close (see Fig. 8.7), but still a reasonable accuracy can be obtained.

Another interesting example of online monitoring is illustrated in Fig. 8.13. It shows the signal of a heavily polluted raffinate stream as well as the raw UV signals at λ_1 and λ_2 , from which the concentrations of uridine and guanosine could be calculated. Due to the

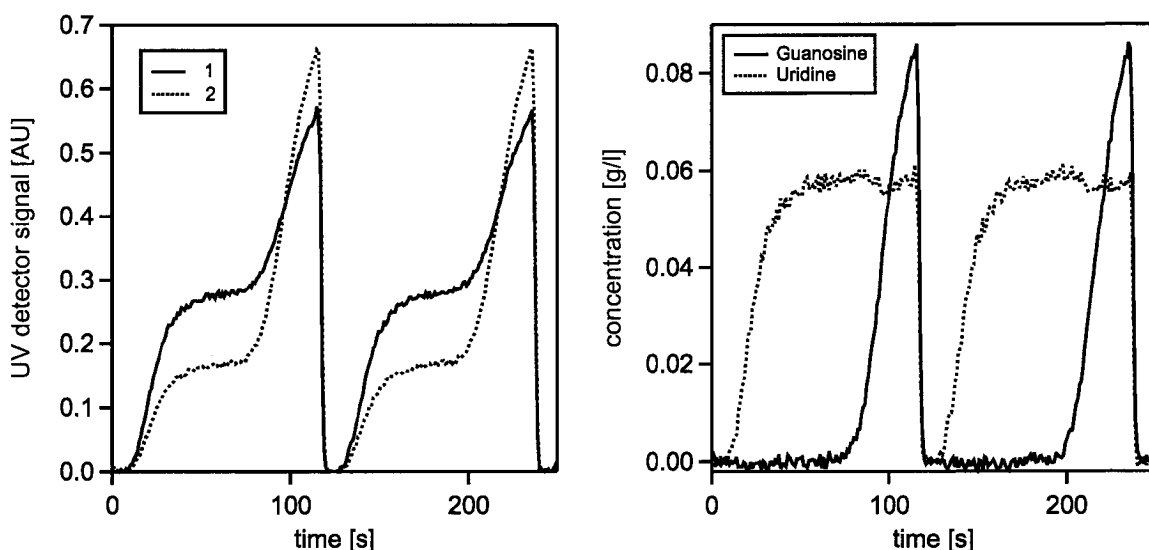


Figure 8.13: Separation at $m_1=3.35$, $m_2=1.96$, $m_3=2.71$, $m_4=1.028$, $t^*=120$ s in cyclic equilibrium. (a) Raffinate signal at the two wavelength $\lambda_1=212$ nm and $\lambda_2=234$ nm; (b) raffinate calculated concentrations for uridine and guanosine ($P_R = 74.9\%$).

large impurity it can be nicely observed how the measurement system divides between the two components. The combined signal is recorded by the UV detector and only its shape indicates the breakthrough of the polluting component, whereas the calculated concentration of the impurity, i.e. guanosine, remains zero for more than half of the switching period and then the time of the breakthrough can clearly be determined.

8.2.3 Comparison of online monitoring results and simulation

To simulate the plant described above, a detailed model was used, that accounts for axial dispersion and mass transfer resistance (see Eqs. (1.11)-(1.13)). The flow in the dead volume elements (see Fig. 8.4) was modeled according to the following equation:

$$\frac{\partial c_i}{\partial t} + u \frac{\partial c_i}{\partial z} = D_D \frac{\partial^2 c_i}{\partial z^2} \quad (8.13)$$

where i is the component index and D_D is the axial dispersion in the dead volume. This model is solved similar to the column model. The right hand side of the equation was accounted for by numerical dispersion and the resulting number of mixing stages is equal to the number of grid points used to discretize the dead volume, as discussed in [11].

In case of the lumped solid diffusion model under linear conditions, the following relationship applies [14]:

$$HETP_i = \frac{L}{N_{p,i}} = \frac{2\varepsilon^* D_{L,i}}{uL} + \frac{2u}{(1-\varepsilon)LH_i a_p k_i} \left(\frac{(1-\varepsilon^*)H_i}{\varepsilon^* + (1-\varepsilon^*)H_i} \right)^2 \quad (8.14)$$

The model parameters for axial dispersion and mass transfer resistance could be obtained by fitting Equ. 8.14 to the experimental points in Fig. 8.3.

The number of grid points used to model the dead volume, i.e. the number of mixing stages, hardly effects the simulation result, whereas it is important to properly account for the hold-up time in the dead volume. For computational efficiency, the minimum number of grid points in each dead volume element was chosen, which is 2.

The experimental run shown in Figs. 8.10 - 8.12 has been simulated and the comparison of online monitoring and simulation is shown in Fig. 8.14 and 8.15.

It can be observed from these figures that the dynamics of the SMB is captured quite well by the online monitoring and the simulated profiles are close to the ones obtained by online monitoring. The differences between the measured peaks, which is more obvious in Fig. 8.14, are due to the column to column variations. The simulation results and the measurements match slightly less for the extract. It is almost impossible to account properly for all influences on the process in a real plant. The fact that the impurity in the extract has not the typical shape as we would expect it (maximum at $t^*/2$) suggests an effect due to the plant hardware, e.g. a not completely flushed dead volume, the model of course can not account for.

Finally it can be said that process dynamics of a real SMB experiment can be modeled

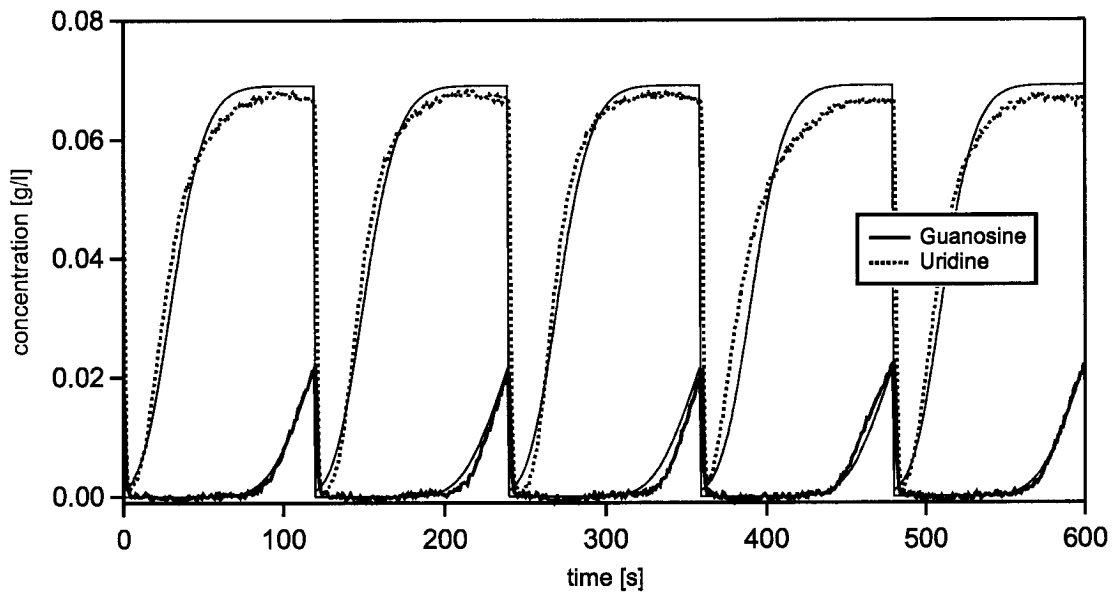


Figure 8.14: Comparison of raffinate online monitoring (bold lines) and simulation (thin lines) for $t^* = 120$ s, $m_1 = 3.35$, $m_2 = 1.36$, $m_3 = 2.4$ and $m_4 = 0.97$ and $T = 25^\circ\text{C}$.

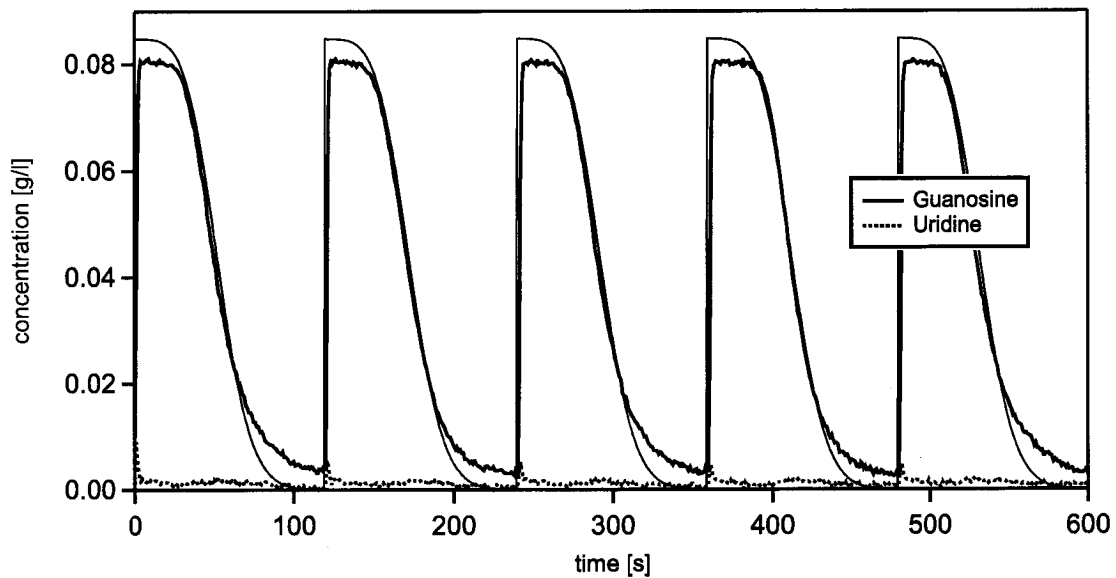


Figure 8.15: Comparison of extract online monitoring (bold lines) and simulation (thin lines) for $t^* = 120$ s, $m_1 = 3.35$, $m_2 = 1.36$, $m_3 = 2.4$ and $m_4 = 0.97$ and $T = 25^\circ\text{C}$. The simulated concentration of uridine $c_U = 0$.

rather accurately, whereas it is hard to account for every influence on the real process properly and model deviations have to be expected.

8.3 SMB control

The developed controller has been implemented experimentally on the separation of nucleosides which is characterized in chapter 8.1 and a first preliminary result can be shown. The controller model uses the separation triangle for 5% ethanol in water and 22°C as illustrated in Fig. 8.6a. The experiment was carried out under model/plant mismatch conditions: the operating temperature was $23 \pm 1^\circ\text{C}$, which causes a downward shift of the separation triangle and uncertainties according to Fig. 8.2. Furthermore, a reduced column efficiency was found in comparison to the experiments shown in Fig. 8.6, which was possibly caused by a damaged column packing. A set point of a minimum purity of 93% for both extract and raffinate was chosen and the plant was started up at $m_1 = 3.32$, $m_2 = 1.31$, $m_3 = 2.55$, $m_4 = 1.09$ and $t^* = 120$ s, which is an operating point above the region of complete separation leading to an unsatisfactory purity of the raffinate and an extract purity above the set point (see Fig. 8.17). The controller was switched on after cycle 6 and the trajectory of the operating point in the (m_2, m_3) plane is illustrated in Fig. 8.16.

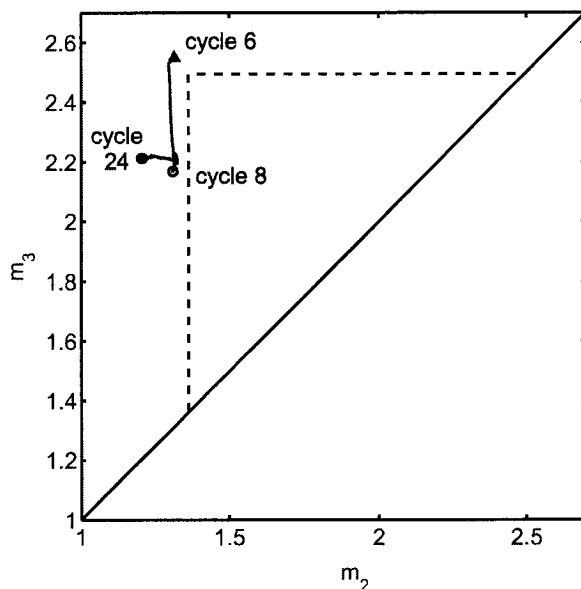


Figure 8.16: Trajectory of the operating point in the (m_2, m_3) plane with respect to the separation triangle used by the controller model (broken line).

The corresponding purities as measured by the online monitoring system are shown in Fig. 8.17. It has to be kept in mind that the real purities might deviate depending on the accuracy of the online monitoring system. However, to assess the performance of the controller one has to look solely at the online monitoring purities. In order to overcome the online measurement uncertainty which can never be avoided completely, a repetitive online/offline adjustment of the monitoring system calibration while the unit is running will have to be implemented.

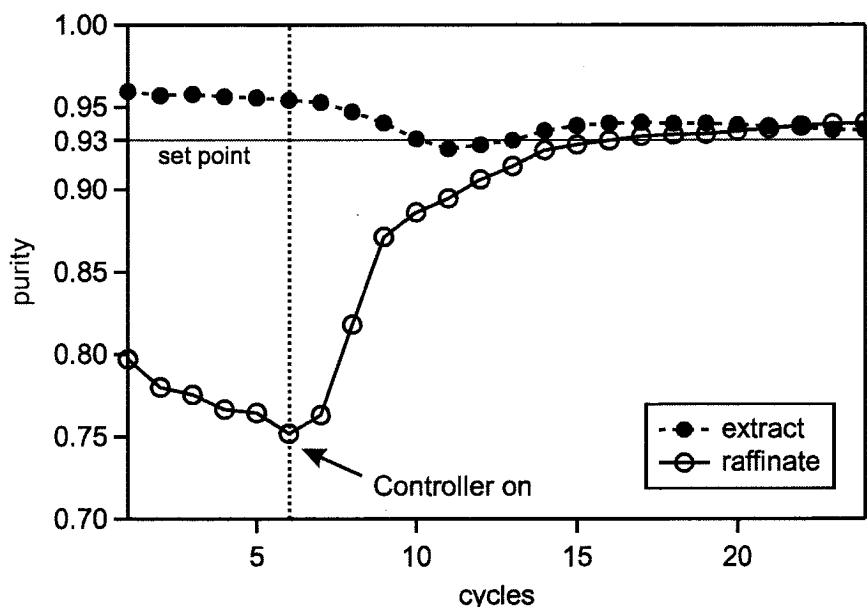


Figure 8.17: Outlet purities for the controlled SMB. The controller is switched on after cycle 6 in order to bring the outlet purities above a set point of 93% minimum purity for both outlets.

It can be observed, that the operating point in the (m_2, m_3) plane moves down in only 2 cycles in order to fulfill the purity constraint, i.e. to improve the low raffinate purity. Then the operating point is shifted left towards lower values of m_2 and from cycle 16 on the purity constraint for both extract and raffinate is fulfilled and no off-spec product is obtained despite a rather big model/plant mismatch. At cycle 24 the plant is not yet in steady state, because the plant had to be shut down due to hardware problems.

This result looks already rather promising and further tuning of the controller should improve the control performance. It has to be emphasized again that this result is preliminary, more experimental work is required and problems have to be solved in order to obtain a robust SMB control system. This first impression of the controller performance shows that the developed controller is able to act in a meaningful way and bring the outlet

purities above the set point.

9 Conclusions and Outlook

The majority of SMB applications are binary separations in the liquid phase using a standard four section SMB in isocratic mode. In this work two new SMB paradigms have been realized to broaden the range of applications and to include not only chiral separations but also multi-component multi-fraction separations, e.g. bio-separations. The goal was not only to improve the separation performance in terms of productivity and solvent consumption, but also to make an SMB separation possible for a number of applications that could not be processed using SMB before. For these applications, e.g. multi-component bio-separations needing a frequent column cleaning step (cleaning in place, CIP), the possibility to apply the continuous high productivity SMB technology is a big advantage compared to the current production using batch processes.

The first SMB paradigm mentioned above is the solvent gradient SMB (SG-SMB). It aims at improving the productivity and decreasing the solvent consumption by applying a step gradient in solvent composition. Design criteria based on equilibrium theory have been developed for linear and nonlinear adsorption isotherms and the concept could be validated by simulations and experiments. It was found that productivity and solvent consumption could be improved for separations with linear adsorption isotherms, i.e. dilute systems, whereas in cases with nonlinear isotherms the solubility limit might diminish the benefit of the gradient mode.

The second paradigm is the three fraction SMB (3F-SMB). It consists of a standard SMB configuration with one or two additional sections between sections 4 and 1, i.e. section 0 and an equilibration section. This setup can be used for purifications or to separate continuously a mixture of three components where one component adsorbs much stronger than the others, which is often the case for bio-separations. This component moves through the SMB columns similar as in a batch process. This combination of batch characteristics and continuous process is exploited in the concept of the 3F-SMB as well as the intrinsic switching mechanism of the SMB, that makes the complete separation into three pure fractions possible. Depending on the application the solvent can be changed in one of the additional sections or it can be used to integrate a continuous cleaning in place (CIP) step, where every column is cleaned once every switching cycle. If necessary the flow direction of the cleaning step can be reversed. This concept of 3F-SMB is considered very attractive for the separation of bio-molecules and is a first step from the batch process to the continuous process in this field.

Finally, to provide a tool for the proper implementation of SMB in the production an optimizing control concept for SMBs has been developed using MPC (model predictive control). The objective of the controller is to optimize the separation performance with respect to productivity and solvent consumption, while the purity doesn't fall below a given minimum purity. The outlet concentrations of all components are measured at extract and raffinate by an online monitoring system and the states of the plant are estimated by a Kalman filter using an approximate plant model. With this information the controller is able to calculate a prediction of the future evolution of the plant and an optimized input in terms of flow rates (controlled variables), which are then implemented. The control system has been successfully tested for several disturbance scenarios using a plant simulation. An experimental separation of nucleosides has been characterized and an online measurement system consisting of two UV detectors measuring at two different wavelength has been implemented. A very promising preliminary result of the implemented experimental SMB control system shows that the developed controller behaves in a meaningful way for both simulations and real plant.

As a result of this work the investigated technical innovations pave the way for many potential SMB applications and provide efficient tools for improved state of the art production, especially in fields with rather fast scientific progress, e.g. biotechnology, where appropriate separation processes are urgently needed.

For a successful implementation of the introduced concepts in production the control concept has to be further extended, e.g. for plants with differing numbers of columns or different SMB operating schemes. The application of the control scheme in industry, which is the ultimate goal, will need a more simplified user interface for handling, which has to be developed as soon as all technical aspects are tackled.

Notation

A, B, C	state space model matrices
A	column cross-section, [cm ²]
a_p	specific surface of the adsorbent particles, [1/cm]
c_i	concentration of species i , [g/l]
c	concentration, [g/l]
D	apparent axial dispersion coefficient, [cm ² /s]
d	internal column diameter, [cm]
$D_{L,i}$	axial dispersion coefficient of component i , [cm ² /s]
D_D	axial dispersion coefficient in the dead volume, [cm ² /s]
F	production cost
H	Henry's constant, [-]
$HETP$	height equivalent of a theoretical plate, [cm]
H_i	Henry's constant of species i , [-]
\tilde{K}	Kalman filter gain matrix
k	parameter in equation (3.2), [-]
k	cycle index
k	langmuir isotherm equilibrium constant, [l/g]
k_q	mass transfer coefficient in the lumped pore diffusion model, [cm/s]
k_i	mass transfer coefficient of component i , [cm/s]
L	column length, [cm]
m	flow rate ratio, [-]
m_j	flow rate ratio in section j , [-]
N	number of time steps per cycle [-]
n	parameter in equation (3.2), [-]
n	time step index
N_c	total number of columns in the SMB [-]
N_g	total number of grid points in the SMB [-]
n_j^{col}	number of columns in section j , [-]
N_p	number of theoretical plates [-]
N_t	number of time steps during a switching period [-]
P	purity, [-]
P_K	purity of product stream K , [-]
Q	volumetric fluid flow rate, [ml/min]
q^*	adsorbed phase concentration at equilibrium, [g/l]
q_i	adsorbed phase concentration of species i , [g/l]
Q_j	volumetric fluid flow rate in section j , [ml/min]
Q_s	volumetric solid flowrate, [ml/min]
S	selectivity, [-]
S_j	distance component A propagates during a switching period t^* in section j , [cm]
s	slack variable, [-]
t	time, [s]
t_R	retention time, [s]
t^*	switch time, [s]

u	vector of manipulated variables
u_j	superficial velocity in section j , [cm/min]
V	column volume, [ml]
v	internal flow rate, [ml/min]
V_j^D	dead volume per column in section j , [ml]
V_d	dead volume element, [ml]
V_{in}^D	dead volume of the tubing measured from inlet port to column inlet, [ml]
V_{out}^D	dead volume of the tubing measured from column outlet to outlet port, [ml]
w_j	propagation velocity of component A in section j , [cm/min]
$w_{1/2}$	peak width at half height, [min]
x	volume fraction of solvent W in the fluid phase, [-]
x	state vector
\tilde{x}	state vector of reduced order model
y	vector of output concentrations
z	axial coordinate, [cm]

Subscripts and superscripts

A, B, C	components of a mixture
A, \dots, H	index for physical columns
$contr$	control horizon
D	desorbent
dA	2'-deoxyadenosine
dC	2'-deoxycytidine
dG	2'-deoxyguanosine
dT	thymidine
E	extract
eq	equilibration
F	feed
g	space index (grid point number)
h	column position index, ($h = 1, \dots, 8$)
i	component index
in	column inlet
I/O	inlet/outlet stream
j	section index, ($j = 1..4$)
j	section index, ($j = 1..4$)
L	lower bound
max	maximum
min	minimum
out	column outlet
P	at operating point P
$pred$	predicted
R	raffinate
ref	reference value
SMB	Simulated Moving Bed
T	third fraction
TMB	True Moving Bed
U	upper bound
W	solvent W
0	reference value at $x = 0$

Greek letters

ε^*	overall bed void fraction, [-]
ε_p	particle porosity, [-]
ε	bed void fraction, [-]
Γ	saturation loading capacity, [g/l]
λ	weighting factor in cost function, [-]

References

- [1] H. Lorenz, P. Sheehan, and A. Seidel-Morgenstern. Coupling of simulated moving bed chromatography and fractional crystallization for efficient enantioseparation. *J. Chromatogr. A*, 908:201–214, 2001.
- [2] M. Amanullah, S. Abel, and M. Mazzotti. Separation of tröger's base enantiomers through a combination of simulated moving bed chromatography and crystallization. *AIChE J.*, to be submitted, 2004.
- [3] M. Amanullah, S. Abel, and M. Mazzotti. Separation of tröger's base enantiomers through a combination of simulated moving bed chromatography and crystallization. *SSCP*, Zurich, March 9-10, 2004.
- [4] D. M. Ruthven and C. B. Ching. Counter current and simulated counter current adsorption separation processes. *Chem. Eng. Sci.*, 44:1011–1038, 1989.
- [5] M. Juza, M. Mazzotti, and M. Morbidelli. Simulated moving-bed chromatography and its application to chirotechnology. *Trends in Biotechnology*, 18:108–118, 2000.
- [6] R.-M. Nicoud. The separation of optical isomers by simulated moving bed chromatography (part II). *Pharm. Technol. Eur.*, 11:28–34, 1999.
- [7] M. Schulte and J. Strube. Preparative enantioseparations by simulated moving bed chromatography. *J. Chromatogr. A*, 906:399–416, 2001.
- [8] R. M. Nicoud. Simulated moving bed: some possible applications of biotechnology. In G. Subramanian, editor, *Bioseparation and bioprocessing*. Wiley-VCH, New York, 1998.
- [9] S. Nagamatsu, K. Murazumi, and S. Makino. Chiral separation of a pharmaceutical intermediate by a simulated moving bed process. *J. Chromatogr. A*, 832:55–65, 1999.
- [10] M. Mazzotti, G. Storti, and M. Morbidelli. Optimal operation of Simulated Moving Bed units for nonlinear chromatographic separations. *J. Chromatogr. A*, 769:3–24, 1997.
- [11] C. Migliorini, M. Mazzotti, and M. Morbidelli. Simulated moving bed units with extracolumn dead volume. *AIChE J.*, 45:1411–1422, 1999.

- [12] G. Storti, M. Mazzotti, M. Morbidelli, and S. Carrá. Robust design of binary countercurrent separation processes. *AIChE J.*, 39:471–492, 1993.
- [13] G. Guiochon. Review preparative liquid chromatography. *J. Chromatogr. A*, 965:129–161, 2002.
- [14] C. Migliorini, A. Gentilini, M. Mazzotti, and M. Morbidelli. Design of simulated moving bed units under non-ideal conditions. *Ind. Eng. Chem. Res.*, 38:2400–2410, 1999.
- [15] O. Ludemann-Hombourger, R. M. Nicoud, and Bailly M. The "VARICOL" process: A new multicolumn continuous chromatographic process. *Separation Science and Technology*, 35:1829–1862, 2000.
- [16] O. Ludemann-Hombourger, G. Pigorini, R. M. Nicoud, D. S. Ross, and G. Terfloth. Application of the "VARICOL" process to the separation of the isomers of the sb-553261 racemate. *J. Chromatogr. A*, 947:59–68, 2002.
- [17] E. Kloppenburg and E. D. Gilles. A new concept for operating simulated moving-bed processes. *Chem. Eng. Technol.*, 22:10–19, 1999.
- [18] Y. Zang and P.C. Wankat. SMB operation strategy - Partial feed. *Ind. Eng. Chem. Res.*, 41:2504–2511, 2002.
- [19] Z. Zhang, M. Mazzotti, and M. Morbidelli. PowerFeed operation of SMB units: changing the fluid flow rates during the switching interval. *J. Chromatogr. A*, submitted, 2002.
- [20] C. Migliorini, M. Wendlinger, M. Mazzotti, and M. Morbidelli. Temperature gradient operation of a simulated moving bed unit. *Ind. Eng. Chem. Res.*, 40:2606–2617, 2001.
- [21] J.Y. Clavier, M. Perrut, and R.M. Nicoud. A new efficient fractionation process: the simulated moving bed with supercritical eluent. In Ph. Rudolf von Rohr and Ch. Trepp, editors, *High Pressure Chemical Engineering*. Elsevier Science, London, 1996.
- [22] O. DiGiovanni, M. Mazzotti, M. Morbidelli, F. Denet, W. Hauck, and R.M. Nicoud. Supercritical fluid simulated moving bed chromatography. II. Langmuir isotherm. *J. Chromatogr. A*, 919:1–12, 2001.

- [23] F. Denet, W. Hauck, R.M. Nicoud, O. Di Giovanni, M. Mazzotti, J.-N. Jaubert, and M. Morbidelli. Enantioseparation through supercritical Simulated Moving Bed (SF-SMB) chromatography. *Ind. Eng. Chem. Res.*, 40:4603–4609, 2001.
- [24] M. Mazzotti, G. Storti, and M. Morbidelli. Supercritical fluid simulated moving bed chromatography. *J. Chromatogr. A*, 786:309–320, 1997.
- [25] T. B. Jensen, T. G. P. Reijns, H. A. H. Billiet, and L. A. M. van der Wielen. Novel simulated moving-bed method for reduced solvent consumption. *J. Chromatogr. A*, 873:149–162, 2000.
- [26] D. Antos and A. Seidel-Morgenstern. Application of gradients in the simulated moving bed process. *Chem. Eng. Sci.*, 56:6667–6682, 2001.
- [27] J. Houwing, H. A. H. Billiet, and L. A. M. van der Wielen. Optimization of azeotropic protein separations in gradient and isocratic ion-exchange simulated moving bed chromatography. *J. Chromatogr. A*, 944:189–201, 2002.
- [28] G. Biressi, O. Ludemann-Hombourger, M. Mazzotti, R. M. Nicoud, and M. Morbidelli. Design and optimisation of a SMB unit: role of deviations from equilibrium theory. *J. Chromatogr. A*, 876:3–15, 2000.
- [29] F. Quattrini, G. Biressi, M. Juza, M. Mazzotti, C. Fuganti, and M. Morbidelli. Enantiomer separation of α -ionone using gas chromatography with cyclodextrin derivatives as chiral stationary phases. *J. Chromatogr. A*, 865:201–210, 1999.
- [30] G. Zenoni, F. Quattrini, M. Mazzotti, C. Fuganti, and M. Morbidelli. Scale-up of analytical chromatography to the simulated moving bed separation of the enantiomers of the flavour norterpeneoids α -ionone and α -damascone. *Flavour Frag. J.*, 17:195–202, 2002.
- [31] MP. Pedferri, G. Zenoni, M. Mazzotti, and M. Morbidelli. Experimental analysis of a chiral separation through simulated moving bed chromatography. *Chem. Eng. Sci.*, 54:3735–3748, 1999.
- [32] G. Hotier, J.-M. Toussaint, G. Terneuil, and D. Lonchamp. Continuous process and apparatus for chromatographic separation of a mixture of at least three constituents into three purified effluents using two solvents. United States Patent No. US005093004A, 1992.

- [33] U. Voigt, J. Kinkel, R. Hempel, and R.-M. Nicoud. Chromatographic process for obtaining highly purified cyclosporin A and related cyclosporins. United States Patent No. US006306306B1, 2001.
- [34] G. Paredes, S. Abel, M. Mazzotti, M. Morbidelli, and J. Stadler. Analysis of a new Simulated Moving Bed unit for three fraction separations (3F-SMB). *Ind. Eng. Chem. Res.*, submitted, 2004.
- [35] P. Marteau, G. Hotier, N. Zanier-Szydlowski, A. Aoufi, and F. Cansell. Advanced control of c8 aromatics separation process with real-time multipoint on-line raman spectroscopy. *Process Control and Quality*, 6:133, 1994.
- [36] K. U. Klatt, F. Hanisch, and G. Dünnebier. Model-based control of a simulated moving bed chromatographic process for the separation of fructose and glucose. *J. of Process Control*, 12:203–219, 2002.
- [37] H. Schramm, S. Grüner, A. Kienle, and E.D. Gilles. Control of moving bed chromatographic processes. *Proceedings of European Control Conference 2001, Porto, Portugal*, pages 2528–2533, 2001.
- [38] C.E. Garcia, D.M. Prett, and M. Morari. Model predictive control - theory and practice - a survey. *Automatica*, 25(3):335–348, 1989.
- [39] A. Bemporad and M. Morari. Model predictive control: A survey. *Lecture Notes in Control and Information Sciences*, 245:207–226, 1999.
- [40] S. Natarajan and J.H. Lee. Repetitive model predictive control applied to a simulated moving bed chromatography system. *Computers and Chem. Eng.*, 24:1127–1133, 2000.
- [41] J. H. Lee, S. Natarajan, and K. S. Lee. A model-based predictive control approach to repetitive control of continuous processes with periodic operations. *J. Process Control*, 11:195–207, 2001.
- [42] G. Guiochon, S. Golshan-Shirazi, and A. M. Katti. *Fundamentals of preparative and nonlinear chromatography*. Academic Press, 1994.
- [43] G. Erdem, S. Abel, M. Morari, M. Mazzotti, and M. Morbidelli. Automatic control of simulated moving beds. *Ind. Eng. Chem. Res.*, 43:405–421, 2004.

- [44] MATLAB®, Control System Toolbox. The MathWorks, Inc.
- [45] R. E. Kalman. A new approach to linear filtering and prediction problems. *Trans. ASME, Journal of Basic Engineering*, 82:35–45, 1960.
- [46] K. S. Lee and J. H. Lee. “Implementations of Iterative Learning Control Method.” *Iterative Learning Control: Analysis, Design, Integration and Applications*. Kluwer Academic Publishers, 1998. Edited by Z. Bien and J. Xu.
- [47] G. Erdem, S. Abel, M. Morari, M. Mazzotti, and M. Morbidelli. Automatic control of simulated moving beds - nonlinear isotherm. *Ind. Eng. Chem. Res.*, in press, 2004.

Curriculum Vitae

Personal Data

Stefanie Abel

born in Karlsruhe, Germany, 10.05.1973

Citizen of Germany

School

08/1979–07/1983 Primary school, Langensteinbach, Germany

08/1983–05/1992 Gymnasium Karlsbad, Langensteinbach, Germany

University

10/1992–04/1998 Chemical Engineering, University of Karlsruhe, Germany

Practical Training Abroad

04/1997–10/1997 CSIRO, Division of coal and energy technology, Sydney, Australia

Professional Experience

10/1998–03/2000 Process Engineer, IBM Speichersysteme GmbH Mainz, Germany

Doctorate

05/2000–04/2004 Swiss Federal Institute of Technology, ETH Zurich
Institute of Process Engineering

Zurich, 06. April 2004

List of Publications

- S. Abel, M. Mazzotti, M. Morbidelli. Solvent gradient operation of simulated moving beds. I. Linear isotherms. *J. Chromatogr. A*, vol. 944, pp.:23-39 (2002)
- S. Abel, M. Mazzotti, M. Morbidelli. Solvent gradient operation of simulated moving beds. II. Langmuir isotherms. *J. Chromatogr. A*, vol. 1026, pp.:47-55 (2004)
- S. Abel, M. Bähler, C. Arpagaus, M. Mazzotti, J. Stadler. Two-fraction and three-fraction continuous SMB separation of nucleosides. *J. Chromatogr. A* (2003), in press.
- G. Paredes, S. Abel, M. Mazzotti, M. Morbidelli, J. Stadler. Analysis of a new SMB unit for three fraction separations (3F-SMB). *Ind. Eng. Chem. Res.* (2004), submitted.
- S. Abel, G. Erdem, M. Mazzotti, M. Morari, M. Morbidelli. Optimizing control of simulated moving beds - linear isotherm. *J. Chromatogr. A*, vol. 1033, pp.: 229-239 (2004).
- G. Erdem, S. Abel, M. Morari, M. Mazzotti, M. Morbidelli. Automatic Control of Simulated Moving Beds. *Ind. Eng. Chem. Res.* 43, pp.:405-421 (2004)
- G. Erdem, S. Abel, M. Morari, M. Mazzotti, M. Morbidelli. Automatic Control of Simulated Moving Beds - Nonlinear Isotherm. *Ind. Eng. Chem. Res.* (2004), in press.
- M. Amanullah, S. Abel, M. Mazzotti. Separation of Träger's base enantiomers through a combination of simulated moving bed chromatography and crystallization. *AIChE J.* (2004), to be submitted.

List of Conference Contributions

- S. Abel, M. Mazzotti, M. Morbidelli. Gradient operation of a simulated moving bed unit. *PREP 2001*, Washington, USA, May 13 - 16.
- S. Abel, C. Arpagaus, J. Stadler, M. Mazzotti. Simulated moving bed separation of nucleosides. *PREP 2001*, Washington, USA, May 13 - 16.

- G. Zenoni, S. Abel, G. Erdem, M. Mazzotti, M. Morbidelli. Liquid phase simulated moving bed for the separation of enantiomers. *FOA7 2001*, Nagasaki, Japan, May 20 - 25.
- S. Abel, G. Erdem, G. Zenoni, M. Mazzotti, M. Morbidelli. Separation of enantiomers through solvent gradient SMB chromatography. *AICHE 2001*, Reno, USA, November 4 - 9.
- G. Erdem, S. Abel, M. Mazzotti, M. Morari, M. Morbidelli. Controlling simulated moving beds. *PREP 2002*, Washington, USA, June 16 - 18.
- S. Abel, L. Aumann, M. Mazzotti, M. Morbidelli. Solvent gradient operation of simulated moving bed processes. *ISPPP 2002*, Heidelberg, Germany, November 10 - 13.
- S. Abel, G. Erdem, M. Mazzotti, M. Morari, M. Morbidelli. Model predictive control of simulated moving bed separations. *SPICA 2002*, Heidelberg, Germany, October 6 - 9.
- S. Abel, M. Bähler, C. Arpagaus, J. Stadler, M. Mazzotti, M. Morbidelli. Simulated moving bed processes for the continuous separation of nucleosides. *ACS 2003*, New Orleans, USA, March 23 -27.
- G. Erdem, S. Abel, M. Mazzotti, M. Morari, M. Morbidelli. Optimization based adaptive control of simulated moving beds. *The 3rd Pacific Basin Conference on Adsorption Science and Technology 2003*, Kyungju, Korea, May 25 - 29.
- G. Erdem, S. Abel, M. Morari, M. Mazzotti, M. Morbidelli. Optimizing control of Simulated Moving Beds. *AICHE 2003*, San Francisco, USA, November 16 - 21.
- S. Abel, G. Paredes, J. Stadler, M. Mazzotti, M. Morbidelli. 3F-SMB operation for the separation of biomolecules. *AICHE 2003*, San Francisco, USA, November 16 - 21.
- M. Amanullah, S. Abel, M. Mazzotti. Separation of tröger's base enantiomers through a combination of simulated moving bed chromatography and crystallization. *SSCP 2004*, Zurich, Switzerland, March 9-10.